

EFFECTS OF PLY DROPS ON THE FATIGUE RESISTANCE
OF COMPOSITE MATERIALS AND STRUCTURES

by

Mark Ethan Scott

A thesis submitted in partial fulfillment
of the requirements for the degree

of

Master of Science

in

Chemical Engineering

MONTANA STATE UNIVERSITY
Bozeman, Montana

August 1997

STATEMENT OF PERMISSION TO USE

In presenting this thesis in partial fulfillment of the requirements for a master's degree at Montana State University, I agree that the Library shall make it available to borrowers under rules of the Library.

If I have indicated my intention to copyright this thesis by including a copyright notice page, copying is allowable only for scholarly purposes, consistent with "fair use" as prescribed in the U.S. Copyright Law. Requests for permission for extended quotation from or reproduction of this thesis in whole or in parts may be granted only by the copyright holder.

Signature _____

Date _____

ACKNOWLEDGMENTS

I would especially like to thank Dr. Mandell and Dr. Cairns for their insight and direction. Dan Samborsky receives special thanks for all his time and suggestions with editing figures, efforts in helping with experiments and keeping the facilities running. Zane Maccagnano for his work using finite element analysis to back up the results obtained experimentally. To all of the students in the composites group for their input and good sense of humor during the frustrating moments of school and research. And finally, to my family who have always encouraged and supported me.

This work was supported by the U.S. Department of Energy and the State of Montana through the Montana DOE EPSCoR Program (Contract # DEFC02-91ER75681) and the National Renewable Energy Laboratory (Subcontract # XF-1-11009-5), and Sandia National Laboratories (Subcontract ANO412).

TABLE OF CONTENTS

LIST OF TABLES	vii
LIST OF FIGURES	ix
ABSTRACT	xii
1. INTRODUCTION	1
2. BACKGROUND	4
Strain Energy Release Rate	4
Tensile Testing of Dropped-Ply Laminates	8
Compression Testing of Dropped-Ply Laminates	9
Damage Accumulation	10
Stress Analysis on Dropped-Ply Laminates	11
Delamination Prevention	13
Existence of a Resin Rich Region	14
Design Considerations	15
Motivation for Thesis	18
3. EXPERIMENTAL METHODS AND MATERIALS	20
Test matrix and description of specimens	20
Material Preparation	29
Fabrics	31
Specimen Preparation	32
Test Facility and Development	33
DCB and ENF test specimens	35
4. RESULTS AND DISCUSSION	37
DELAMINATION STUDY	37
Effect of Ply Drop Location	37
Effects of laminate thickness and multiple ply drops at the same position	43
The ESE and ESF laminates	44
Effect of Ply Drop Spacing	45
Effects of “Z-Spiking”	46
Effect of Tough Adhesive at Ply Drop	49
Effect of Butt-Joints	50
Effects of $\pm 45^\circ$ Ply Drops	51
Effect of A130 warp unidirectional fabric	52
Other attempts to prevent delamination	53

Repairing Delaminated Samples	55
Comparing different laminates	56
EFFECT OF PLY DROPS ON LIFETIME	57
Fiber Volume Content Effect	57
A130 fabric vs. D155 fabric	59
Resin Rich Region	61
COMPRESSION TESTING	64
Residual Strength of Coupons	67
PLY DROPS IN BEAMS	70
Flange laminate ESA	73
Beam 39	73
Beam 44	76
Beam 48	78
Flange laminate ESB	80
Beam 40	80
Flange laminate ESG	81
Beam 41	81
Beam 42	85
Flange laminate ESH	86
Beam 49	86
Beam 50	89
Comparison of Delamination Rate in Beams and Coupons	90
STRAIN ENERGY RELEASE RATE AND MODELING RESULTS	94
Determination of Critical Strain Energy Release Rate	94
Static and Threshold Strain Energy Release Rates at Ply Drops	97
5. CONCLUSIONS AND RECOMMENDATIONS	100
Conclusions	100
Delamination at Ply Drops	100
I-Beam Study	101
Effect of Ply Drops on Lifetime	101
G _c Tests	102
Recommendations	102
REFERENCES CITED	103
APPENDIX A.....	108
APPENDIX B.....	118

LIST OF TABLES

Table	Page
1. Lay-up of fiberglass materials with Ply Drops	22
2. Test matrix	24
3. Comparison of delamination resistance of different ply drop configurations.	42
4. Slenderness ratios calculated using Equation 4	65
5. Comparison of ESH laminate compressive strength with and without ply drops.	66
6. Residual strength of ESH laminate after being fatigued (R=0.1)	69
7. List of I-beams tested with ply drops	72
8. Reference notation for Beams 39, 44 and 48 with ESA Laminate	74
9. Delamination length vs. fatigue cycles for Beam 39	75
10. Average delamination length vs. cycles for compression and tension flanges for Beam 44.	77
11. Delamination length vs. cycles for tension and compressive flanges on Beam 48.	79
12. Reference notation for Beam 40 with ESB laminate	81
13. Reference notation for Beams 41,42 with ESG laminate	83
14. Cycles vs. average tension and compression flange delamination length for beam 41	84
15. Cycles vs. average tension flange delamination for Beam 42.	85
16. Cycles for tension and compression flange delamination on beam 49.	87
17. Reference notation for Beams 49 and 50 with ESH laminate.	88
18. Cycles vs. tension flange delamination length for beam 50.	91

19. Critical strain energy release rate for Mode I and Mode II cracks 97

20. ESA and ESB critical static strength. 97

21. Static strain energy release rates 98

22. Threshold strain energy release rates 99

LIST OF FIGURES

Figure	Page
1. Common structural elements with discontinuities from Ref. 1	2
2. The three modes of fracture from Broek [2]	5
3. Typical load vs actuator displacement for DCB specimen.	7
4. Typical load vs actuator displacement for a ENF specimen.	8
5. Cross-sectional and edge view of ESB laminate showing ply drop.	28
6. Different delamination prevention techniques.	30
7. Lay-up of laminate with ply drops in mold	31
8. DCB and ENF specimens	35
9. Delamination of exterior zero degree ply drop.	38
10. Typical static failure of laminate with ply drop.	38
11. Delamination length vs. cycles for ESA laminate, R = 0.1, Exterior 0° Ply Dropped	39
12. Delamination at an interior ply drop showing two delamination fronts.	39
13. Delamination length vs cycles for ESB (Single interior 0°ply drop) laminate, R=0.1.	40
14. Delamination length vs. cycles for ESC (Single center interior 0°ply drop) laminate, R=0.1.	41
15. Illustration of resin rich region in ESH laminate.	45
16. Delamination length vs. cycles for laminates ESB, ESH, ESF (all interior ply drops) at a maximum running stress of 275 MPa, R=0.1	46

17. Effect of different spacing between ply drops, R=0.1, ESI laminate (Two, 0° ply drops) at 276 MPa, $V_f=0.35$ 47

18. ESI coupons run at 276 MPa, R=0.1. 47

19. Delamination length vs. cycles for ESJ “Z-Spiked” laminate compared to ESA (Single, exterior 0° ply drop) laminate, R= 0.1. 48

20. Delamination length vs. cycles for laminates ESA, ESK, ESG, ESE (all exterior ply drops) at a max. running stress of 138 MPa, R=0.1. 49

21. ESL laminate in tension at the ply drop (Interior 0° ply drop with Hysol adhesive) failed at 276 MPa. 50

22. Delamination length vs. cycles for ESA, JKA "Feathered" and JKA random laminates at a maximum running stress of 207 MPa, R=0.1. 53

23. Delamination initiating along tows which were pulled out. 54

24. Delamination length vs. cycles for ESB and JKB "Feathered" at a maximum running stress of 275 MPa, R=0.1. 54

25. Delamination length vs. cycles at 207 MPa, R=0.1, initial ESA laminate compared to repaired ESA laminate. 55

26. Effect of fiber content on the normalized S-N Data, R=0.1, for DD materials [0/±45/0]s compared to ESH laminate (Two interior 0° Ply drops). 58

27. S-N curve (R=0.1) comparing D155 Fabric (DD6) to A130 Fabric (DD11) control materials with no ply drops, from Reference 50. 60

28. Fatigue life of ESH (Two D155 ply drops) vs. ESQ (Two A130 ply drops) laminates (Maximum stress is on the thin side of the ply drop). 60

29. Tensile fatigue S-N data for ESQ (Two 0° internal ply drops) vs. control DD11 (no ply drops) laminates, A130 unidirectional fabric. 61

30. Damage developing around thermoplastic beads as a result of fatigue loading, R=0.1. 62

31. Photomicrograph of ESH laminate showing resin rich regions ahead of ply drops. 62

32. Side view of crack propagating through ESH laminate	63
33. Tensile fatigue (R=0.1) S-N curves for ESB (Single 0° internal ply drop) and ESH (Two interior 0° ply drops).	63
34. Compressive stress vs. percent strain for ESH 804 coupon.	65
35. I-Beam testing apparatus	71
36. Beam coordinate system	71
37. Beam 39 with ESA laminate for flange material.	76
38. Tension and compression flange on Beam 44.	78
39. Beam 48, ESA laminate, tension and compression flanges.	80
40. Beam 40	82
41. Beam 41	84
42. Beam 42, ESG laminate (Two exterior 0° ply drops) on flanges	86
43. Beam 49 with ESH (Two internal 0° ply drops) flange material.	89
44. Beam 50 with ESH (Two interior 0° ply drops) laminate as flange material.	90
45. Beam (Tension Flange) vs. Coupon Data (R=0.1) for ESA (Single exterior 0° ply drop), R=0.1.	92
46. Beam (tension flange) vs. coupon data for ESH laminate (Two Interior ply drops), R=0.1.	92
47. Mode I coupon geometry.	95
48. Mode II specimen geometry.	96

ABSTRACT

Material thickness variations are required to optimize the design of laminated composite structures. These thickness variations are accomplished by dropping layers of material (plies) along the structure to match the load carrying requirements. Unfortunately, these ply drops produce internal stress concentrations as a consequence of material and geometric discontinuities. This thesis provides a parametric experimental investigation of ply drops in E-Glass stranded fabric reinforced polyester composites and structures. These parameters include: ply drop location, laminate thickness, number of plies dropped at one location, fabric type, loading condition, fiber content, and spacing between ply drops. The damage which develops at ply drops is typically delamination cracks which propagate between the layers of reinforcing fabric.

There were two parts to this study: (1) to examine delamination propagation rates at ply drops and determine crack growth threshold levels, and (2) to determine the effect of ply drops on the lifetime of various composite materials. Tests were conducted on both small coupons of material and beam structural elements with ply drops in the flanges.

A strong sensitivity to ply drop position and manufacturing details is shown for fatigue damage initiation and growth. The results indicate that it will be difficult to completely suppress damage and delamination initiation in service. For 0° plies, single internal ply drops provide the greatest delamination resistance. Multiple ply drops should be spaced at correct intervals so that the delaminations from each do not overlap prior to arrest. It was found that, in most cases, there is a threshold loading under which little growth after initiation is noted. Delamination retardation techniques such as ply edge feathering, "Z-Spiking" and adhesive layers improve the delamination resistance in many cases. After delamination has occurred, especially with exterior ply drops, it can be repaired with adhesives. Ply drops adversely affect fatigue lifetime of low fiber content laminates more severely than for high fiber content laminates. The choice of fabrics used in a laminate can have a significant impact on delamination rates, but the lifetime of the laminate is insensitive to fabric type.

CHAPTER 1

INTRODUCTION

Today's need for stronger, lighter and cheaper structures has generated much interest in materials development, especially in composite materials. Fiber-reinforced composites have played a leading role in the technological advancement of structural material systems. Typically, fiber-reinforced composites are known for being light weight, high strength materials which are more durable than conventional materials. The use of composite materials in structural applications is rapidly increasing for commercial applications. With this increased use comes the need for a better understanding of the performance of the structures fabricated from composite materials, called composite structures. A large portion of composite structures are comprised of layered, laminated composite materials; thickness variations in such laminates are achieved by changing the number of plies in proportion to the thickness change. This requires the termination of layers, or plies, within the laminate, which then introduces a characteristic flaw into the material.

Laminated composites typically are fabricated from planar sheets of material, so that all fibers are oriented in a plane. Careful design and selection of the in-plane fiber

orientation can create a laminate that is designed to carry the loads very efficiently in the plane of the fiber reinforcement. However, an inherent weakness of the laminate is the lack of fiber reinforcement in the direction normal to the fiber orientation. Consequently, the interlaminar direction, normal to the plane of reinforcement, is the weakest direction of the laminated material system. Therefore, any interlaminar loads that are applied to or induced within the structure are of particular concern in terms of structural integrity.

Figure 1, from Ref. 1, illustrates five structural elements used in laminated composite structures that produce interlaminar stresses. These common elements are the free edge, the open hole, the ply drop, and bonded or bolted joints. Free edges are unavoidable in many structures. Open holes are commonly employed to allow access to the internal parts of the structure. When the design calls for a laminate that is tapered in thickness, discontinuous layers or plies are utilized. It is also common to insert

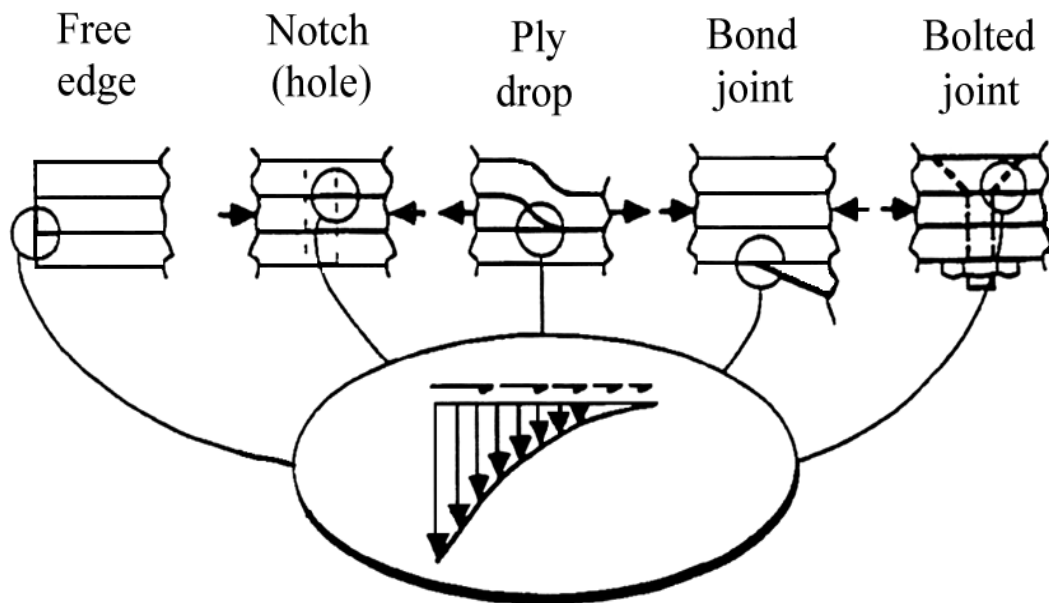


Figure 1. Common structural elements with discontinuities from Ref. 1

discontinuous plies to create a local build-up or thickening at high stress points. Finally, bonded or bolted joints are required to attach multiple sub-components of the structure. Each of the structural elements shown in Figure 1 develop significant out-of- plane normal and shear forces when the component is under load. These interlaminar loads are acting on the plane of minimum strength and toughness of the laminated structure. Therefore, each of these structural elements have the potential to cause a delamination of the individual layers. In addition, most analyses and failure models do not account for these interlaminar loads. The interlaminar performance of these critical structural elements provides a limit to the structural performance of the composite structure. It is important to note that the approach taken in this thesis is also directly applicable to some degree to all of the interlaminar stress risers illustrated in Figure 1.

The approach in this work was to focus on the ply-drop configuration. This is an unavoidable flaw if the thickness is to be tapered, and has received limited attention in the literature with respect to low cost composites of this type under fatigue loading. A parametric experimental study of the influence of various geometric details of ply drops was carried out using laminate coupons, in terms of both the delamination resistance and the reduction in fatigue lifetime. The work is then extended to ply drops in the flanges of larger I-beam structures.

CHAPTER 2

BACKGROUND

This Chapter reviews the basic mechanics of delamination in terms of the strain energy release rate. Several key problem areas associated with thickness transitions in composite laminates are then identified and discussed. Issues in need of an increased research effort are identified.

Strain Energy Release Rate

Once a crack is initiated in a structure it can be further propagated in any of three different modes, or a combination of these. Figure 2 shows the three modes of crack growth. Mode I is an “opening mode” crack, which is caused by normal stresses. In-plane shear causes Mode II or “sliding mode” cracks and Mode III cracks are caused by out-of-plane shear and are known as “tearing mode” cracks [2].

The strain energy release rate, G , is based on the Griffith criterion [2]. Griffith stated that crack propagation will occur if the energy released upon crack growth is sufficient to provide all the energy that is required for crack growth. The Griffith equation can be represented as

$$\frac{dU}{da} = \frac{dW}{da} \quad (1)$$

where U is the elastic strain energy and W the energy required for crack growth. G is equal to dU/da and is sometimes called the crack driving force. The energy consumed during crack propagation is denoted by R , which is equal to dW/da , and is called the crack resistance. Thus, R is equal to the critical strain energy release rate to cause crack extension.

There is a different critical strain energy release rate for each mode of crack growth. A subscript denotes the particular mode. The critical strain energy release rate is

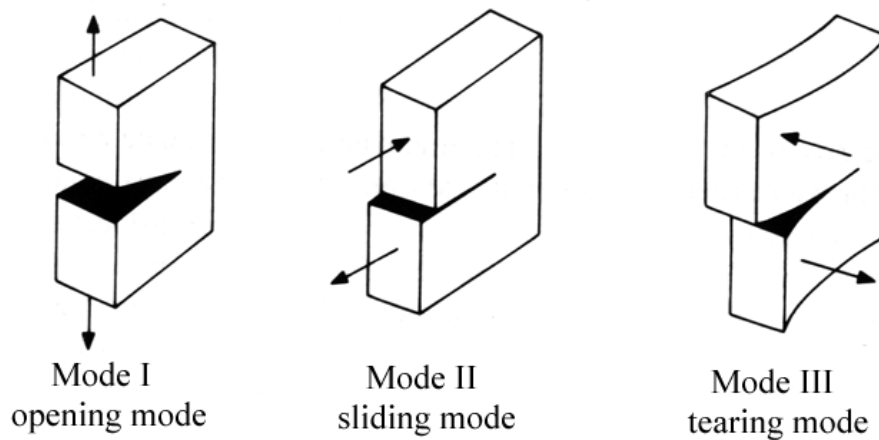


Figure 2. The three modes of fracture from Broek [2].

denoted with a “c” in the subscript following the mode designation. Above this value of G , in simple linear elastic fracture mechanics [2], a crack will propagate unstably in the structure. If there is a mechanism which produces increased crack resistance as the crack

extends, the crack will propagate according to some R-curve behavior, requiring higher G values as crack extension occurs [2].

To determine an opening mode, or Mode I, strain energy release rate for delamination, a double cantilever beam (DCB) specimen is used. The critical strain energy release rate can be obtained by determining the area enclosed by the loading and unloading curves on a load-displacement diagram, which is the incremental change in stored strain energy, U, with crack extension Δa . A typical loading-unloading diagram for a DCB specimen can be seen in Figure 3. Another method to determine G_I values

$$G_{Ic} = \frac{12P_c^2 a^2}{EB^2 h^3} \quad (2)$$

uses an analytic formula (Eq. 2) proposed by Benbow and Roesler [3] and Gilman [4] which takes into account the strain energy generated due to the bending moment of the DCB test, where a is the crack length, E the modulus parallel to the crack direction, B the laminate width, h is the half height and P_c is the critical load. Many G values can be obtained from a single DCB specimen which allows a crack resistance (R) curve to be generated, indicating how (and if) the resistance to crack growth changes with increasing crack length.

To determine Mode II crack growth resistance, it is necessary to use a different test method to determine the corresponding strain energy release rate. End notched flexure (ENF) tests apply a load to the center of the coupon; when the applied load

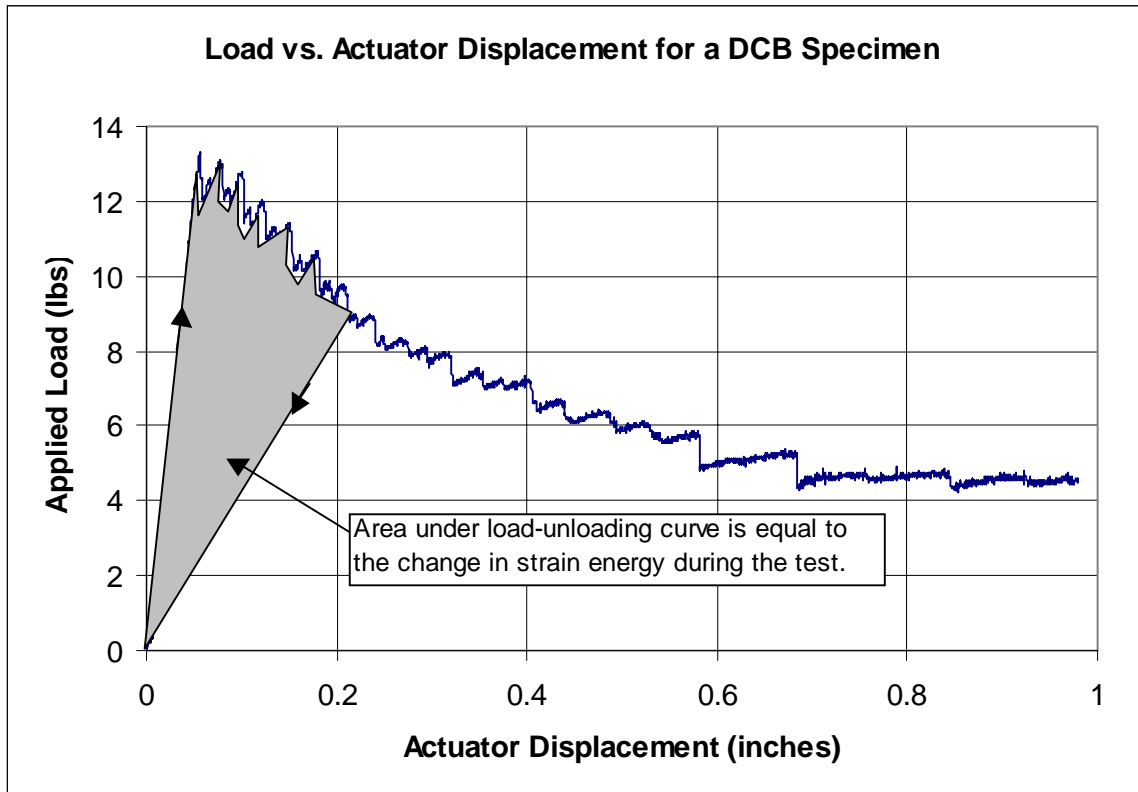


Figure 3. Typical load vs. actuator displacement for DCB specimen.

reaches a critical value, the crack propagates suddenly toward the center where the load is applied. In this type of test, there is only one data point collected as compared with the many points for the DCB specimen due to the instability of crack growth in the ENF specimen. A typical load-actuator displacement graph is shown in Figure 4. Since the load-displacement diagram is unstable for Mode II tests, an analytic formula is necessary to determine a G value. The formula proposed by Russell and Street [5] to calculate G_{IIc} is

$$G_{IIc} = \frac{9P_C^2 a^2}{16E_x w^2 h^3} \quad (2)$$

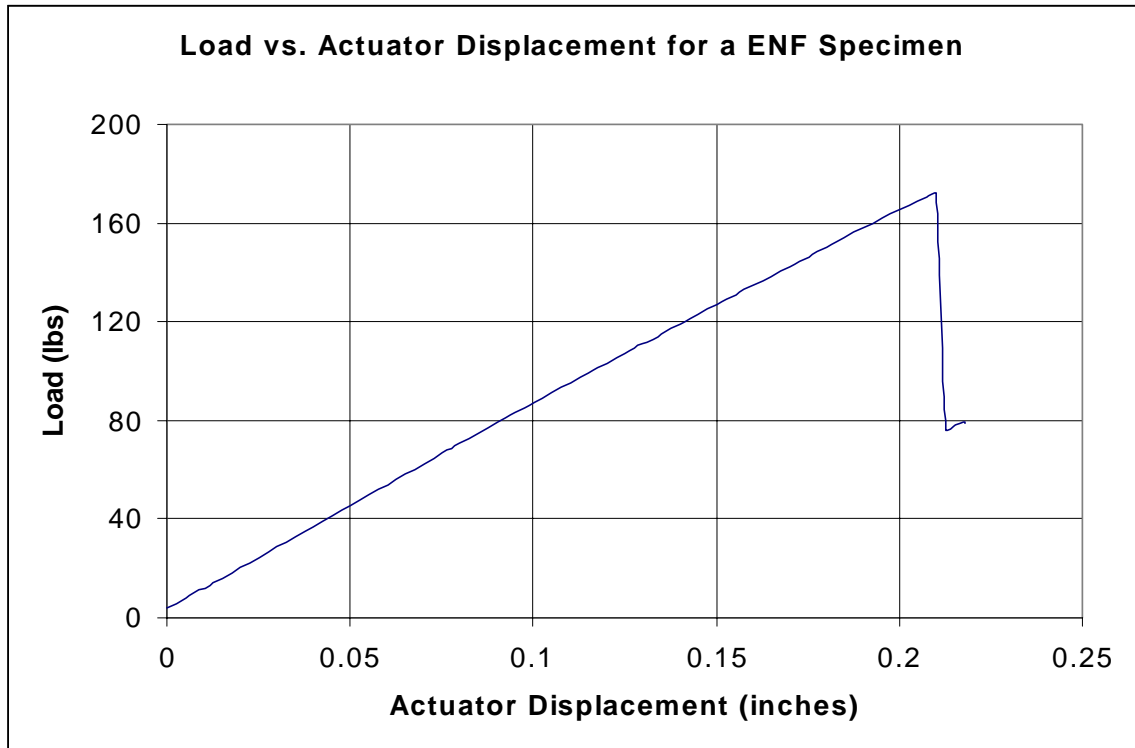


Figure 4. Typical load vs. actuator displacement for a ENF specimen.

Where P_c is the critical applied load, a is the initial crack length, E_x is the modulus in the long direction of the specimen, w is the width of the specimen and h is the half thickness of the specimen.

Tensile Testing of Dropped-Ply Laminates

The DCB and ENF specimens are used to induce crack growth in pure Mode I and II, respectively. Ply drops do not cause a pure mode of crack growth, but generally display a combination of at least Modes I and II, as discussed later. Lagace and Cannon [6] conducted an experimental program investigating the influence of discontinuous internal plies on the tensile response of graphite/epoxy laminates. The fiber orientation was chosen to minimize the occurrence of the edge delamination failure mode. For the

configurations investigated, little change in the global stress-strain behavior and ultimate load carrying capability were observed relative to similar constant thickness laminates. The work illustrated an effect due to the placement of multiple ply drop-offs. When discontinuous plies were distributed along the specimen length, the laminate failed similar to a laminate without ply drops. However, when multiple plies were dropped at one position in the laminate, a delamination failure resulted. It was suggested that the apparent penalty in the in-plane response may be more severe for compression loading.

Wisnom [7] looked at the size effect of coupons on delamination rate. Larger size coupons showed a decreasing delamination rate. Also, when the number of plies dropped in one location was increased, there was a significant increase in the rate of delamination.

The effect of the fiber content on ply drop effect has not received much attention. The apparent reason for this lack of research is that the majority of work has been centered around the use of pre-preg laminates which generally have ply thicknesses of less than 0.2 mm, with fiber volume contents ranging narrowly in the fifty to sixty percent range. The fiberglass laminates being studied for use in this project ranged in fiber content from the low thirties to the mid-fifty percent range. Mandell, et al. [8] showed that the tensile fatigue resistance decreases with increasing fiber content. The cause of this is postulated as due to the decreased amount of resin between plies which acts as a buffer to reduce stress concentrations resulting from matrix cracks in adjacent layers.

Compression Testing of Ply Drop Laminates

Grimes and Dusablon [9] investigated the static and fatigue compression behavior of graphite/epoxy composites with internal ply drop-offs subjected to severe operating

environments. A $[\pm 45/0/90]_s$ family laminate with up to four dropped plies was tested. The static strength and stiffness were insignificantly affected by the discontinuities. However, the endurance limit was decreased by up to 30 percent depending on the orientation of the discontinuous layers.

Curry, et. al. [28] noted that dropped plies can cause a significant reduction in compressive strength. Also, the greater the change in axial stiffness between the thick and thin sections, the greater the reduction in strength. The reduction in compressive strength is much greater than the reduction in tensile strength.

Damage Accumulation

Ulman et al. [10] conducted an extensive experimental program with graphite/epoxy laminates with single ply drops. Damage initiation and growth from both open holes and ply terminations were evaluated during both static testing and constant amplitude fatigue testing of a $[0/\pm 45/90]$ family laminate. The results indicated that although the loading mode greatly influenced the damage development process, interfacial delamination was present in both static and fatigue loading before ultimate failure. Tapered specimens were shown to be dominated by the ply drop. Under tensile loads, the damage progressed from matrix cracking in the resin-rich zone, to transverse cracks at the ply termination. Continued loading induced delamination which increased in size until final failure. In fatigue loading, the damage development was similar, but, delamination growth dominated the last 75 percent of the structural life. A similar fracture response was illustrated for compression loading; however, the process occurred much more rapidly.

Reifsnider [11] showed that the residual (remaining) strength of typical composites does not deteriorate from the static value until a few hundred cycles before failure. This was because the accumulated damage in fatigue samples was similar in type and amount to that in quasi-static tests near failure.

Stress Analysis of Ply Drop Laminates

A numerical study of a 30-ply carbon fiber laminate containing two zero degree dropped plies at different locations through the thickness was performed by Adams, et al. [12]. A three-dimensional finite element analysis incorporating nonlinear orthotropic lamina properties was conducted to assess the effect of compressive load, moisture and temperature. Although the residual thermal stresses resulting from post cure cooling were found to be significant, the interlaminar stresses were negligible compared to the in-plane stresses. It was concluded that the dropped plies have little effect on the in-plane stresses.

Kemp and Johnson [24] presented a failure analysis of an eight-ply quasi-isotropic graphite/epoxy laminate containing up to three dropped zero degree plies, in a single drop step. The finite element method was applied to determine the resulting three-dimensional state of stress. Interlaminar stresses were found to be significant at the location of the dropped plies. In-plane failure loads were calculated based on both resin failure near the dropped plies and intralaminar failure in tension and compression. A maximum principal stress criterion was applied to predict resin failure and the Tsai-Wu criterion was applied to predict intralaminar failure. The analysis predicted initial failure to occur in the resin. No experimental data was generated to correlate with the numerical results.

Curry et al. [28] studied sixteen-ply graphite/epoxy laminates, containing four plies terminated at the mid-plane. A stress based failure theory was applied to predict the axial compressive strength. The results were shown to under estimate experimentally determined failure loads by 33 percent. Experimental results indicated that both the tensile and compressive strength are reduced by the presence of a thickness discontinuity. However, the reduction was larger for compressive loading. In addition, the reduction in strength was shown to be inversely related to the increase in axial stiffness of the thick section relative to the thin section.

Fish and Lee investigated the tensile strength of tapered glass/epoxy laminates with multiple internal ply drops [13]. A three-dimensional finite element analysis was conducted and the average stress concept was applied to predict the initiation of failure. Strength predictions, based on the stress in the inter-ply resin layers and an averaging distance of one ply thickness, were found to correlate with the experimentally observed delamination failure. However, the predictions were valid only for delamination initiation and not delamination growth. Laminates both with and without significant edge effects were tested. The failure mode for those with negligible free edge effects was an unstable delamination growth across the width of the laminate, followed by stable delamination growth in the axial direction. One of the tapered laminates showed an increase in strength while the other showed a decrease. Alternatively, laminates containing 90° plies showed a significant free edge effect. The corresponding failure mode was a combination of free edge delamination and delamination growth in the axial direction [14].

A similar analysis for laminates with external ply drop-offs was conducted by Wu and Webber [15]. A two-dimensional finite element analysis was performed.

Interlaminar peel and shear stresses were found to peak in the corner regions of the external steps. The failure of the laminates in delamination was attributed to these peak stresses.

Unidirectional glass/epoxy and graphite/epoxy laminates with internal drop-offs were studied by Hoa et al. [16]. Under tensile loading, the laminates failed in delamination at load levels well below the in-plane strength. Stress and strain variations within the taper were obtained using a three-dimensional finite element model employing a quadratic displacement based element. An acoustic emission was found to correspond to the initiation of delamination while no change in the stress-strain response was observed. Reasonable correlation between experimental and numerical results was reported when the interlaminar stresses were compared to the interlaminar strength of the material.

Delamination Prevention

Another type of ply drop occurs in laminates with discontinuous interlaminar layers in the use of buffer strips [17,18]. A buffer strip is added or constructed by either discontinuing specific fiber layers of a laminate, usually the stiff zero degree plies, or inserting additional plies of lower longitudinal modulus. The objective is to create discrete region of increased local compliance within the component. The result is a superior construction in terms of damage tolerance. As damage in the main laminate grows, it can be arrested and controlled by the more compliant buffer strips. Such a

construction has been shown to reduce the sensitivity of composite structures to inherent damage and to increase the lifetime of the component [19].

Another method currently being used is called “Z- Spiking”. Aztex Co. (Waltham, Mass.) uses fibers positioned in foam which is then vacuum pressed into the laminate to reinforce laminates in the thickness direction. This reinforcement is especially useful for bonded joints, where the strength of the joint is matrix dominated. Aztex [20] reports a minimal decrease in the in-plane properties and a 30-fold increase in interlaminar fracture toughness. Tanzawa [21] showed that although the z reinforcing fiber content was approximately 0.6%, the normally brittle carbon fiber/epoxy plates had the same critical strain energy release rate as carbon fiber/PEEK plates. By increasing the critical strain energy release rate, the structure becomes more delamination resistant without having to increase the cost by using the more expensive PEEK thermoplastic matrix.

Chan [22] used narrow, tough thermoplastic interlayers to prevent coupon edge delamination. In another study, Masters [23] used an entire layer of adhesive to improve the impact toughness of composites. These interlayers provided a tough region where propagating cracks could be arrested before growing long enough to cause a catastrophic failure in the component.

Existence of a Resin Rich Region

It has been shown that during processing of a variable thickness laminate, a pure resin region develops at the end of the discontinued plies. Therefore it is the resin flow from surrounding layers during processing that creates this neat resin zone. After the

resin fills the mold, porosity can become entrapped in the resin in this area creating stress concentrations which can initiate delamination. The volume and dimensions of this region are clearly a function of the number of discontinuous layers at a given location and the orientation of the surrounding layers. The existence of this neat resin region has been observed in several works [24-28]. A common method employed to account for this micro structural detail is to inspect actual laminates with photo microscopy. Although this identifies the size and shape of the neat resin zone, there has been little effort to address the change in fiber volume content near a discontinuous layer. Chan and Ochoa [26] did attempt to account for the change in ply properties that occur local to the discontinuous plies.

Design Considerations

In metallic structures, damage tolerance technology has been used effectively to characterize crack growth under cyclic loading for a material, predict the rate of crack growth in the structure under service loads, and establish inspection intervals and nondestructive test procedures to ensure operational safety [29]. Because composite delamination represents the most commonly observed macroscopic damage mechanism in laminated composite structures, many efforts have been undertaken to develop similar procedures for composite materials by characterizing delamination growth using fracture mechanics [30-33]. Although this approach is promising, there are some fundamental differences in the way fracture mechanics characterization of delamination in composites may be used to demonstrate fail safe designs compared with the classical damage tolerance treatment used for metals.

Many papers have been published recently where the rate of delamination growth rate with fatigue cycles has been expressed as a power law relationship in terms of the strain energy release rate, G , associated with delamination growth [1-4]. This fracture mechanics characterization of delamination growth in composites is analogous to that of fatigue crack growth in metallic structures, where the rate of crack growth with cycles is correlated with the stress intensity factor at the crack tip. However, delamination growth in composites, with a relatively high crack growth exponent, may change too rapidly over too small a range of load, and G , to be incorporated into a classical damage tolerance analysis for fail safe designs [2,34,35]. Where in metals the range of fatigue crack growth may be described over as much as two orders of magnitude in G , the growth rate for a delamination in a composite is often characterized over less than one order of magnitude in G . Hence, small uncertainties in applied loads may yield large (order of magnitude) changes in delamination growth. Different damage mechanisms may also interact with the delamination and increase the resistance to delamination growth. Delamination growth resistance curves may be generated to characterize the retardation in delamination growth from other mechanisms [36,37,38]. This delamination resistance curve is analogous to the R-curves generated for ductile metals that account for stable crack growth resulting from extensive plasticity at the crack tip. However, unlike crack tip plasticity, composite damage mechanisms such as fiber bridging and matrix cracking, may not always be present to the same degree.

One alternative to using the classical damage tolerance approach for composites would be to use a strain energy release rate threshold, below which no delamination

growth occurs, and design to stress levels below this threshold. Metals are macroscopically homogeneous, and the initial stress conditions that create cracks at particular locations in preferred directions cannot be easily identified beforehand. Composites, however, are macroscopically heterogeneous, with stiffness discontinuities that give rise to stress risers at known locations such as free edges, internal ply drops, and matrix cracks. Although these stress fields are not the classical variety observed at crack tips, and hence cannot be characterized with a single common stress intensity factor, they can be characterized in terms of the strain energy release rate, G , associated with eventual delamination growth [4].

The most common technique for characterizing delamination onset in fatigue for composite materials is to run cyclic fatigue tests on standard composite specimens, where G for delamination growth is known, at maximum load or strain levels below that required to propagate a delamination monotonically. A strain energy release rate threshold for delamination onset may be developed by running tests at several maximum cyclic load levels and plotting the cycles to delamination onset versus the maximum cyclic G , corresponding to the maximum cyclic load or strain applied[39-43]. This G curve may then be used to determine a threshold value of G for delamination and to predict delamination onset in other laminates of the same material, or at other points [44].

Uncertainty inherent in predicting service loads has generated concern for using a no-growth threshold design criterion for high cycle fatigue applications. If G values exceed no-growth threshold levels, a catastrophic delamination propagation may occur. O'Brien [45] outlines a damage threshold/fail-safety approach for composite fatigue

analysis that involves the following steps:

- 1.) Predict the delamination onset thresholds using fracture mechanics.
- 2.) Assume that surpassing the delamination threshold corresponds to complete propagation.
- 3.) Determine the remaining load carrying capability of the composite with delamination present using composite mechanics (i.e., check for fail-safety).
- 4.) Iterate on Steps 1 to 3 to account for multiple sources of delamination.

Step 1 may be used to demonstrate the delamination durability of any composite structure. Step 2 reflects a way to deal with relatively high exponent delamination growth observed for composites as compared to metals. An alternative would be to predict the delamination growth rate using growth laws that incorporate R-Curve characterization, thereby taking into account the resistance provided by other damage mechanisms. Finally, Step 3 acknowledges that the residual strength of the composite is a function of structural variables, and it is not uniquely a question of material characterization. This proposed damage-threshold /fail-safety concept incorporates generic material properties of fracture mechanics and also takes into consideration the unique characteristics of laminated composites.

Motivation for Thesis

Previous research has focused on graphite/epoxy [6] or pre-impregnated E-glass and S-glass [7] laminates containing ply drops. Graphite/epoxy laminates have better fatigue resistance than do glass fiber composites [7]. The pre-impregnated composites usually have thinner plies than do typical laminates of the type used in this study, which

may minimize ply drop effects. To achieve efficient designs, wind turbine blades require severe thickness tapering to reduce the overall weight. Blades are also subjected to very high cycle fatigue loading, which can lead to delaminations over a period of many years. This, along with an absence of adequate data on the effects of ply drops in laminates using the E-glass stranded fabrics typical of blade and other low cost composite applications, gives motivation for this thesis.

CHAPTER 3

EXPERIMENTAL METHODS AND MATERIALS

Test matrix and description of specimens

This section provides a brief overview of the different cases tested. Table 1 gives the lay-up of each case as well as other comments. Table 2 gives the test matrix used to determine the properties of the laminates listed in Table 1, including the number of coupons tested at each stress level, and the loading conditions (tension or compression). In the following paragraphs, plies which are terminated (near mid-length of the coupon) are shown with asterisks. As described later, all laminates were resin transfer molded using stitched or woven fabric reinforcement.

The laminates were based on the DD set of laminates, which exhibited the best fatigue performance of the laminates previously tested [47]. Selected cases of ply drops, both interior and exterior (on the surface), were introduced into laminates. After initial delamination studies with single ply drops were completed, multiple ply drops at the same location, as well as spaced along the length, were also studied. Attempts to suppress delamination with the addition of adhesives, feathering and “Z-Spiking” were then studied. All of these attempts investigated dropping 0° plies. The effect of dropping single and multiple $\pm 45^\circ$ layers was then studied. In addition, A130 woven fabric for the

zero degree layers was also substituted for the standard D155 fabric used in the DD family of laminates.

The ESA laminate included a single exterior zero degree ply drop. The actual configuration of the laminate is $[0^*/0/\pm 45/0/0/\pm 45/0]$, where the angle given is relative to the applied load direction. Ply configurations follow standard laminate notation [46]. The ESB laminate has the configuration $[0/0^*/\pm 45/0/0/\pm 45/0]$, while the ESC laminate has the configuration $[0/\pm 45/0/0^*/0/\pm 45/0]$, with a central ply being terminated. In terms of percentages, the ESA, ESB and ESC laminates have a 14% drop in thickness, with 20% of the zero degree layers being dropped. The ESD laminate has two internal plies being dropped with the laminate configuration $[0/\pm 45/0^*/0^*/\pm 45/0]$. This is a 33% drop in the total thickness, with 50% of the zero degree layers being dropped. Figure 5 shows an actual polished cross-section through an ESB coupon prior to testing. The edge of the ply drop is somewhat smeared during molding, with a resin rich area ahead of the drop. The thickness taper coincides with the ply drop as closely as possible, to give an approximately constant fiber content along the length.

In the next set of laminates thicker materials were used to investigate less severe thickness tapering. The ESE laminate had the configuration $[0^*/(0/\pm 45/0)_3]$, while the ESF laminate incorporated a single internal ply drop into the thicker laminate $[0/0^*/\pm 45/0/0/\pm 45/0/0/\pm 45/0]$. In each of these laminates the thickness was tapered 10%, while the percentage of zeros being dropped was 15%. The ESG and ESH laminates both

Table 1. Lay-up of fiberglass materials with ply drops

Lay up of Fiberglass Materials with Ply Drops		
Laminate	Ply Configuration	Description
ESA	$[0^*/(0/\pm 45/0)_s]$	Single Exterior Ply Drop
ESB	$[0/0^*/\pm 45/0/0/\pm 45/0]$	Single Interior Ply Drop
ESC	$[0/\pm 45/0/0^*/0/\pm 45/0]$	Single Center Ply Drop
ESD	$[0/\pm 45/0^*/0^*/\pm 45/0]$	Double Central Ply Drop
ESE	$[0^*/(0/\pm 45/0)_3]$	Single Exterior Ply Drop, with thicker laminate
ESF	$[0/0^*/\pm 45/0/(0/\pm 45/0)_2]$	Single Interior Ply Drop with thicker laminate
ESG	$[0^*/0^*/(0/\pm 45/0)_3]$	Two exterior ply drops with thicker laminate
ESH	$[0/0^*/0^*/\pm 45/0/(0/\pm 45/0)_2]$	Two interior ply drops with thicker laminate
ESI	$[0/0^*/0^*/\pm 45/0/0/\pm 45/0]$	Two interior ply drops with different spacing between the ply drops.
ESJ	$[0^*/(0/\pm 45/0)_s]$	“Z-Spiking” of a single exterior ply drop.
ESK	$[0^*/(0/\pm 45/0)_s]$	Single exterior ply drop, Hysol EA9309.2NA adhesive applied to ply drop before polyester resin was put in the mold.
ESL	$[0/0^*/\pm 45/0/0/\pm 45/0]$	Single interior ply drop, Hysol EA9309.2NA adhesive applied to ply drop before polyester resin was put in the mold.
ESM	$[0/0^*/\pm 45/0/0/\pm 45/0]$	Attempted “Z-Spiking” with an interior ply drop. The zero degree ply being dropped was slipped through a cut ± 45 layer.
ESN	$[0^{**}/\pm 45/0/0/\pm 45/0]$	Outside zero degree layer used as a butt-joint.
ESO	$[0/\pm 45^{**}/0/0/\pm 45/0]$	Inside $\pm 45^\circ$ degree layer contains a butt-joint.
ESP	$[0/\pm 45^*/\pm 45^*/\pm 45/0/(0/\pm 45/0)_2]$	Two interior $\pm 45^\circ$ layers being dropped.
ESQ	$[0/0^*/0^*/\pm 45/0/(0/\pm 45/0)_2]$	Two interior ply drops with thicker laminate A130 fabric instead of D155 fabric
ESR	$[0/\pm 45/0/\pm 45^*/\pm 45^*/0/\pm 45/0]$	Two interior ± 45 ply drops at the centerline
Lay up of Fiberglass Materials with Ply Drops		
Laminate	Ply Configuration	Description
JKA “Feathered”	$[0^*/(0/\pm 45/0)_s]$	Alternating tows were pulled one half inch past the adjacent tows in the ply drop layer.
JKA Random	$[0^*/(0/\pm 45/0)_s]$	Random mat laid down underneath the ply drop
JKB “Feathered”	$[0/0^*/\pm 45/0/0/\pm 45/0]$	Alternating tows were pulled one half inch past the adjacent tows in the ply drop layer.
<p>* Ply being terminated ** Ply contains a butt-joint oriented at 90° to the load direction. The subscript s denotes a symmetrical lay-up about the location of s, while the notation ()_n indicates that the lay-up in () is repeated n times [46].</p>		

Table 2. Test matrix

Laminate Configuration	Tension Coupons (R=0.1)*		Compression Coupons (R=10)*	
	Maximum. Stress (MPa)	# of Tests	Minimum Stress (MPa)	# of Tests
ESA	Static	6	-207	2
	207	3	-138	2
	138	3	-----	
ESB	Static	4		
	345	2		
	310	3		
	276	5		
ESC	Static	2		
	345	3		
	276	3		
ESD	Static	1		
	138	1		
ESE	Static	2		
	207	2		
	138	2		
	121	1		
ESF	345	1		
	276	4		
	207	1		
ESG	Static	1		
	345	1		
	207	1		
	138	2		
	103	1		

Laminate Configuration	Tension Coupons (R=0.1)*		Compression Coupons (R=10)*	
	Maximum. Stress (MPa)	# of Tests	Minimum Stress (MPa)	# of Tests
ESH	Static	8	-276	3
	454	1	-207	2
	414	5	-----	
	345	3		
	276	7		
	207	6		
ESI1	310	1		
	276	3		
ESI2	310	2		
	276	3		
	246	1		
ESI3	276	3		
	241	2		
	207	1		
ESI4	310	1		
	276	4		
	241	1		
ESJ	276	1		
	207	3		
ESK	276	1		
	207	2		
	138	1		
ESL	276	2		
	241	2		

Laminate Configuration	Tension Coupons (R=0.1)*		Compression Coupons (R=10)*	
	Maximum. Stress (MPa)	# of Tests	Minimum Stress (MPa)	# of Tests
ESM	276	1	-----	
ESN	276	1		
	172	1		
	138	1		
	103	2		
ESO	345	1		
	310	2		
	276	3		
ESL	Static	3		
	552	2		
	414	3		
	276	3		
	207	1		
ESR	276	2		
	241	2		
JKA "Feathered"	276	3		
JKA Random	276	3		
JKB "Feathered"	276	3		

* R = minimum load/maximum load

included more than one ply drop at the same position. ESG had two exterior zero degree layers dropped while the ESH laminate had two interior plies dropped. The laminate

configurations were $[0^*/0^*/(0/\pm 45/0)_3]$ for the ESG laminate and $[0/0^*/0^*/\pm 45/0/0/\pm 45/0/0/\pm 45/0]$ for the ESH laminate. In both of these laminates the thickness was tapered 18% , while the percentage of zero degree layers being dropped was 25 percent.

The ESI laminate contained multiple single ply drops with each ply drop separated by multiples of 13 mm spans. For example, the ESI2 had a 25 mm spacing between ply drops, while the ESI3 laminate had a 38 mm spacing in between ply drops. The laminate lay-up, $[0/0^*/0^*/\pm 45/0/0/\pm 45/0]$, had a 25% thickness taper while the percent of zeros being dropped was 33%.

ESJ and ESK used special details shown in Figure 7 in an attempt to increase delamination resistance. The ESJ laminate used “Z-Spiking” [47], to provide a thickness reinforcement. This was accomplished by interlacing the exterior zero degree ply drop with a continuous zero degree layer. This helped to prevent the surface ply drop from peeling away when the coupon was loaded. The ESK laminate also was an exterior ply drop; to prevent delamination, a tough epoxy adhesive, Hysol EA 9309.2NA, was applied to the ply drop zero degree layer and the first continuous layer and then allowed to cure before the resin was introduced into the mold. The fabric lay-up for both the ESJ and ESK laminates was the same as for the ESA laminate, $[0^*/0/\pm 45/0/0/\pm 45/0]$. The ESL and ESM laminates considered delamination prevention for internal ply drops. The ESL laminate used the same Hysol adhesive as the ESK laminate. Again the adhesive was applied both underneath and above the ply drop and allowed to cure before the resin was introduced into the fabric. The ESM laminate represents an attempt to “Z-Spike” an

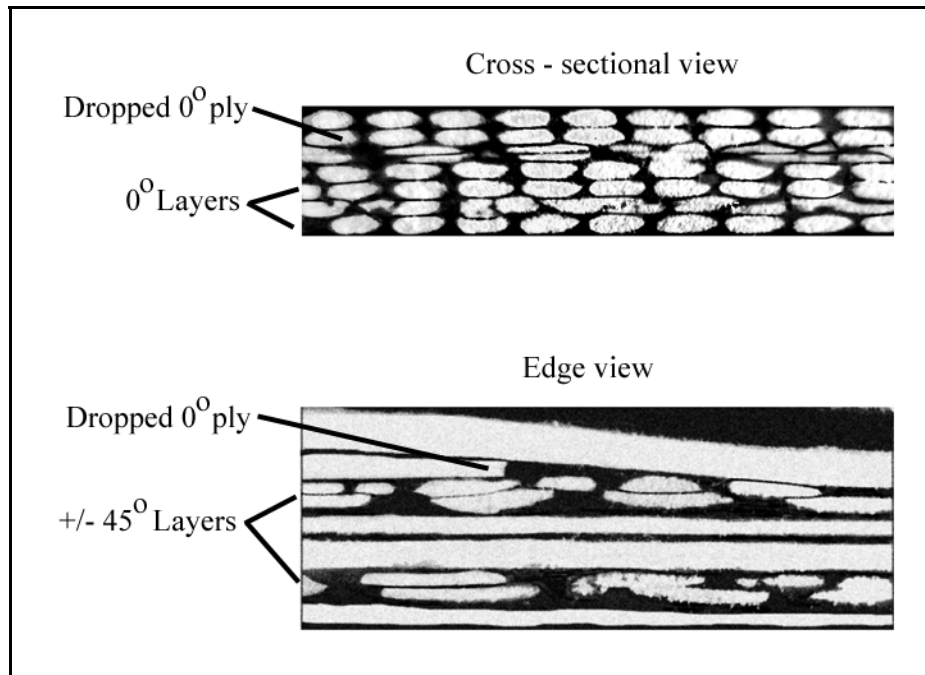


Figure 5. Cross-sectional and edge view of ESB laminate showing ply drop.

internal ply drop. This was accomplished by cutting the $\pm 45^\circ$ degree layer underneath the ply drop and pushing the layer being terminated through the $\pm 45^\circ$ layer. Both of these laminates used the same lay-up as the ESB laminate, $[0/0^*/\pm 45/0/0/\pm 45/0]$.

The ESN and ESO laminates incorporated butt-joints in plies. In order to use some glass fabrics which are only available as weft unidirectionals, butt-joints are necessary. In both the ESN and ESO laminate there are no dropped plies, but the butt joints cause a stress discontinuity similar to the effect caused by ply drops. The ESN laminate had an exterior zero degree layer as the butt joint, while the ESO laminate had an interior $\pm 45^\circ$ layer as the butt-joint. The actual lay-up in the ESN and ESO laminates was $[0/\pm 45/0]_s$.

. The ESP laminate had the lay-up, $[0/\pm 45^*/\pm 45^*/\pm 45/0/(0/\pm 45/0)_2]$, to evaluate the

effect of dropping $\pm 45^\circ$ layers. In this laminate the thickness was tapered 18%, with no zero degree layers being dropped. The ESQ laminate had the same lay-up as the ESH laminate, two interior zero degree ply drops, but the fabric being used for the zero layers was the warp unidirectional woven A130. The last laminate is ESR, which had the lay-up $[0/\pm 45/0/\pm 45^*/\pm 45^*/0/\pm 45/0]$. This looked at the effect of dropping multiple $\pm 45^\circ$ layers in a thinner laminate. No zero degree layers were dropped, and the thickness was tapered 25%.

Additional coupons investigated the possibility of suppressing delamination by adding to or tailoring the laminate properties. The first configuration used the ESA laminate as a basis for comparison, and a second configuration used the ESB laminate as a basis. For the JKA coupons, random mat fabric was included between the ply drop and the first continuous zero layer. Random mat was not used in the internal ply configuration case. A second modification is called “feathering.” In this case, alternating tows were pulled one half inch past the adjacent tows to provide a less defined delamination site. This modification along with “Z-Spiking” can be seen in Figure 6.

Material Preparation

The various E-glass/polyester materials used in this thesis were all manufactured by RTM (Resin Transfer Molding), which consisted of a peristaltic pump forcing the resin into a closed, vented mold containing the reinforcing layers[48]. To incorporate ply drops into the manufacturing process, the following procedure was used to prepare the mold. First the mold was coated with a mold release (Frekote 700- NC), air dried, then the individual fabric layers were placed in the mold. The lay-up of a laminate with ply

drops is shown in Figure 7. Ply drop layers (4) were cut to shorter lengths and placed in the desired position along with the continuous layers (3). Fluoro-Peel release film (2) was added to the laminate to accomplish the thickness reduction in the desired area, with

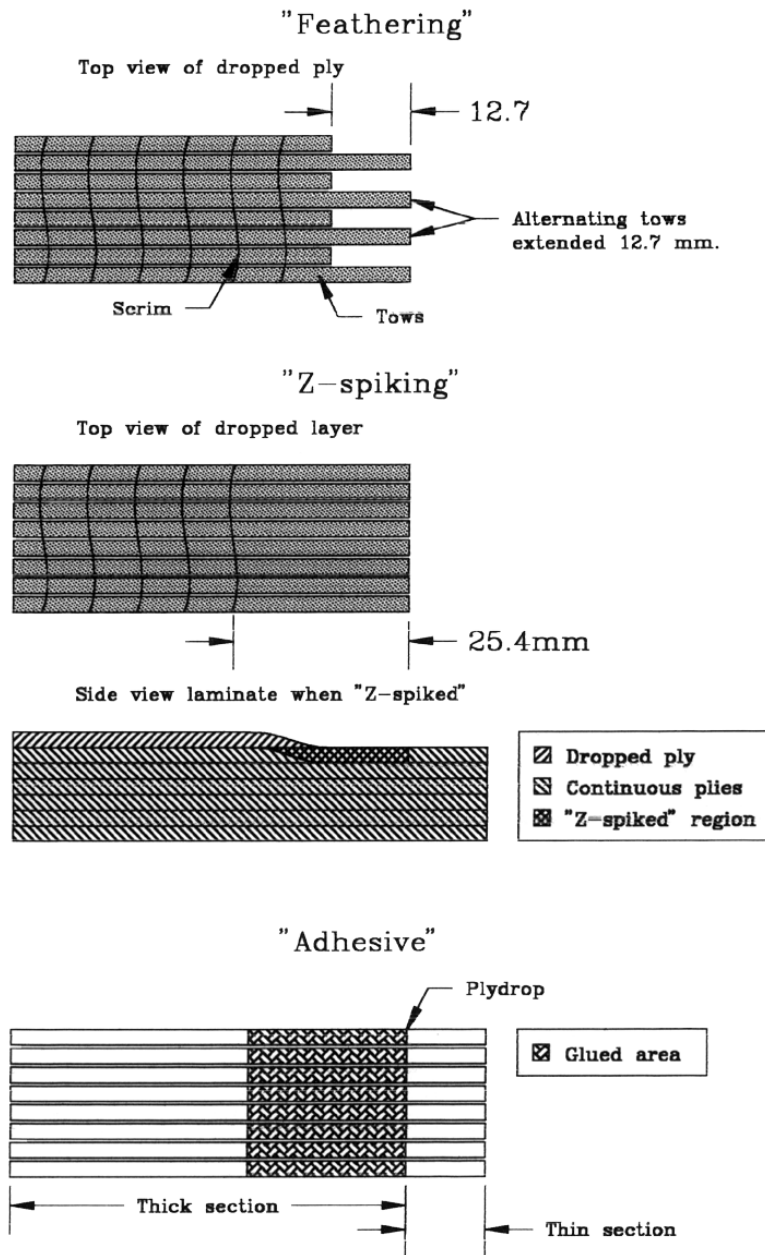


Figure 6. Different delamination prevention techniques.

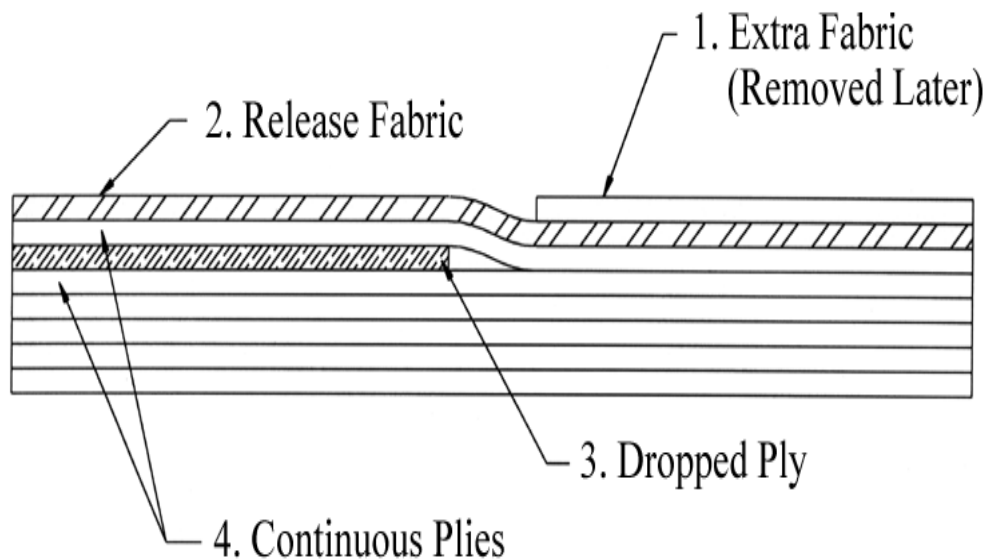


Figure 7. Lay-up of laminate with ply drops in mold

fabric layers (1) added over the release film so that the fiber content was the same in the thin and thick sections. When the resin was injected into the mold, the porosity of the sample was low (<1%), except for the resin rich region in front of a ply drop which was often observed to have some localized higher porosity.

Fabrics

The E-glass fabrics used in these experiments were from Owens-Corning Fabrics (formerly Knytex). Three different types of fabric were used in these experiments. Wind turbine blades, because they are long and thin need to use a high percentage of continuous warp unidirectional fabric oriented with fibers in the length (0°) direction to give them stiffness. They also usually incorporate $\pm 45^\circ$ fabrics to control twisting. Unidirectional fabrics, from Owens-Corning, are available in either the warp or the weft direction. Warp fabric means that the individual tows of glass fibers are oriented parallel to the long

direction of the fabric when it is rolled up; conversely, weft fabrics have the unidirectional tows oriented so they are perpendicular to the length of the roll, which is generally only 1.3 meters wide. D155 fabric is a unidirectional fabric which weighs approximately 526 grams/ m². The D155 fabric is available in the weft direction only, and while the properties are good, the current manufacturing lengths makes it unsuitable for structures longer than 1.3 meters. The second type of unidirectional fabric used in this thesis is A130. This fabric is a woven warp unidirectional fabric which has good tensile properties, but because of the curves introduced from large thermoplastic beads connecting the tows, creating the weave, the compressive properties are significantly less than the D155 properties [49]. Finally the $\pm 45^\circ$ fabric layers involve the DB120 fabric, the DB representing double bias fabric of 407 grams/m².

The resin used in these experiments was CoRezyne 63-AX-051, an unsaturated orthophthalic polyester, manufactured by Interplastic Corporation. This resin was combined with methyl ethyl ketone peroxide (MEKP), 2% by volume, to catalyze the cross-linking reaction. Curing of the materials was at ambient conditions, followed by two hours at 60°C

Specimen Preparation

After the plates had been left to cure for at least five hours, they were removed from the mold. The edges were trimmed off to eliminate any edge anomalies. All specimens were cut using a water-cooled diamond saw. The coupon edges were then polished in sequential steps down to 400 grit emery paper from Buehler. This helps to suppress, but not eliminate, edge generated delamination. For coupons run to more than

10^5 cycles, fiberglass tabs were bonded onto the ends with Hysol EA 9309.2NA adhesive. The coupons were then post-cured a second time at 60 °C for two hours. Tensile coupons were 20 cm long by 2.5 cm wide with a gage section of 13 cm. Compressive coupons were 10 cm long by 2.5 cm wide with a gage section of 5 cm.

All coupons were tested for the fiber content using a matrix burn-off method described under ASTM D 2584. The only deviation from the ASTM standard was in the amount of material used in the burn off test, 15 to 20 grams rather than the prescribed 5 grams.

Test Facility and Development

All of the coupons were tested using an Instron 8501 servo-hydraulic machine. This machine allowed maximum and minimum peak loadings to be accurately maintained while varying the loading wave forms and counting the number of cycles applied to the specimen. The specimens were clamped into the Instron using hydraulic grips. The amount of pressure used to clamp the specimens was varied according to the maximum stress experienced by the specimen, to prevent coupon crushing. If, during the course of the test, the grip hydraulic pressure gauges fluctuated, which could indicate sample slipping, the test would be stopped and additional pressure would be added to the grips. This method was used to avoid over-clamping the specimens and causing excessive gripping or tab failures.

An extensometer (Instron 2620-525) was used to determine strains for calculation of the initial modulus. The extensometer was attached to the edge of the coupon via rubber bands. In all cases the initial longitudinal elastic modulus, E_x , was

measured on the thin section of the coupon by taking a least squares fit of at least five equally spaced load intervals. The modulus of the thin section then provided a basis for calculating the maximum running strain for a given stress.

A minimum of three static tests were performed to obtain an accurate ultimate tensile strength for each laminate. These static tests were performed under displacement control, with a displacement rate of 12.7 mm/sec. Fatigue tests used a sine-wave cyclic waveform with the testing machine in load control. The first coupons were set to run at a maximum stress of approximately 60% of the ultimate stress, with a minimum stress of 10% of the maximum stress, giving an R value of 0.1 ($R = \text{minimum stress} / \text{maximum stress}$). After these coupons failed, a best fit line through the two points was used to predict the approximate lifetime of coupons being run at different stress levels. All test coupons were run at frequencies where the coupon temperature did not rise more than 5 °C above room temperature. A fan was placed approximately one meter away to provide additional cooling of the coupons. Fatigue tests were either performed until failure, which was defined as the inability of the coupons to carry the maximum load, or until delamination at the ply drop extended along the entire length of the coupon and into the grips.

DCB and ENF test specimens

These experiments were run to characterize the pure Mode I and Mode II delamination resistance, G_{Ic} and G_{IIc} . These lay-ups were $[0]_{10}$, $[(0)_5/\pm 45/(0)_4]$, and $[\pm 45]_{10}$. Figure 8 shows typical DCB and ENF specimens. The main requirement for double cantilever beam (DCB) specimens is to ensure that delamination propagates along the mid-plane. This was accomplished by inserting a 25 mm wide piece of Fluoro-Peel release fabric between the layers of interest to form the starter crack. Once the mold had

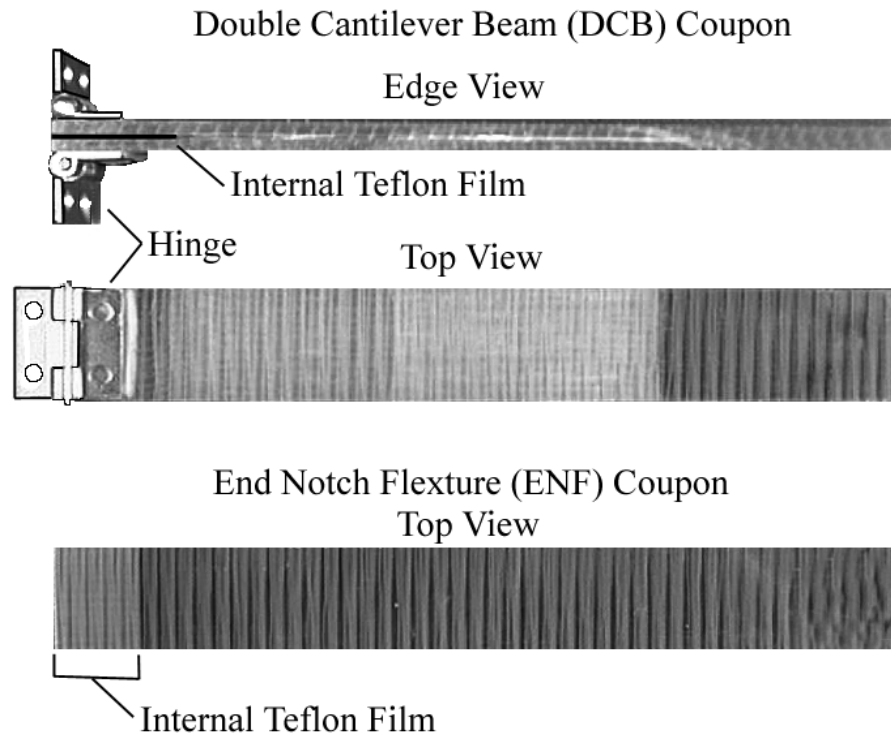


Figure 8. DCB and ENF specimens

time to cure the plate was cut into test coupons with dimensions of 25 mm wide by 200 mm long, and a nominal thickness of 5 mm. A starter crack, 3 mm long, was introduced

into the coupons, to bypass the resin-rich area ahead of the release fabric, with a flat head screwdriver. The area where the hinges were to be mounted for loading was then sanded to remove any release agent from the molding process. Typical piano stock hinges were then mounted to the coupon ends using Hysol EA 9309.2NA adhesive. The end notch flexure (ENF) specimens had the same dimensions as the DCB specimens, but with no hinges.

CHAPTER 4

RESULTS AND DISCUSSION

This chapter is divided into four sections. The first section presents results for the delamination resistance of various laminates, where the delamination was allowed to progress over the entire specimen length. Comparison between various ply drop combinations are made in terms of delamination growth rates as well as initiation and arrest. The second section looks at the influence of ply drops on the fatigue lifetime of the laminates, including design knockdown factors. Appendix A contains the fiber content, elastic modulus, maximum running stress and the number of cycles to which each coupon was fatigued. Appendix B contains the delamination length versus cycles for all of the coupons tested in the first section. The third section presents results for composite I-beams containing ply drops, comparing results in these structural components with coupon results. The last section presents basic results for critical strain energy release rates in Modes I and II delamination using double cantilever beam and end notch flexure coupons, respectively.

DELAMINATION STUDY

Effect of Ply Drop Location

Table 1 lists details of laminates ESA, ESB, and ESC, each of which contained a single 0° ply drop. The ESA laminate has a single exterior 0° ply drop. Static tensile tests

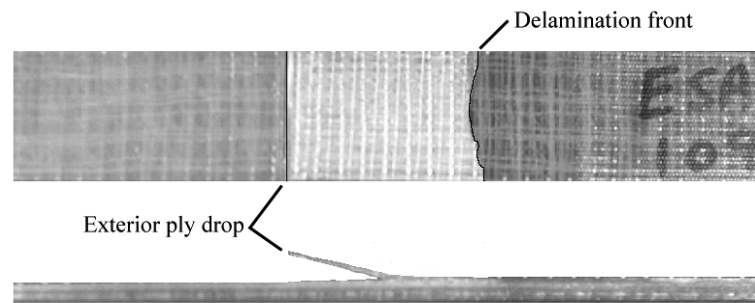


Figure 9. Delamination of exterior zero degree ply drop.

produced delamination of the dropped ply over the entire specimen free length, as seen in Figure 9, followed by a brooming type of failure of the remaining cross-section, shown in Figure 10. This type of dramatic failure is typical for all laminates tested statically, and Figure 10 is also typical of laminates without ply drops.

The ESA laminate was tested in tensile fatigue at various maximum stress levels at an R value of 0.1 to characterize the fatigue crack growth of the delamination. Figure

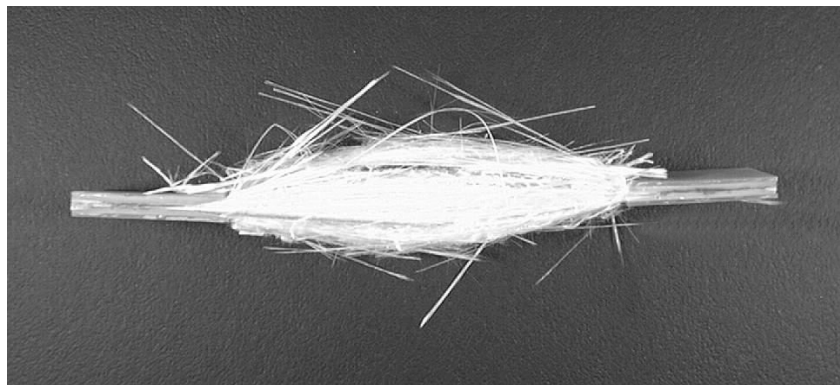


Figure 10. Typical static failure of laminate with ply drop.

11 shows results for delamination length versus cycles at three maximum stress levels.

These are results for typical individual tests; results for all tests are given in Appendix B.

These coupons delaminated uniformly across the coupon width and along the gage length.

Measuring the length of the delamination was straight-forward, because the initially

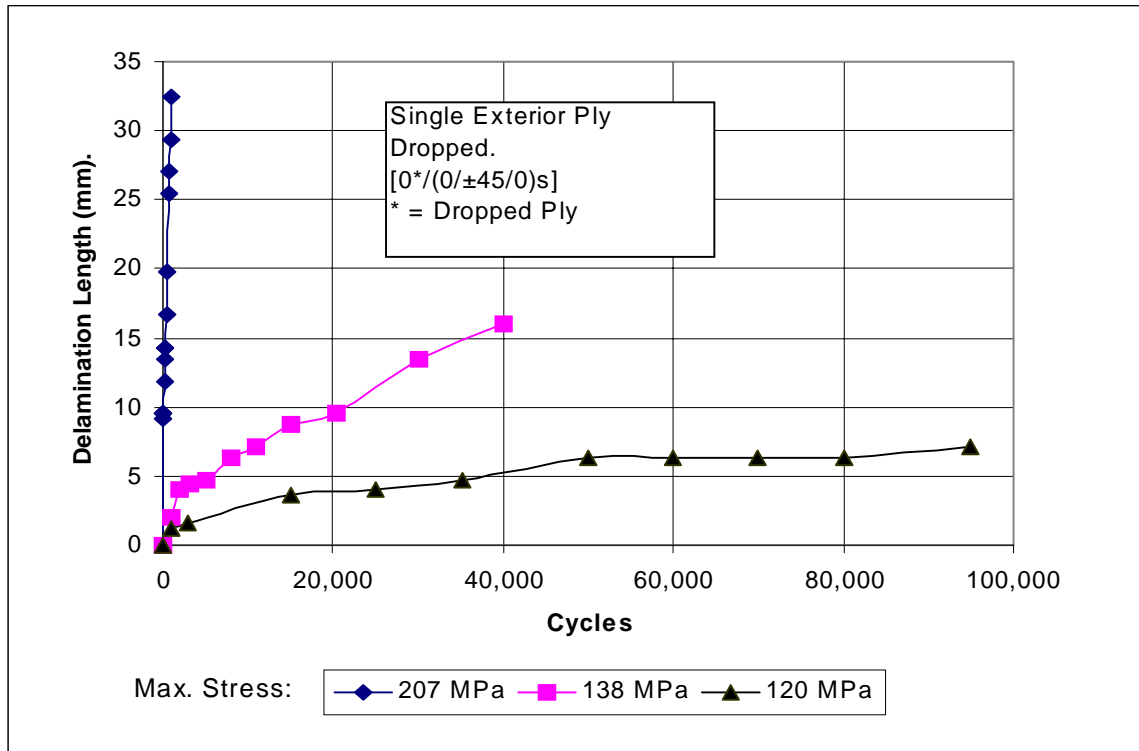


Figure 11. Delamination length vs. cycles for ESA laminate, R = 0.1, Exterior 0° Ply Dropped.

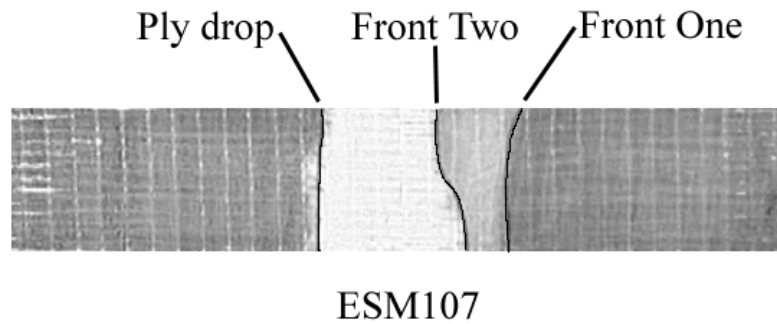


Figure 12. Delamination at an interior ply drop showing two delamination fronts.

translucent coupons became opaque due to the delamination. In Figure 9, an ESA coupon is shown with the exterior 0° delaminated. This type of delamination is typical for all of the laminates with exterior ply drops. The coupons showed no other signs of fatigue damage. Unlike laminates with an exterior ply drop, interior ply drops developed two different delamination fronts. These two delamination fronts can be seen in Figure 12 for the ESB laminate [0/0*/±45/0/0/±45/0]. The crack initially started in between the +45° and -45° plies under the ply drop, labeled Front One in the Figure 12. The delamination then propagated along the length ahead of the second delamination front, labeled Front

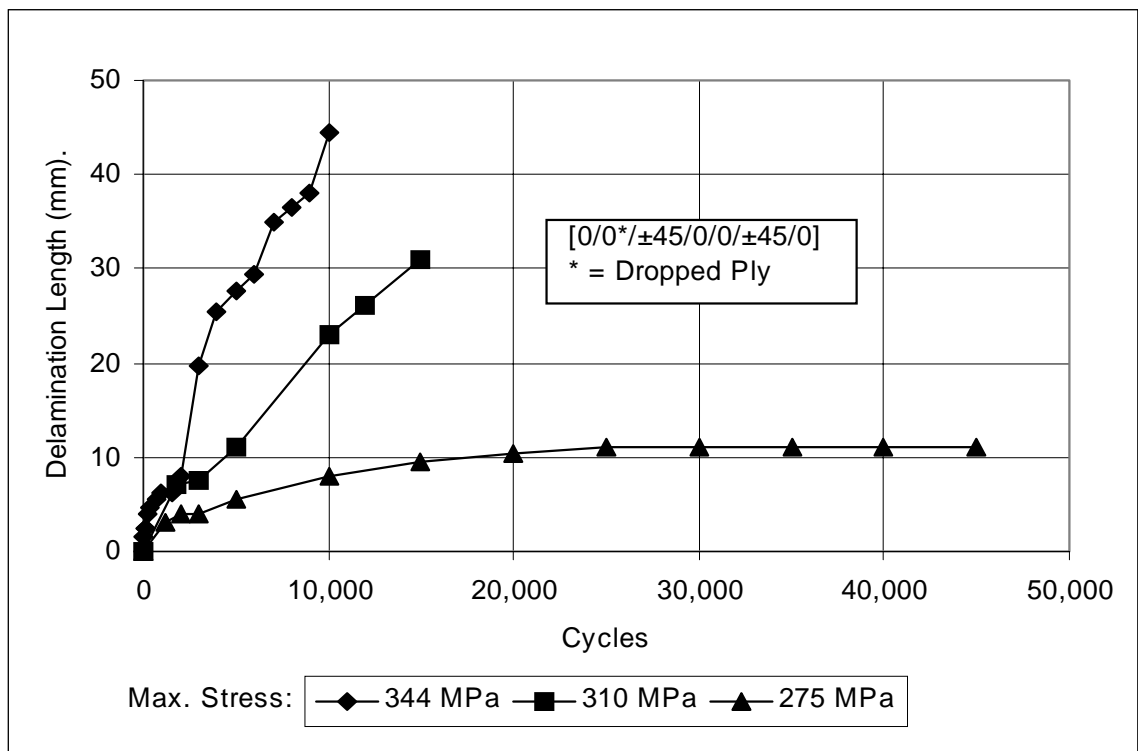


Figure 13. Delamination length vs. cycles for ESB (Single interior 0°ply drop) laminate, R=0.1.

Two, which developed between the exterior zero ply and the ply drop layer. For the interior ply drop, in the ESB laminate, delamination required about twice as high a

maximum stress level as for the ESA laminate, apparently due to the two shear surfaces, as discussed later. The delamination rate for various stress levels for both the ESB and ESC laminates can be seen in Figures 13 and 14. The ESC laminate, with a central ply drop, showed a slightly higher delamination resistance than ESB.

Table 2 provides an approximate measure of delamination resistance based on the delamination test results. The Table rates delamination resistance for different laminates in terms of the maximum strain under tensile fatigue loading to produce a one-inch long

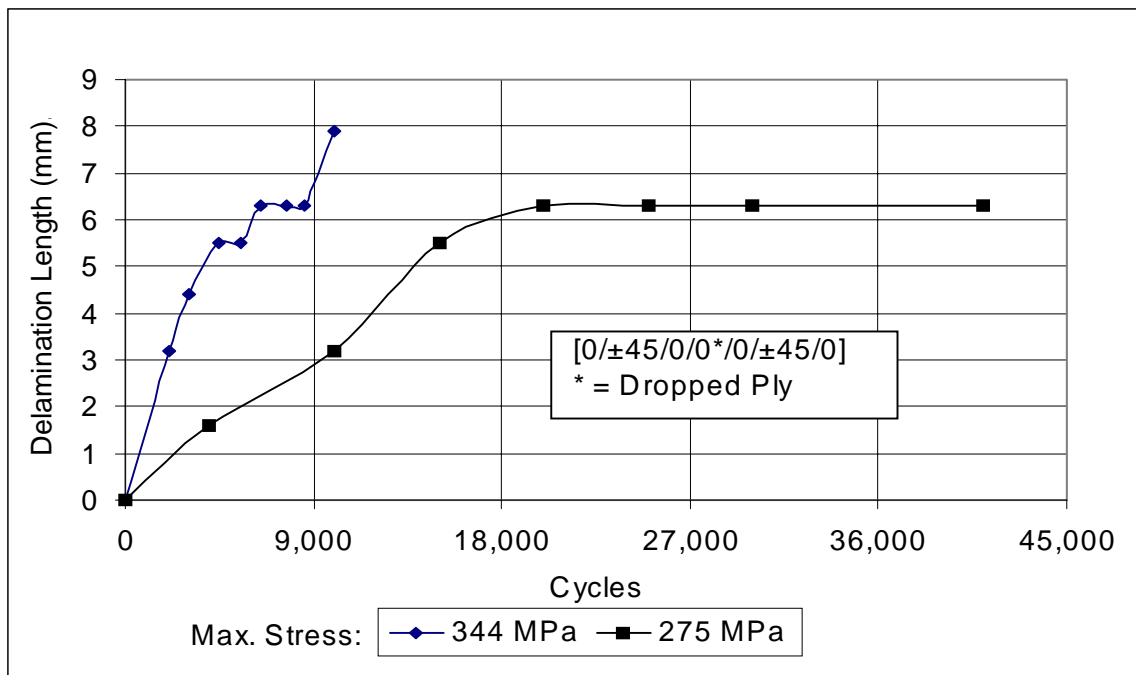


Figure 14. Delamination length vs. cycles for ESC (Single center interior 0°ply drop) laminate, R=0.1.

delamination in 10^5 cycles. The ESA laminate with an exterior ply drop required only 0.6% maximum strain in fatigue to produce a 25 mm delamination in 10^5 cycles, while the ESB and ESC laminates required about 1.1% maximum strain. The stresses and strains in each case are the values measured and calculated for the thin cross-section side of the ply drop. The arrest strain values are obtained from the highest stress where the

Table 3. Comparison of delamination resistance of different ply drop configurations.

Laminate	Lay-up	% Strain for 25.4 mm delamination in 10 ⁵ cycles	Arrest % strain ¹	Threshold % strain ²
ESA	[0*/(0/±45/0) _s]	0.6	0.5	0.4
ESB	[0/0*/±45/0/0/±45/0]	1.1	1.1	0.8
ESC	[0/±45/0/0*/0/±45/0]	1.1	1.1	0.8
ESE	[0*/(0/±45/0) ₃]	0.6	0.4	0.4
ESF	[0/0*/±45/0/(0/±45/0) ₂]	1.0	1.0	0.7
ESG	[0*/0*/(0/±45/0) ₃]	0.4	--	--
ESH	[0/0*/0*/±45/0/(0/±45/0) ₂]	0.7	0.6	0.5
ESI	[0/0*/0*/±45/0/0/±45/0]	1.1 ^A	1.0	0.7
ESJ	[0*/(0/±45/0) _s] "Z-Spiked"	0.8	--	--
ESK	[0*/(0/±45/0) _s] Hysol EA 9309.2NA	0.7	--	--
ESM	[0/0*/±45/0/0/±45/0] Hysol EA 9309.2NA	1.1 ^B	--	--

¹- no further growth over most of the 10⁵ cycles
²- no delamination after at least 10⁵ cycles.
 Fabrics: 0°: D155; ±45°: DB120 except as noted
 Laminates ESO, ESR and ESP not shown, ±45° layers did not delaminate.
^A- Same as ESB, except multiple ply drops.
^B- No delamination; however, failure of coupon occurred at ply drop.

delamination arrested after 10⁵ cycles. The threshold strain values are obtained from the highest stress where no delamination had formed after 10⁵ cycles. These results are limited to the 10⁵ cycle range, and could vary at high cycles.

Effects of laminate thickness and multiple ply drops at the same position

Two significant parameters in dropping plies are the percentage of the total thickness (and total 0° plies) which are dropped, and the number of plies which are dropped at the same position. These parameters were explored with laminates ESD through ESH. Laminate ESD had two interior 0° ply drops, while maintaining the same basic lay-up as the thin sections of the ESA, ESB and ESC laminates, without adding

additional 0° plies to be dropped. This resulted in a 33 percent drop in thickness (a 50% drop in the percent 0° plies), whereas the ESA, ESB and ESC laminates were only tapered 14 percent, with 20% of 0° plies dropped. This interior ply drop did delaminate when statically loaded to failure, but no delamination occurred when the coupon was fatigued. The laminate simply broke through the thickness at the ply drop. The difference can also be seen in the moduli of the thick and thin sections, 22 GPa versus 15 GPa, respectively, resulting from a higher percent of 45° material in the thin section (Table 1). This bounds the practical range of thickness taper that can be used successfully in a design. Having too much taper can prevent delamination, but only because the thin section can only support very low loads. Only two coupons were tested since no delamination occurred prior to tensile failure.

The ESE and ESF laminates

The ESE and ESF laminates incorporated a single 0° ply drop into a base laminate that was thicker than the ESA laminate. The percent thickness change in these laminates was reduced to 10% as compared to the 14% for the ESA laminate. The ESE laminate had an exterior ply drop while the ESF laminate had an interior ply drop. The delamination rate was slightly lower for the ESE laminate than for the ESA laminate (Figure 17), but the strain to produce a 25 mm delamination in 10^5 cycles was about the same, 0.6% (Table 2). The ESF laminate also had a slightly slower delamination rate than the ESB laminate, but the strain value in Table 2 was slightly lower at 1.0% for ESF versus 1.1% strain for ESB. The delamination mode of both of these laminates was very

similar to their thinner counterparts.

The ESG and ESH laminates were also thicker in cross-section, plus, in an attempt to simulate a manufacturing situation, two plies were dropped instead of one. The ESG laminate contained two dropped plies on the outside while the ESH laminate contained two dropped plies in the interior (Table 1). In both cases these configurations behaved poorly compared with their single ply drop counterparts. During testing of the ESH laminate, the resin rich area ahead of the ply drop was observed to crack extensively during the fatigue test. When the coupon was at the maximum stress of the fatigue cycle, fracture and fragmentation in the resin pocket occurred. No matrix material was left ahead of the ply drop after the initial cycles. This is illustrated in the Figure 15.

The ESG laminate, with a double external ply drop, delaminated more easily than a single ply drop on the outside. The percent strain for a one-inch delamination in 10^5 cycles for ESG and ESH were 0.4% and 0.7%, respectively. These are significantly lower than the values for their counterparts single-ply-drop cases, ESE and ESF at 0.6% and 1.0% strain, respectively (Table 2). A comparison of laminates having internal ply drops is presented in Figure 16. As noted, the ESH laminate with two interior ply drops had the highest delamination rate. (The ESK laminate is discussed later).

Effect of Ply Drop Spacing

The ESI laminate was constructed to look at the effect of multiple individual ply drops with spacing ranging from 13 to 48 mm, and are compared with the ESB laminate having the same ply configuration and a single ply drop. The results for the various cases in Figure 17 are scattered with no clear effect of spacing. The closest spacing, 12 mm, gives results which are essentially the same as for ESB laminate with a single, interior ply

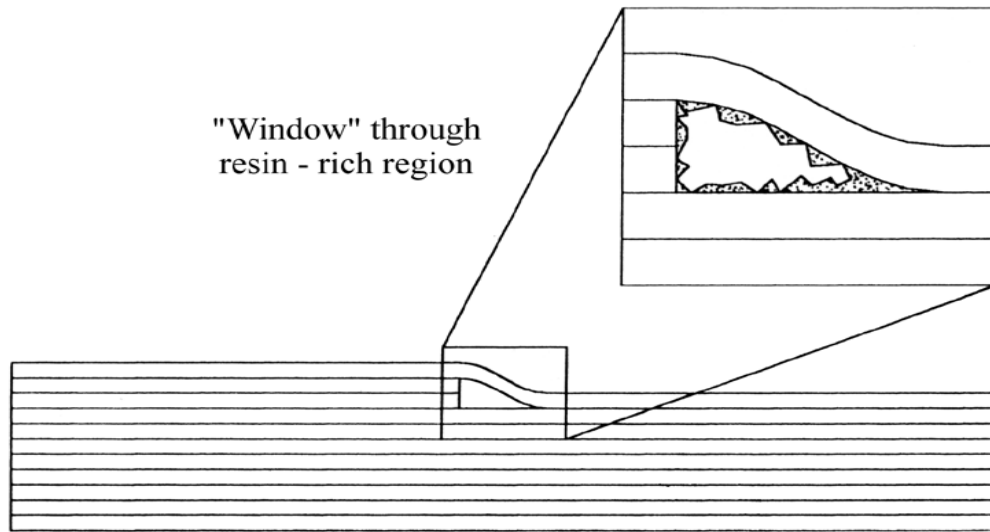


Figure 15. Illustration of resin rich region in ESH laminate.

drop. However, if the two delaminations merge together, then a single system is created

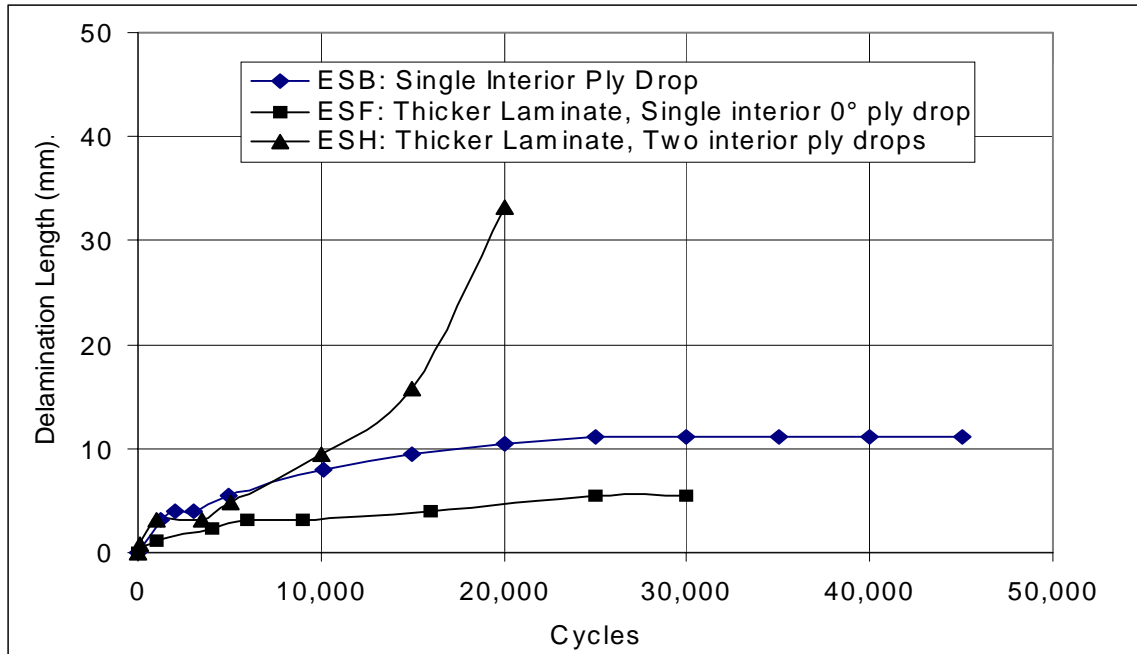


Figure 16. Delamination length vs. cycles for laminates ESB, ESH, ESF (all interior ply drops) at a maximum running stress of 275 MPa, R=0.1

which might propagate like the case with two dropped plies at the same location.

Complete data to explore this question were not generated, but typical coupons containing multiple ply drops with delaminations can be seen in Figure 18. All the coupons were run at the same stress level, 275 MPa, with $R = 0.1$. A coupon with ply drops too close together can be seen at the top of Figure 18 right before both ply drops delaminated together. In the lower two coupons the delamination has arrested after some crack propagation, prior to the delamination combining into a single system.

Effects of “Z-Spiking”

The ESJ laminate with “Z-Spiking” is not shown in Figure 19, which compared laminates with exterior ply drops at a maximum stress of 138 MPa, because there was no

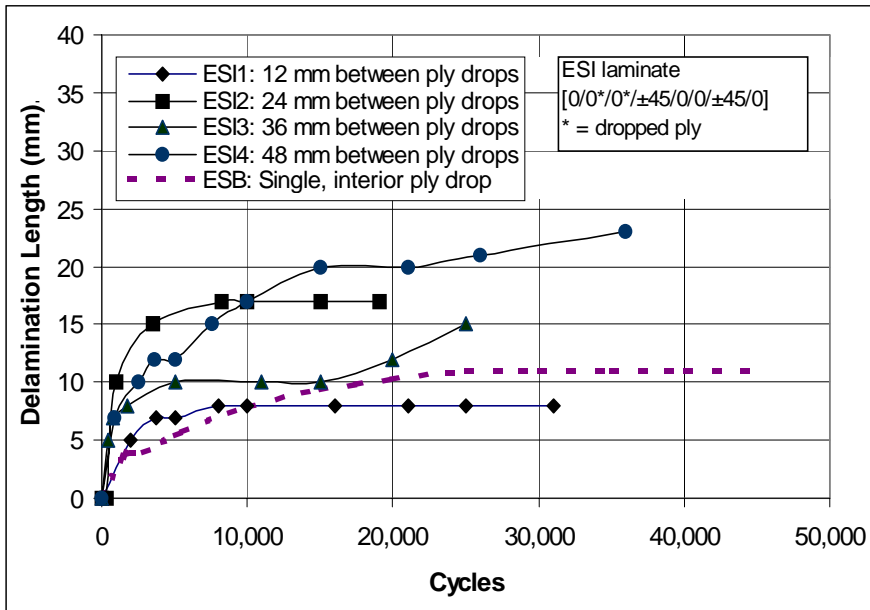


Figure 17. Effect of different spacing between ply drops, R=0.1, ESI laminate (Two 0° ply drops) at 276 MPa.

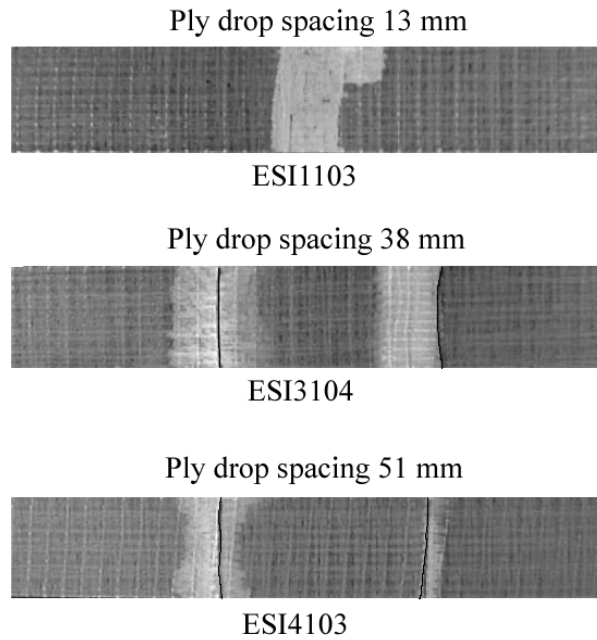


Figure 18. ESI coupons run at 276 MPa, R=0.1.

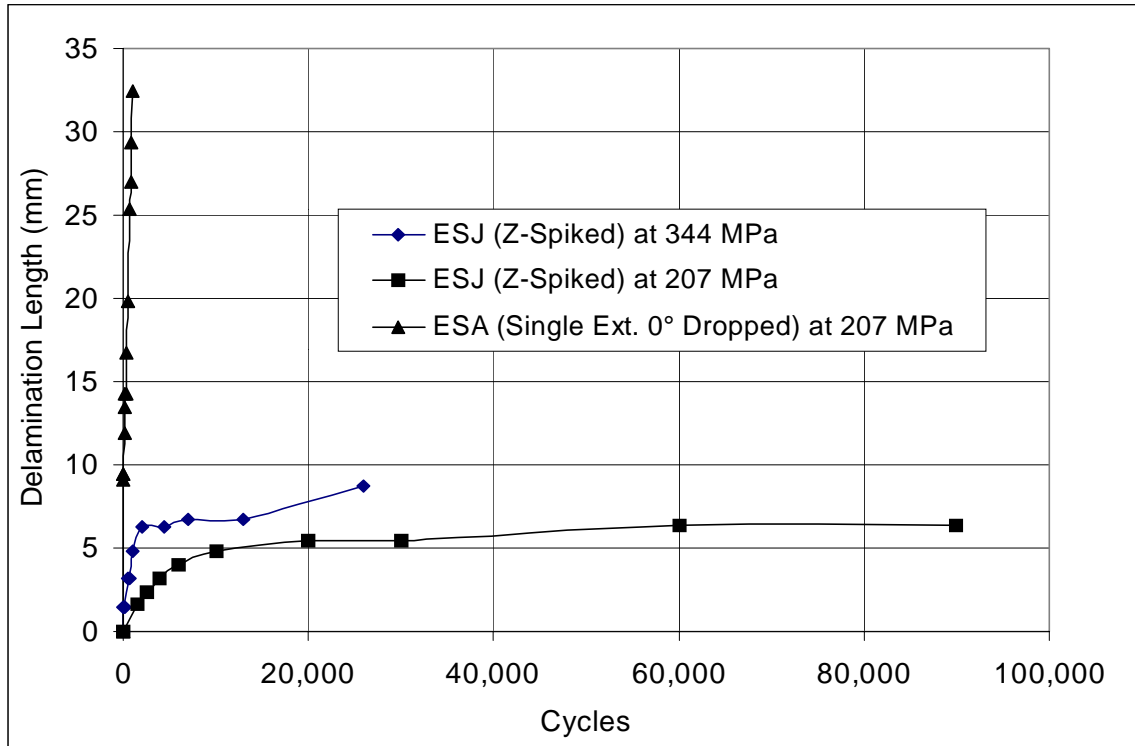


Figure 19. Delamination length vs. cycles for ESJ “Z-Spiked” laminate compared to ESA (Single, exterior 0° ply drop) laminate, R= 0.1.

delamination until more than 200,000 cycles. Delamination at higher stresses in the “Z-Spiked” laminate initiated locally around the tows and then proceeded into the ply drop. The delamination initiation took longer than for a normal exterior ply drop.

Delamination rates at various stress levels for the “Z-Spiked” laminate can be seen in Figure 19 compared with data for the ESA laminate. At the lowest stress level shown using the “Z-Spiked” configuration (207 MPa), the ESA laminate completely delaminated rapidly, but the “Z-Spiked” laminate had reached a level where the delamination arrested. The laminates with interior ply drops and “Z-Spiking” showed a definite improvement in delamination resistance over laminates that were constructed

normally. The ESM laminate, with a “Z-Spiked” internal ply drop, was not successful in preventing delamination. A delamination immediately formed in the area where the $\pm 45^\circ$ layer was completely severed to allow the ply drop to be inserted. The delamination then propagated at the same rate as a typical ESB laminate.

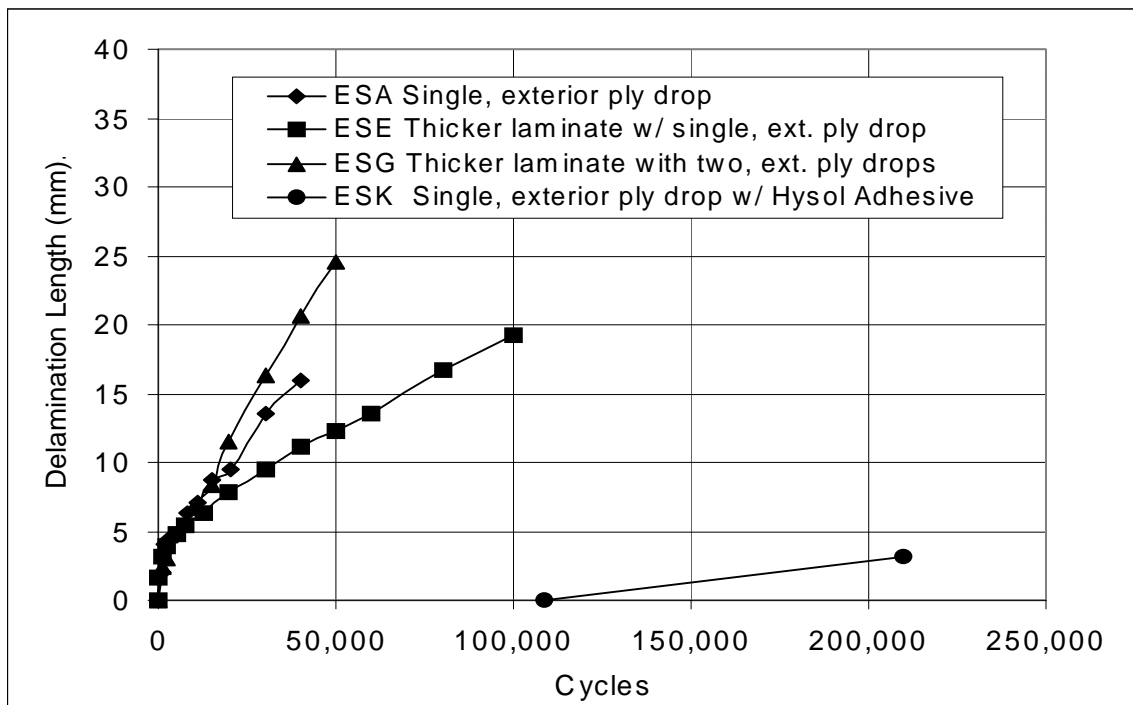


Figure 20. Delamination length vs. cycles for laminates ESA, ESK, ESG, ESE (all exterior ply drops) at a max. running stress of 138 MPa, R=0.1.

Effect of Tough Adhesive at Ply Drop

The ESK and ESL laminates had single ply drops where the ply drop area was impregnated with Hysol EA9309.2NA epoxy adhesive prior to resin impregnation. In Figure 20, the ESK laminate with the Hysol adhesive is compared with three other laminates that incorporated an exterior ply drop. The ESK laminate showed a significant improvement over the other configurations tested. The delamination in the ESK laminate

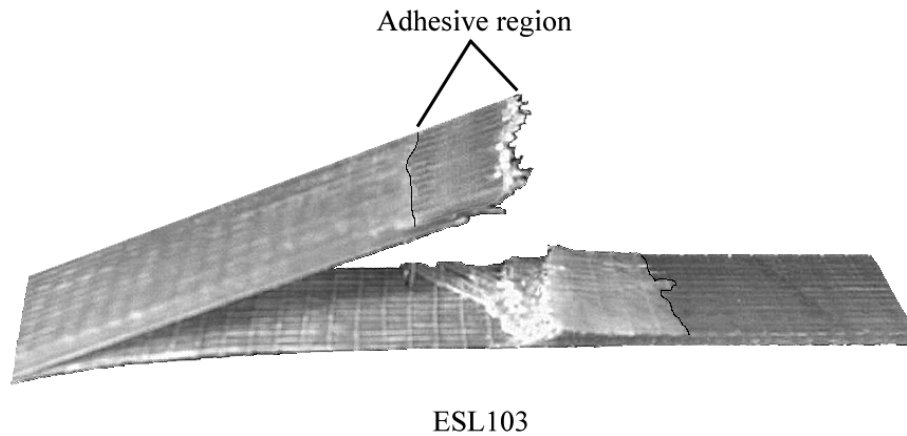


Figure 21. ESL laminate in tension at the ply drop (Interior 0° ply drop with Hysol adhesive) failed at 276 MPa.

did not initiate until the other laminates had completely delaminated. The delamination did not initiate in the adhesive, but at the point right behind the adhesive, in the thicker section. Once the crack had propagated to the grip, the adhesive failed, totally separating the plies. The ESL laminate, with an interior ply drop with adhesive, showed no visible delamination prior to coupon failure. A typical failure can be seen in Figure 21. The region where the adhesive was allowed to cure did not delaminate prior to total laminate failure. Failure occurred near the ply drop location, apparently due to the stress concentration from the ply drop. This type of prevention technique provided significant delamination prevention, while not reducing the life of the coupon when compared with the ESB laminate at the same number of cycles, as discussed later.

Effect of Butt-Joints

The ESN and ESO laminates were used to investigate the effect of butt-joints on

the delamination properties of typical laminates used in this thesis. The ESN laminate contained an exterior 0° butt-joint. This had the same effect as dropping a ply, as the ply delaminated at the same rate as for the ESA laminate. However, the ESO laminate contained an interior $\pm 45^\circ$ layer butt-joint. The $\pm 45^\circ$ layer did not delaminate and caused no damage which influenced the lifetime of the coupon. This suggests that dropping $\pm 45^\circ$ layers makes for a less delamination critical design. This is not surprising since zero degree layers carry the majority of the load and have the greatest influence on stiffness. However, dropping $\pm 45^\circ$ layers can only be used to a limited extent, since they are not present in great numbers in this class of laminates.

Effects of $\pm 45^\circ$ Ply Drops

To confirm the effect of dropping $\pm 45^\circ$ degree layers on delamination rate, the ESR laminate was laid up similar to the ESC laminate. However, instead of incorporating two interior 0° ply drops, the ESR laminate incorporates two $\pm 45^\circ$ ply drops along the centerline. This laminate showed no signs of delamination into the thick section as did all the other laminates, as the delamination actually propagated into the thin section. This delamination may have been artificially influenced by the high degree of tapering, 25% of the thickness, which caused a severe shape change.

To get a better estimation of the influence of $\pm 45^\circ$ layer ply drops, the ESP laminate was manufactured with two $\pm 45^\circ$ ply drops (four total plies). The laminate showed no signs of delamination, even after 300,000 cycles at maximum stress of 276 MPa, whereas the ESH laminate, with two interior 0° layers, had delaminated. However, after this many cycles the coupons had premature end failures. This laminate shows

results that are consistent with the laminate containing the $\pm 45^\circ$ butt-joint. The $\pm 45^\circ$ layers are much more compliant than 0° layers and are less prone to delamination at ply drops.

Effect of A130 warp unidirectional fabric

The ESQ laminate used the same laminate lay-up as the ESH laminate, but made use of the A130 unidirectional woven warp direction fabric in place of the D155 weft fabric used in other laminates. The delamination could not be measured with any consistency from coupon to coupon. The A130 fabric is constructed of unidirectional strands woven around a transverse thermoplastic bead every 25 to 30 mm. The delamination would propagate from one bead to the next and then arrest. After continued fatigue the delamination would jump to the next bead. However, the A130 fabric overall showed less delamination resistance than the D155 fabric, with the delamination propagating unstably between beads. A typical example of this is that at 310 MPa level, a laminate using the A130 fabric would delaminate to the grips in under one thousand cycles, whereas a laminate using the D155 fabric would not delaminate that far until after 30,000 cycles.

Other attempts to prevent delamination

The JKA “Feathered” and “Random” laminates used the ESA laminate with an exterior ply drop as a model to incorporate delamination suppression techniques, in addition to the “Z-Spiked” and adhesively bonded ply drops. The results in Figure 22 show that the random mat had no effect on the delamination rate, while incorporating feathering in the laminate is very successful at retarding delamination. The delamination of the JKA “Feathered” laminate began at the tip of the tows that had been pulled out so they extended beyond the fabric edge, and propagated along those tows until it reached

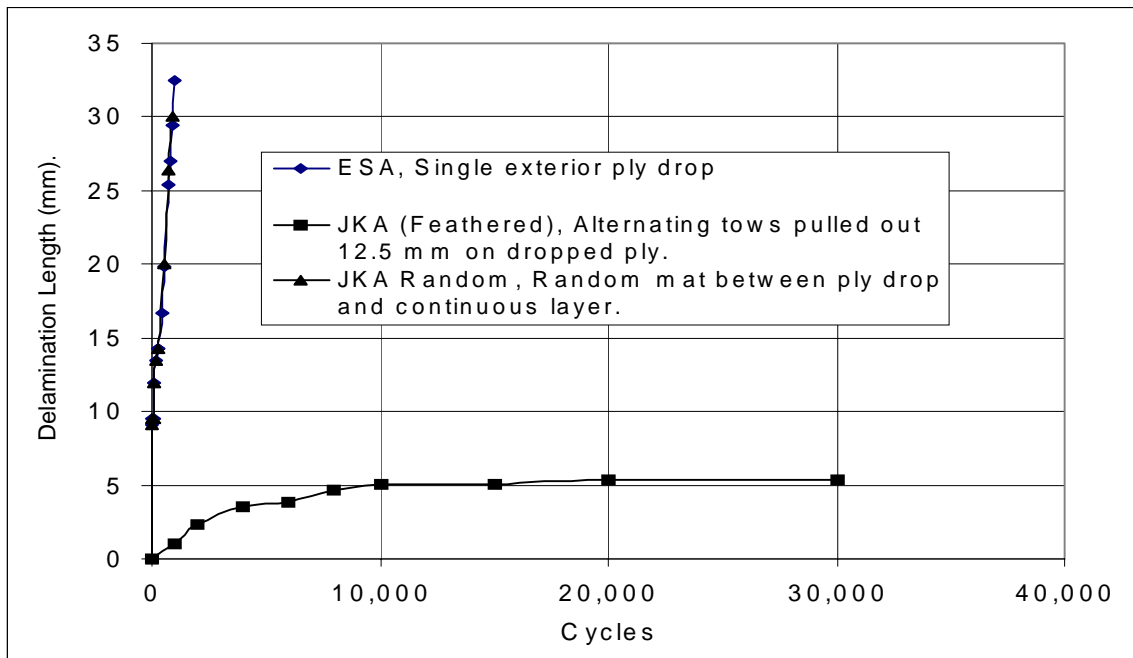
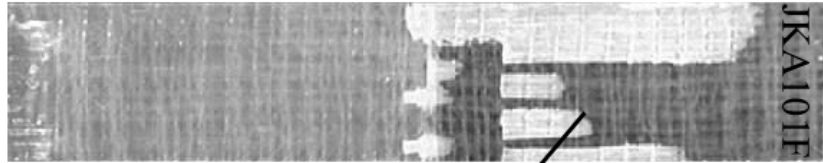


Figure 22. Delamination length vs. cycles for ESA, JKA “Feathered” and JKA random laminates at a maximum running stress of 207 MPa, R=0.1.

the tows which were not pulled out. The delamination can be seen propagating along the pulled out tows in Figure 23. The JKB “Feathered” used the same scheme to prevent



Delamination initiating along
tows that are pulled out

Figure 23. Delamination initiating along tows pulled out.

delamination in an internal ply drop laminate. The delamination progressed the same way as with the JKA “Feathered”. The JKB “Feathered” delamination rate is compared to a standard ESB laminate in Figure 24. The “feathering” has a significant effect on reducing the delamination length.

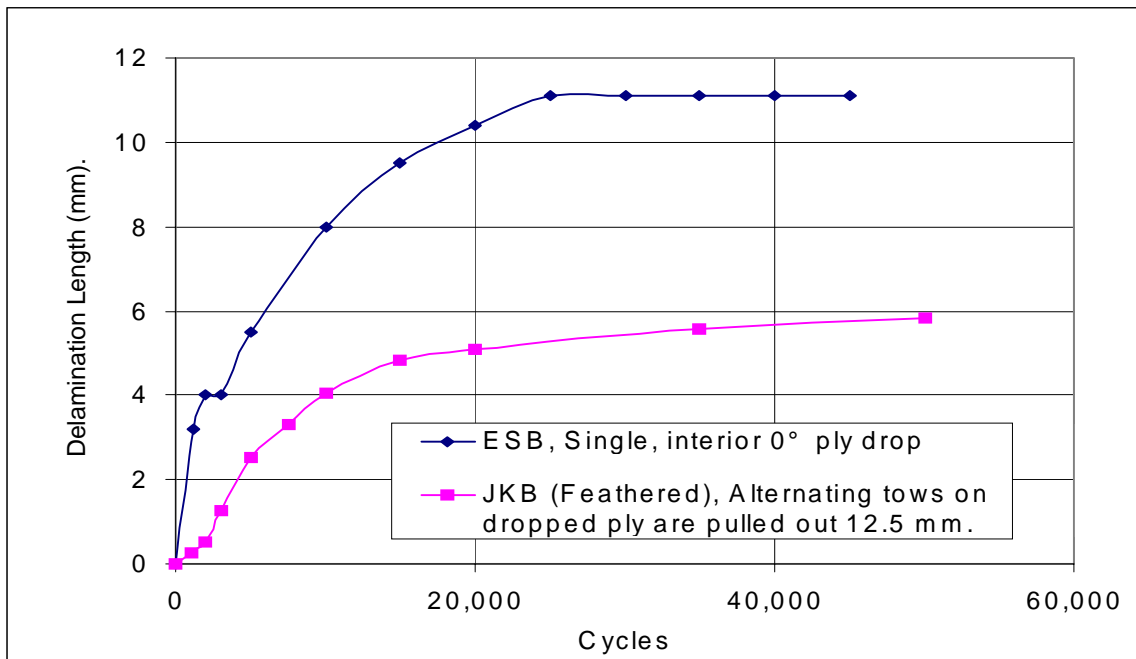


Figure 24. Delamination length vs. cycles for ESB and JKB "Feathered" at a maximum running stress of 275 MPa, R=0.1.

Repairing Delaminated Samples

If exterior ply drops are to be used in a design and an overload condition takes place, it would be desirable to repair the delamination. Two epoxy adhesives, Hysol EA 9309.2NA and Hysol EA 9412, were used to repair the delamination. After the initial test was run on an ESA laminate, causing delamination, the adhesive was injected into the delamination and a C-clamp was applied to the specimen until the adhesive had cured. The specimen was then retested at the same stress level and the delamination rate was

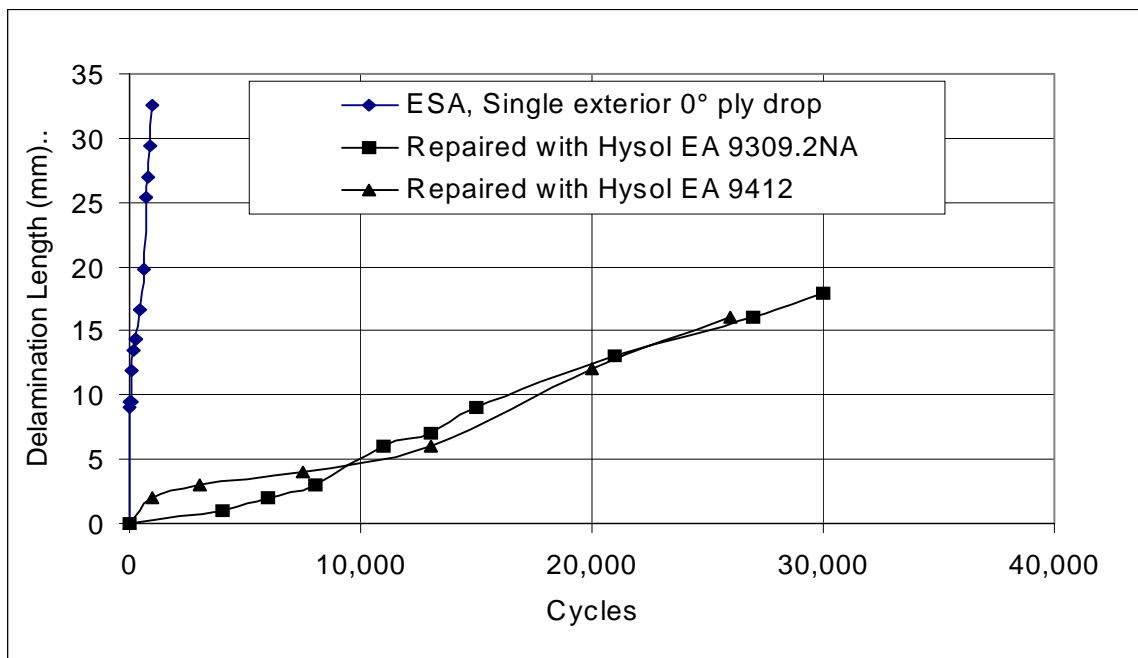


Figure 25. Delamination length vs. cycles at 207 MPa, R=0.1, initial ESA laminate compared to repaired ESA laminate.

compared to the original rate, which can be seen in Figure 25. From Figure 25, the two adhesives had a similar delamination rate and provided a significant reduction in delamination rate compared with the original laminate.

So far the only attempts to repair delamination have involved exterior ply drops, since interior ply drops present an access problem. One possible method of repair would be drill a hole into laminate that is smaller than the critical flaw size and draw a vacuum around the hole. This would draw the repair adhesive into the delamination and possibly extend the lifetime of the component. (This has not yet been demonstrated.)

Comparing different laminates

In order to make this work useful to a designer needing to incorporate ply drops into a design, Table 2 compares the various laminates, by listing the percent strain needed to cause a 25 mm delamination at 10^5 cycles. By knowing the apparent penalty for using different ply drop configurations, more efficient designs can be developed. For example, by using an exterior ply drop instead of an interior ply drop, there would be an 83% reduction in the strain carrying capability of the laminate. Another example would be if two plies are dropped on top of one another instead of the plies being distributed along the length, there would be an 57 % reduction in the strain carrying capability of the laminate. Similar conclusions are evident for the strains to arrest a delamination and for the threshold strain to initiate a delamination, also listed in Table 2.

EFFECT OF PLY DROPS ON LIFETIME

In the previous sections, different lay-ups were tested in relatively short fatigue tests to determine the rate of delamination. This section describes a study of the ESB and ESH configurations at extended fatigue cycling, in terms of the effect of ply drops on total coupon lifetime. The ESH laminate consisted of the lay-up [0/0*/0*/±45/0/0/±45/0/0/±45/0], where the asterisk plies are being dropped. The ESB laminate, with a single ply drop, had a lower delamination rate than the ESH laminate in the delamination fatigue tests.

Fiber Volume Content Effect

The results are represented in terms of conventional S-N fatigue data sets for control and ply drop cases. In Figure 26 the performance of the ESH laminate at two different fiber contents can be seen. The fiber volume content had little effect on the laminate with ply drops, contrary to the significant effect reported for control materials [50]. The low fiber content control DD5 laminate with no ply drop has an S-N curve slope of about 10% of the static strength per decade of cycles. This fatigue performance is optimal for glass fiber composites, and is used as a standard to compare other laminates [50]. The delamination rates and lifetimes for the laminates containing ply drops are about the same for both low and high fiber contents. This is contrary to fiberglass laminates without ply-drops previously tested (DD5 & DD7), Mandell, et.al. [50], which

show improved normalized fatigue performance at lower fiber contents. This trend can also be seen in Figure 26 for control materials. From this figure, the good performance at lower fiber content is lost due to the presence of ply drops. However, the performance of higher fiber content laminates containing ply drops is not affected. The effect of dropping plies can be seen when comparing the ESH laminate to the material performance of the DD5 laminate. While the DD5 laminate was capable of running at one percent strain at a million cycles, both ESH laminates were reduced to 0.63% strain at one million cycles,

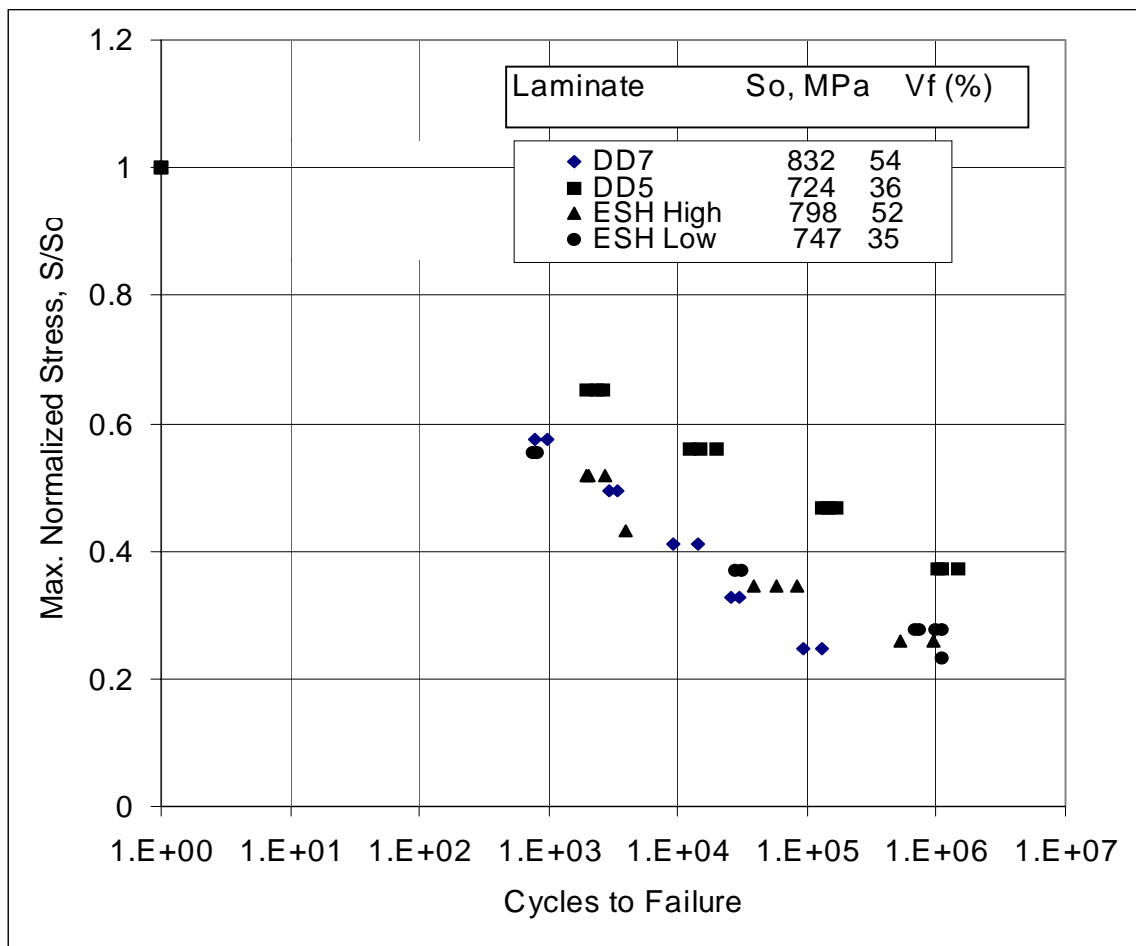


Figure 26. Effect of fiber content on the normalized S-N Data, $R=0.1$, for DD materials $[0/\pm 45/0]_s$ compared to ESH laminate (Two interior 0° ply drops).

similar to the high fiber content control material, DD7. By introducing ply drops, the effective strain carrying capacity of the laminates was reduced by forty percent.

The ESB and ESH laminates delaminated to the grips before the coupon failed. After coupons had been fatigued for 10^6 cycles they were labeled as run-outs. In the majority of these coupons the delamination had not propagated to the grips. The first section of the thesis presented levels of stress where delamination had arrested, but the delamination might have been growing at a slow enough level where it just appeared to have arrested. Threshold levels of strain, where delamination did not initiate before 10^6 cycles, were not found. These strain levels would be low enough to prevent the laminate from being used.

A130 fabric vs. D155 fabric

While the D155 unidirectional fabric has the best fatigue properties at low fiber content of currently available fabrics, it is only available in the weft direction with a maximum width of 127 cm. While the D155 fabric is held together by stitching, which does not cause fiber waviness, the A130's have a thermoplastic bead which runs perpendicular across the tows to keep them together. Since, currently, this would be the fabric of choice for the zero degree layers in composites longer than 127 cm, the ESQ laminate was constructed using this fabric to see how the A130's would behave with ply drops in the laminate. When control laminates containing the two different 0° fabrics, DD11 and DD6 were compared, the fatigue properties were approximately the same, as can be seen in Figure 27.

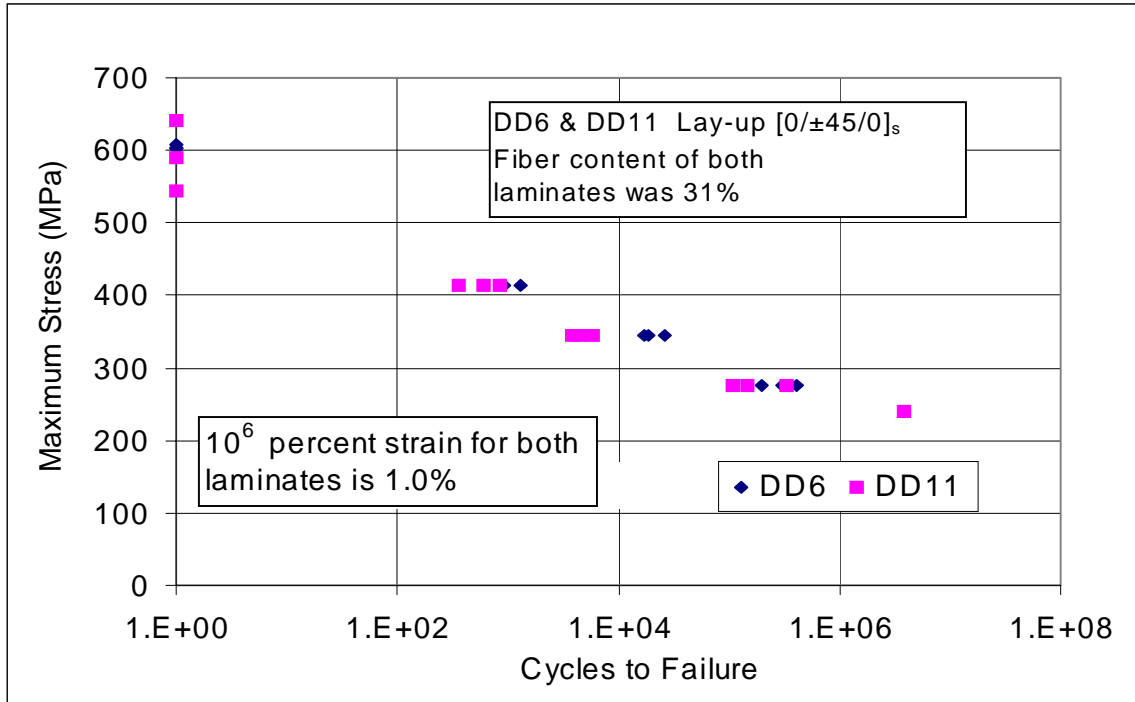


Figure 27. S-N curve (R=0.1) comparing D155 Fabric (DD6) to A130 Fabric (DD11) control materials with no ply drops, from Reference 50.

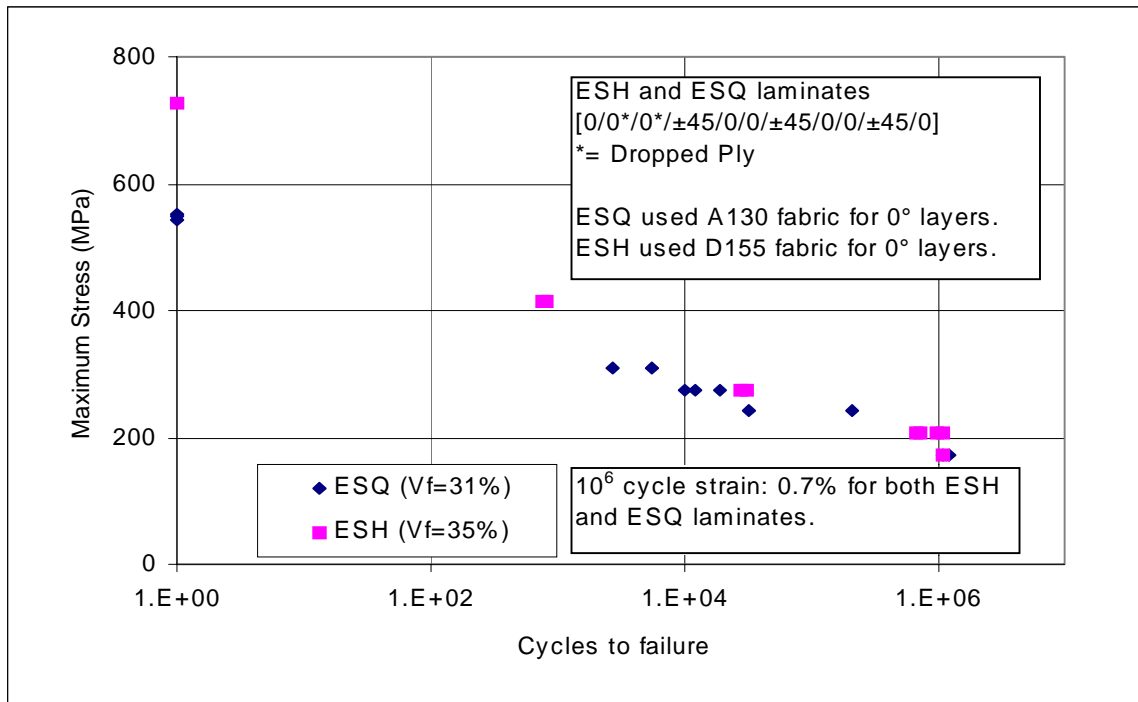


Figure 28. Fatigue life of ESH (Two D155 ply drops) vs. ESQ (Two A130 ply drops) laminates (Maximum stress is on the thin side of the ply drop).

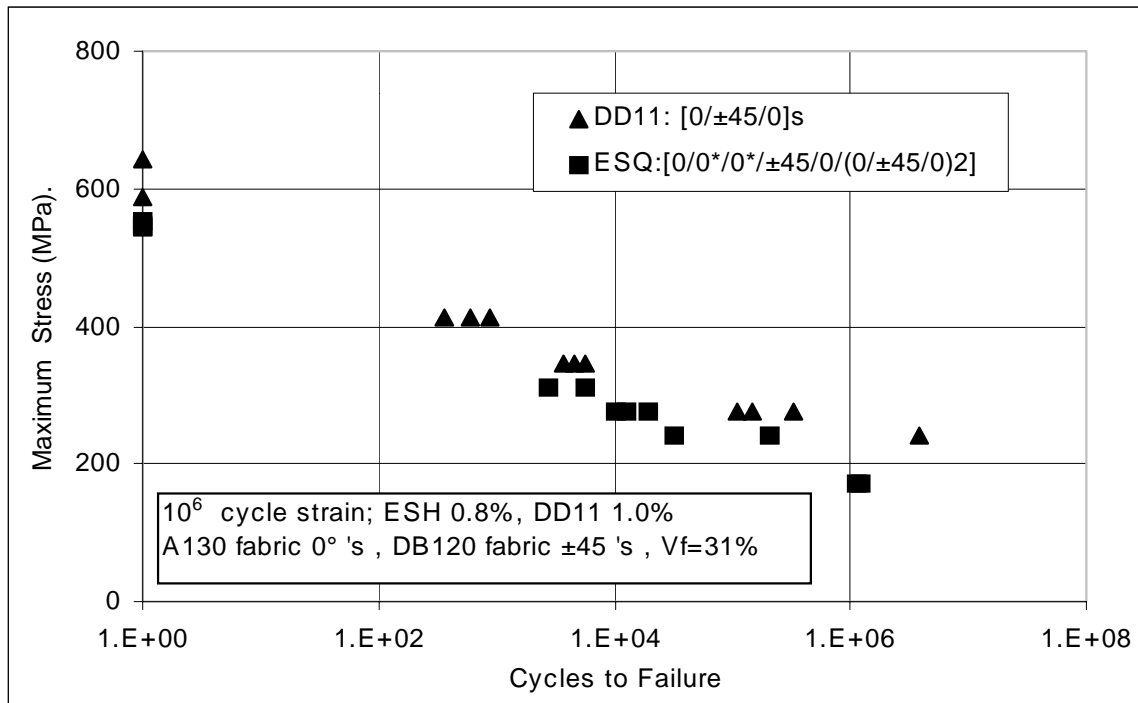


Figure 29. Tensile fatigue S-N data for ESQ (Two, 0° internal ply drops) vs. control DD11 (no ply drops) laminates, A130 unidirectional fabric.

Introducing ply drops into the laminates appears to have a negligible effect. In Figure 28, the performance of the laminates with A130 and D155 0° ply drops is very similar, with the greatest difference shown in the static (1 cycle) strength, where the A130's were lower. Figure 29 compares the A130 based laminate with and without ply drops; as in Figure 26, the ply drops at low fiber content lower the fatigue life, but to a lesser extent in Figure 29. The fatigue properties of the A130 fabric might be higher if the thickness of the thermoplastic bead could be reduced or the spacing increased. In Figure 30, the damage zone appearing around those beads can be seen.

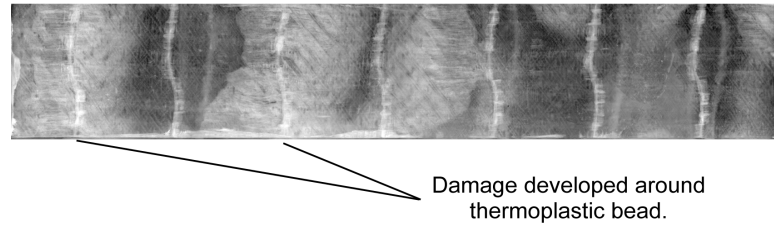


Figure 30. Damage developing around thermoplastic beads as a result of fatigue loading, $R=0.1$.

Resin Rich Region

The size of the resin rich area at the ply drop has a large effect on delamination properties. In Figure 31, two resin rich areas can be seen, due to ply movement which caused the two ply drops to be misaligned. The delamination initiates at this resin rich

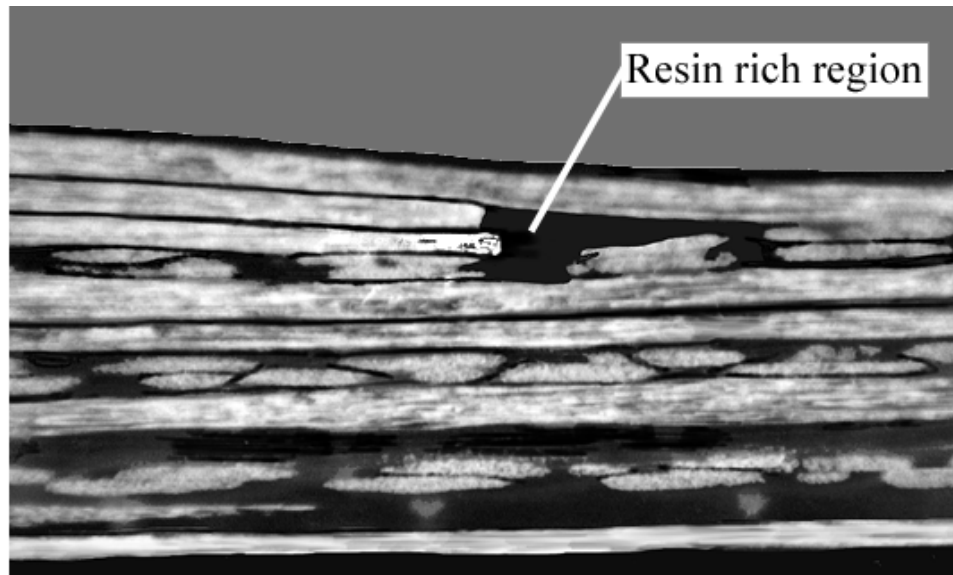


Figure 31. Photomicrograph of ESH laminate showing resin rich regions ahead of ply drops.

region and propagates into the ply drop layers. A typical crack in an ESH laminate can be seen in Figure 32. The delamination on the thicker side grows above and below the ply dropped layers, not between the two ply drops. Also, the crack propagates a short distance

into the thin cross-section and then arrests.

The more plies dropped, the worse the fatigue properties of the laminate, as can be

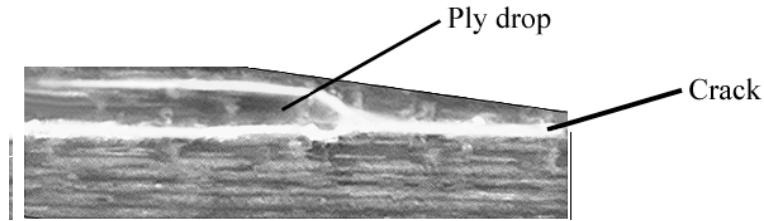


Figure 32. Side view of crack propagating through ESH laminate

seen in Figure 33. Here the fatigue properties of the ESB laminate are compared with the ESH laminate. The ESB laminate has only one interior ply drop, which forms a smaller

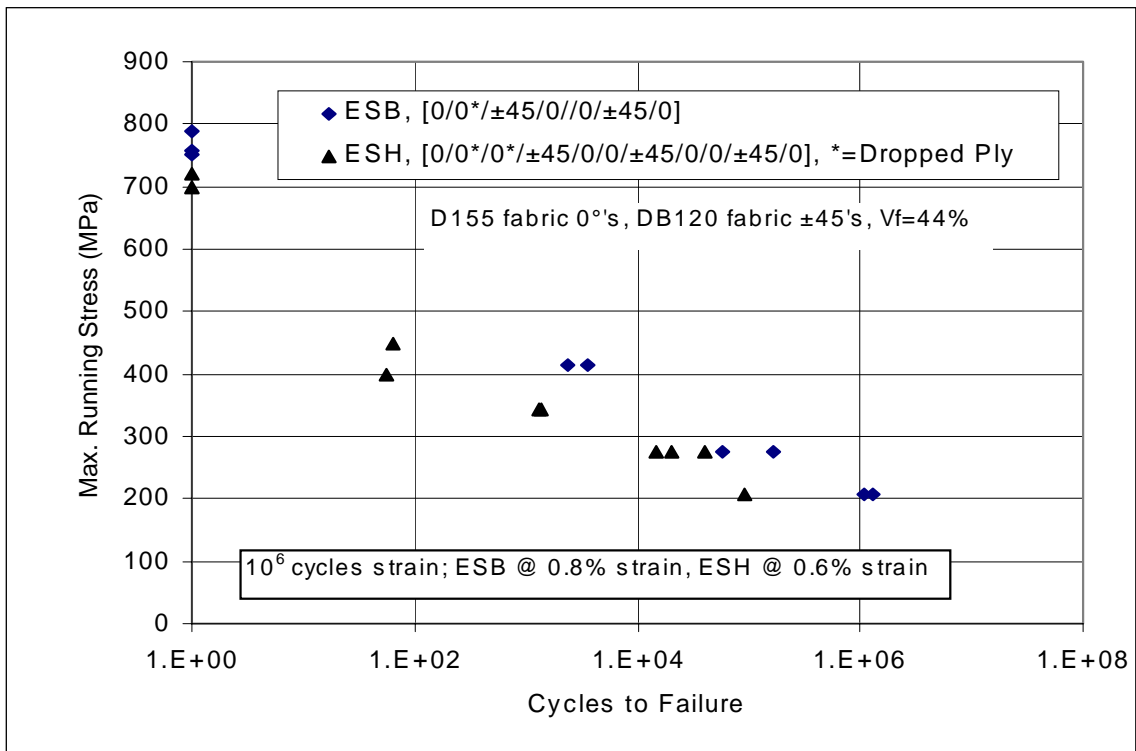


Figure 33. Tensile fatigue (R=0.1) S-N curves for ESB (Single 0° internal ply drop) and ESH (Two interior 0° ply drops).

resin pocket than the ESH laminate which drops two plies. The strain energy release rate

will also increase by dropping more layers. The ESB laminate was able to operate at 0.8% strain out to a million cycles, while the ESH laminate was just above 0.6% strain.

COMPRESSION TESTING

Due to the unsymmetric geometry caused by the ply drop, when a coupon is loaded in axial compression, it tends to buckle. The ESH laminate was studied since it had a thicker cross-section to resist buckling, while at the same time giving a worst case scenario, with two interior ply drops being terminated at the same location. Another problem also arises due to the short specimen used in compression testing. A 13 mm gage length specimen with a ply drop and delamination may be influenced by the grip pressure or stress concentrations associated with the grip. Considering these two problems, the challenge is to have a large enough gage length to create a uniform axial strain field, while avoiding buckling at the test load.

The first approach taken to determine the tendency of a compression coupon to buckle was by calculating its slenderness ratio. The slenderness ratio (SR) is calculated by [50]

$$SR = \frac{\sqrt{12}L_e}{t} \quad (4)$$

Where L_e is the effective length of the test coupon, which for fixed-fixed end conditions is equal to the length multiplied by 0.5, t is the composite thickness in the gage length. A study by Adams and Lewis [51] indicates that a slenderness ratio less than 30 was not

prone to buckling failure in glass epoxy unidirectional composites with uniform cross sections.

For the control coupons tested, Table 4 summarizes the results using Equation 4. While the numbers calculated are less than the proposed numbers for buckling, strain gauges were used to confirm whether buckling was occurring.

Table 4. Slenderness ratios calculated using Equation 4

Slenderness Ratios calculated from Equation 4			
	Thickness (t)	13 mm Gage length	25 mm Gage length
Thick Section Control	4.06 mm	5.5	10.6
Thin Section Control	3.30 mm	6.8	13.1

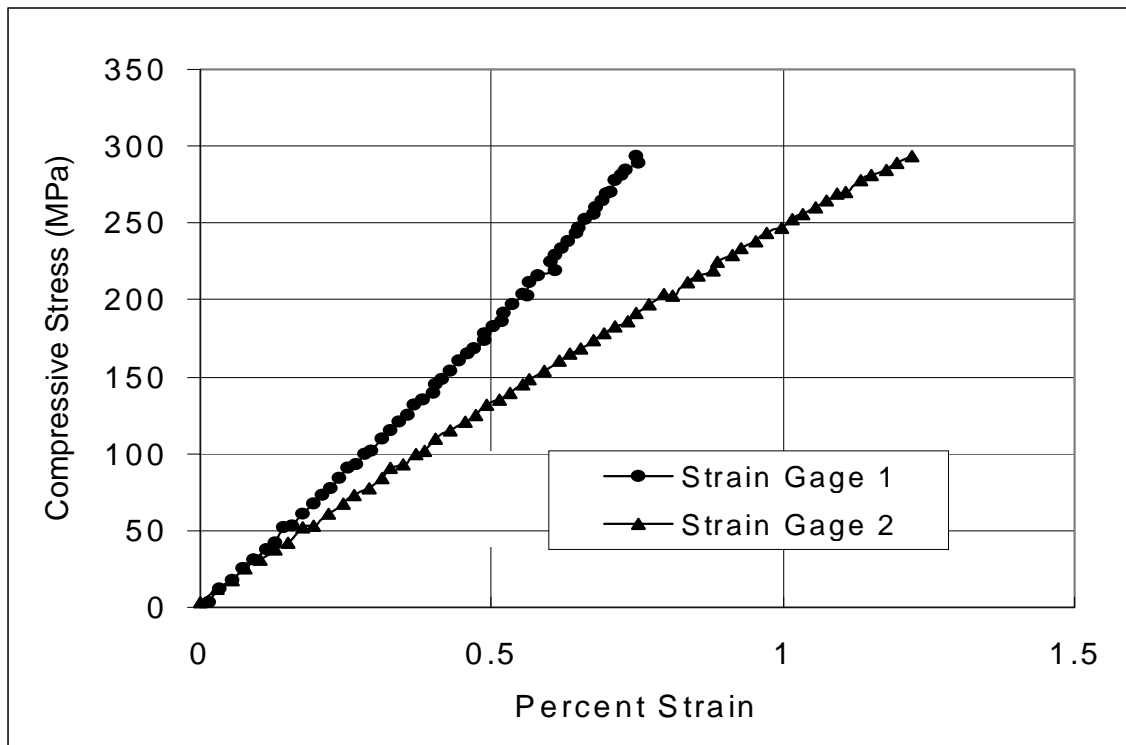


Figure 34. Compressive stress vs. percent strain for ESH 804 coupon.

BLH Electronics strain gages (FAE-25-12-513EL) were mounted on the front and back sides of the coupons to determine when the coupon starts to buckle. In Figure 34, the coupons were loaded to less than 70 MPa before buckling occurred. This had the result of reducing the ultimate compressive strength (UCS) of the coupons, from approximately 579 MPa for control material with no ply drop to 386 MPa with a ply drop. To verify the strength of the laminate without ply drops, control samples were made from the thick and thin sections of the ESH plate, using both 25 mm and 13 mm gage length coupons. The 13 mm gage length was tested to see if the 25 mm gage length was influencing the strength.. The results from these control samples showed that there was no decrease in strength in the thick control samples using either the 25 mm or 13 mm gage lengths. However, when the thin cross-section control coupons were tested using the 25 mm gage length the coupons decreased in UCS from 579 MPa down to 489 MPa. Therefore, when the coupon with the ply drop is tested, the section of the gage length containing the thin section is only 13 mm in height, which means it should not be affecting the strength. This suggests that the ply drop test coupon probably does not have a uniform strain field due to the presence of the ply drop.

Table 5. Comparison of ESH laminate compressive strength with and without ply drops

Comparison of ESH laminate compressive strength with and without ply drops				
Gage length (mm)	Thin control section strength, MPa	Thick control section strength, MPa	Specimen with ply drop strength, MPa	Ply drop specimen bonded back-to-back, MPa
13	551	558	--	--
25	489	558	386	550

Delamination of the coupons in compression occurred at a low number of cycles relative to expectations from tensile tests. In order to obtain more valid tests, two ESH coupons were bonded together back-to-back, using Hysol EA9309.2NA adhesive, to increase the stiffness of the coupon and avoid non-symmetry. These tests showed compressive behavior results that were similar to control cases in Table 5, and also similar to tests with ply drops located in the flange material of the beams described later. When compared to tensile results with ply drops, compressive behavior is less delamination resistant. At strain levels (0.6%) where delamination arrested in the tensile coupons, the compression coupons totally delaminated. The delamination of compression coupons did not show any stable delamination growth, similar to Mode II, ENF specimens discussed later. Typically, the fatigue coupons would not show any delamination until a few hundred cycles before complete delamination over the entire gage length. It was then decided to explore compression behavior in the context of beam flanges, which are more typical of blade structures.

Residual Strength of Coupons

Another interesting aspect of laminates containing ply drops is how well they retained their residual strength during fatigue, prior to failure at the fatigue condition. While the delamination in tension specimens was extensive, reaching into the tabbed area of the coupons, the overall strength after delamination was only reduced by 15% relative to the original coupon strength. In Table 6, the residual strength of ESH coupons is compared at various fractions of the cyclic lifetime (n/N_o).

The high residual strength values give the opportunity to inspect for damage, such as delamination from ply drops caused by overload conditions, while still maintaining the strength to carry the load. However, even though the strength might remain close to the initial strength tests in laboratory conditions, by introducing delamination, the laminate is now more susceptible to environmental effects, which can rapidly reduce the properties of fiberglass laminates.

Table 6. Residual strength of ESH laminate after being fatigued (R=0.1)*

Residual Strength of ESH laminate after being fatigued							
Coupon #	V _F , %	Max. Cyclic Stress, MPa	Cycles	n/N _o	Initial Strength, S _o , MPa	Residual Strength, S _r , MPa	S _r /S _o
ESH 205	36	276	40,000	0.8	703	600	0.853
ESH 213	36	276	20,000	0.4	703	675	0.960
ESH 409	44	207	1.1E6	1.1	746	686	0.920
ESH 404	44	176	1.1E6	0.11 ^A	746	717	0.961
^A - Lifetime estimate used was 10 ⁷ cycles, however test was stopped at 10 ⁶ cycles after no delamination. * Individual specimen results							

PLY DROPS IN BEAMS

Ply drops are a critical issue for the tapered sections of composite structures. Structures may differ from test coupons in several respects: (1) size, (2) stress field characteristics, and (3) manufacturing details. This part of the study was intended to validate the findings of the coupon studies in the context of a small I-beam sub-structural element developed in other parts of the research program [52,54]. Ply drops were incorporated into the tensile and compressive flanges of the beam, which was then loaded in four-point-loading flexural fatigue. Thus, results were obtained from both the tensile and compressive areas of the beam simultaneously, for comparison with coupon data. The results for each beam are presented, followed by a comparison with coupon data with pictures showing typical delaminations, for specific ply drop data. Beams were loaded in one direction only (not reversed), so that the tensile flange experienced an $R=0.1$, and the compressive flange $R=10$; these values correspond to the coupon test values.

Beam Geometry, Fabrication, and Materials.

Figure 35 shows the four-point beam testing apparatus, and Figure 36 indicates the beam coordinate system used in describing the various aspects of the beams. The tested beams are summarized in Table 7. Further details of the beams can be found in Reference [54]. The beam numbering system used here is relative to the overall beam study.

Material DD5 was modified to study the effect of dropping exterior and interior

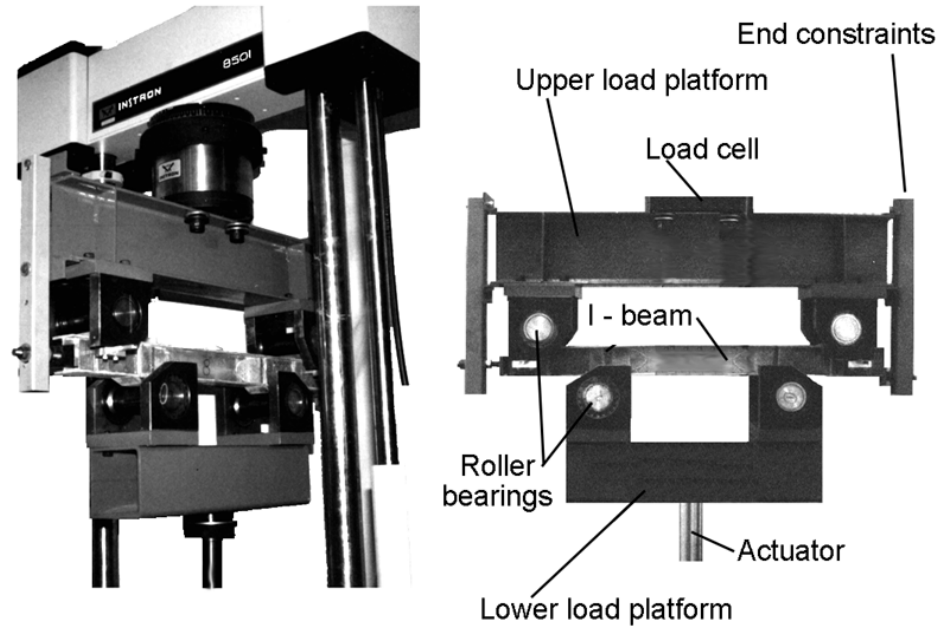


Figure 35. I-Beam testing apparatus

plies in the beam flanges. The ESA laminate configuration was used in beams 39,44 and

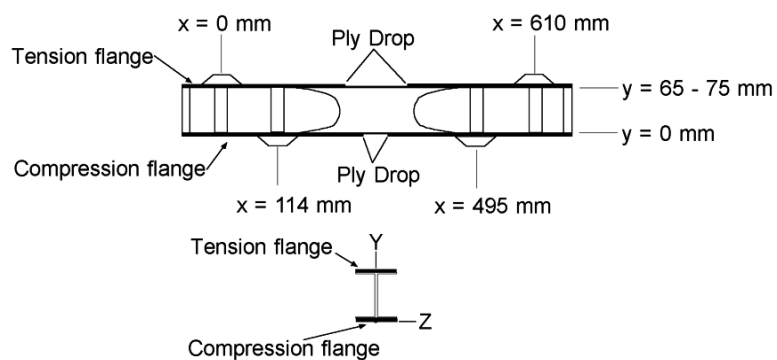


Figure 36. Beam coordinate system

Table 7. List of I-beams tested with ply drops

I - Beam Summary of Static and Fatigue Data						
Beam	Materials Flange / Web	Deflection Constant, K, kN/m	Max. / Min Load, kN	Max. / Min. Strain, %	Cycles	Failure Notes
39	ESA / CH12	4,804	35.6 / 3.6	0.62 / -0.64	1,225,650	ESA ply drop delamination
40	ESB / CH12	4,787	35.6 / 3.6	0.96 / -0.85	264,137	Compression flange delamination
41	ESG / CH12	5,213	49.0 / 4.9	0.74 / -0.76	13,997	ESG ply drop delamination
42	ESG / CH12	5,524	35.6 / 3.6	0.55 / -0.54	436,508	ESG ply drop delamination
44	ESA / CH12	4,527	35.6 / 3.6	0.57 / -0.58	600,000	ESA ply drop delamination
48	ESA/CH12	4,650	35.6 / 3.6	0.66 / -0.67	72,000	ESA ply drop delamination
49	ESH / CH12	6,625	57.8 / 5.8	0.76 / -0.73	25,500	ESH ply drop delamination
50	ESH / CH12	6,054	48.9 / 4.9	0.63 / -0.63	204,000	ESH ply drop delamination
			88.2 (r)	---	1	Compression flange
Web Material (3.0 mm) CH12- ($\pm 45/0/\pm 45$) _s - Fabric 0's- D155 (39%), ± 45 's - DB240 (61%), $V_f = 0.34$, $E_{coupon} = 17.7$ GPa ESA - [$0^*/(0/\pm 45/0)$] _s], Fabric 0's- D155 (71%), ± 45 's - DB120(29%), $V_f = 0.35$, $E_{coupon} = 24.1$ GPa ESB - [$0/0^*/\pm 45/0_2/\pm 45/0$], Fabric 0's- D155 (71%), ± 45 's - DB120 (29%), $V_f = 0.35$, $E_{coupon} = 24.1$ GPa ESG - [$0^*/0^*/(0/\pm 45/0)$] ₃], Fabric 0's- D155 (73%), ± 45 's - DB120 (27%), $V_f = 0.44$, $E_{coupon} = 33.1$ GPa ESH - [$0/0_2^*/\pm 45/0_2 / \pm 45/0_2/\pm 45/0$], Fabric 0's- D155 (73%), ± 45 's - DB120 (27%), $V_f = 0.44$, $E_{coupon} = 33.1$ GPa (r) - residual ultimate strength						

48, ESB in beam 40, ESG in beams 41 and 42, and ESH in beam 49 and 50. The beam flanges were fabricated with the smooth surface on the inside (web side), and the thickness steps on the outside. The respective material lay-ups are detailed in the following sections. During the fatigue tests, the length of delamination on the tension and compression flanges was determined by averaging the two flange edge delaminations, respectively, as each flange contained two ply drops.

Flange laminate ESA

Beam 39

Beam 39 was fatigued at a rate of 4 Hz with a maximum load of 35.6 kN and a minimum load of 3.6 kN. The maximum load produced an initial maximum tension flange measured strain of 0.62% and a minimum compressive flange strain of -0.64%. The initial

beam stiffness was measured as 4,804 kN/m. The flange material was the ESA laminate, which had a single, exterior ply drop (ply 1, Table 8). The ply drops on the tension flange were at $x = 277$ and 328 mm. The ply drops on the compression flange were at $x = 292$ and 314 mm. On the tension flange, the delamination started immediately between the surface 0° ply and first internal 0° ply (ply 1 and 2, Table 8). This delamination was uniform across the width of the tension flange. The delamination on the tension flange continued to grow at an average rate of $6.95E-5$ mm/cycle (Table 9) until the beam was taken out of the apparatus after 1,225,650 cycles. The tension flange itself did not delaminate from the web. The compression flange did not start to show delamination until approximately 11,000 cycles. The compression flange delamination also occurred between the two top 0° plies (plies 1 and 2, Table 8) and grew approximately 30 mm in length over 600,000 cycles and then arrested for the duration of the test. Table 9 lists the average delamination length versus cycles corresponding to the lines on the beam in Figure 37. No shear stiffener, torsional stiffener or other flange damage or delaminations were visible. Indicated materials such as DD5 and CH12 are described in Refs. 49 and 54.

Table 8. Reference notation for Beams 39, 44 and 48 with ESA laminate

Reference Notation for Beams 39, 44 and 48 with ESA Laminate			
Ply Number	Ply Angle	Fabric	Description
1	0°	D155	Dropped Ply
2	0°	D155	DD5 material
3	+45°	DB120	
4	-45°		
5	0°	D155	
6	0°	D155	
7	+45°	DB120	
8	-45°		
9	0°	D155	
Adhesive Layer Hysol EA 9309.2NA, 0.1 - 0.4 mm			
10	+45°	DB240	Web material CH12 I - Beam shape, 3 mm thick, $V_F = 0.35$
11	-45°		
12	0	D155	
13	-45°	DB240	
14	+45°		

Table 9. Delamination length vs. fatigue cycles for Beam 39

Cycles	Average Tension Flange Delamination Length, mm	Average Compression Flange Delamination Length, mm
500	6	0
5,000	10	0
10,000	14	0
41,000	20	6
50,000	22	7
93,000	28	7
171,000	36	11
390,000	51	30
600,000	55	30
812,000	66	--
1,200,000	79	--

Beam 44

Beam 44 was fatigued at a rate of 4 Hz with a maximum load of 35.6 kN and a minimum load of 3.6 kN. The maximum load produced an initial maximum tension flange strain of 0.57% and a minimum compressive flange strain of -0.58%. The initial beam stiffness was measured as 4,527 kN/m. This beam had the same exterior ESA ply drops as Beam 39, except the ply drops were positioned over the ends of the shear stiffeners. The tension flange ply drops were at $x = 152$ and 455 mm (Figure 36). The compression flange ply drops were at $x = 222$ and 383 mm. This ply drop position did not allow the flanges to reach a uniform stress

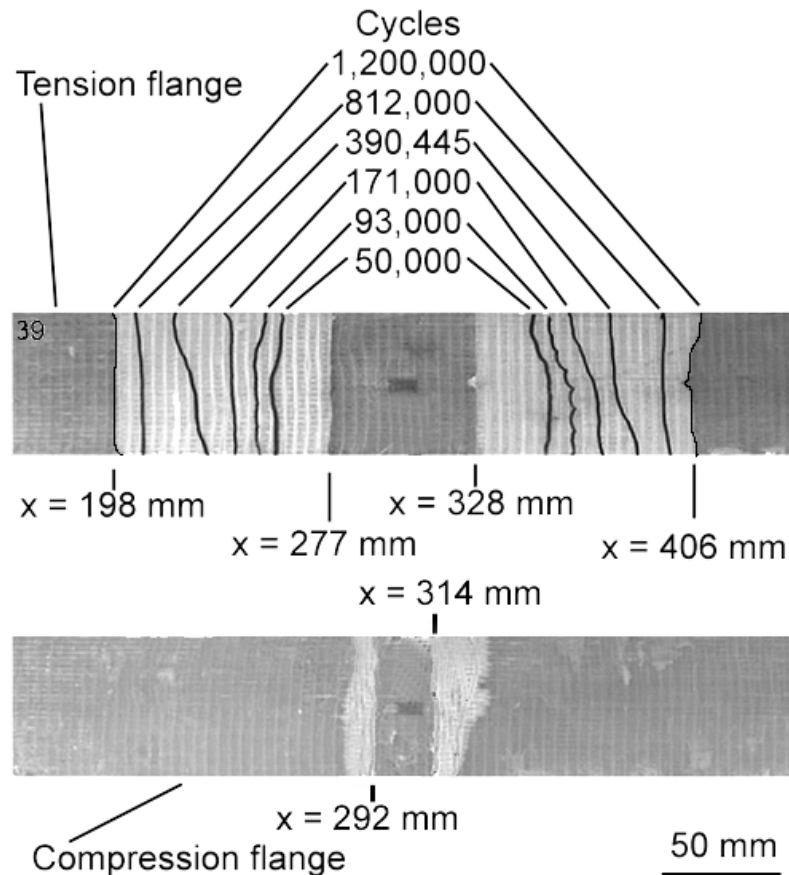


Figure 37. Beam 39 with ESA laminate for flange material.

condition away from the influence of the load introduction and geometry changes. The average delamination length versus cycles is listed in Table 10. The tension flange had a calculated average delamination rate of $2.66E-5$ mm/cycle, while the delamination on the compression flange did not start growing until 185,000 cycles, grew suddenly, and arrested at 5 mm. No shear stiffener, torsional stiffener or other flange damage or delaminations were visible. The beam is shown in Figure 38.

Table 10. Average delamination length vs. cycles for compression and tension flanges for Beam 44.

Cycles	Average Tension Flange Delamination length, mm	Average Compression Flange Delamination length, mm
200	3	--
2,000	4	--
6,300	5	--
40,000	8	--
79,000	11	--
184,000	13	5
213,000	14	5
289,000	16	5
382,000	16	5
600,000	16	5

Beam 48

Beam 48, again with the ESA laminate configuration, was fatigued at a rate of 4 Hz with a maximum load of 35.6 kN and a minimum load of 3.6 kN. The maximum load produced an initial maximum tension flange strain of 0.66% and a minimum compressive flange strain of -0.67%. The initial beam stiffness was measured as 4,650 kN/m. Unlike Beam 44, the ply drops were situated over the constant moment section of the beam with the tension ply drops at $x = 272$ and 327 mm and the compression flange ply drops were at

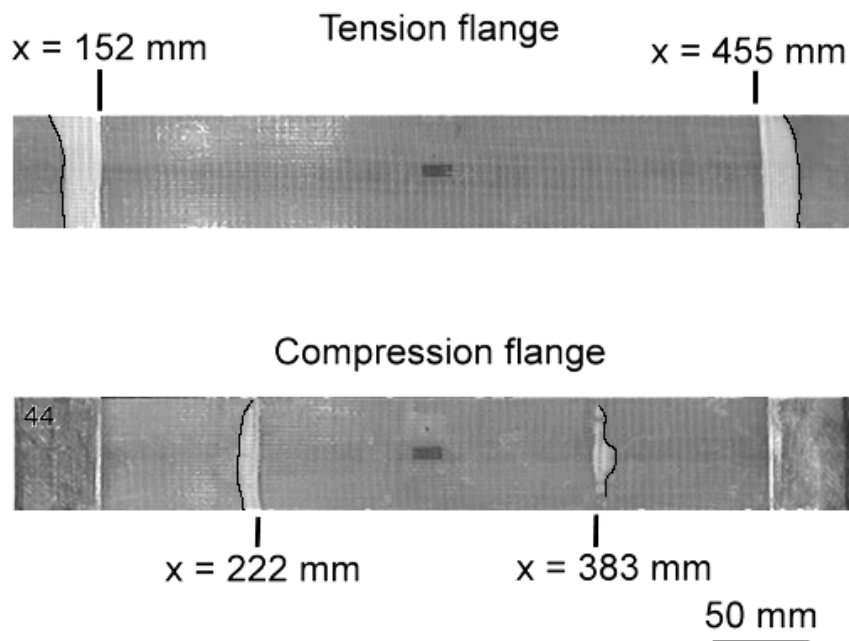


Figure 38. Tension and compression flange on Beam 44.

$x = 295$ and 320 mm. The delamination on the tension flange was uniform across the width and propagated at an average rate of $6.3E-4$ mm/cycle. The compression flange did not start to delaminate until approximately 2,500 cycles and grew at an average rate of $5.5E-5$ mm/cycle. The web and shear stiffeners showed no damage after 72,000 cycles.

The delamination length versus cycles is shown in Table 11 and the beam is shown in

Figure 39.

Table 11. Delamination length vs. cycles for tension and compressive flanges on Beam 48.

Cycles	Average Tension Flange Delamination length, mm	Average Compression Flange Delamination length, mm
2,500	11	--
4,000	13	--
6,000	16	--
7,500	16	--
10,000	19	--
16,000	22	--
37,500	34	4
72,000	45	6

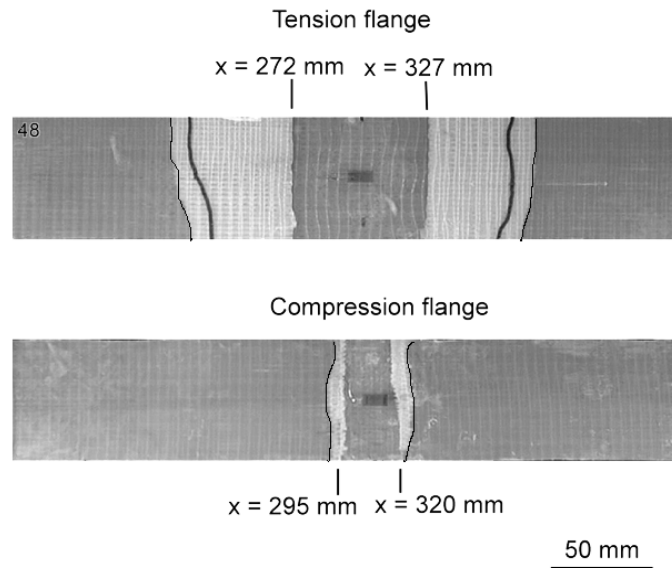


Figure 39. Beam 48, ESA laminate, tension and compression flanges.

Flange laminate ESB

Beam 40

The flange laminate of beam 40 was ESB, which had a single, interior ply drop, that was located between plies 1 and 3, as shown in Table 12. It was fatigued at a rate of 3 Hz with a maximum load of 35.6 kN and a minimum load of 3.6 kN. The maximum load produced an initial maximum tension flange strain of 0.96% and a minimum compressive flange strain of -0.85%. The initial beam stiffness was measured as 4,787 kN/m. The tension flange ply drops were located at $x = 145$ and 452 mm, while the compression flange ply drops were located at $x = 226$ and 376 mm. The compression flange delaminated from the web after 264,137 cycles within the adhesive layer between $x = 150$ and 690 mm which led to subsequent web failure. No ply drop delaminations were visible after this failure. No other shear stiffener, torsional stiffener or other flange

damage or delaminations were visible. Figure 40 shows the failed beam.

Table 12. Reference notation for Beam 40 with ESB laminate

Reference Notation for Beam 40 with ESB Laminate				
Ply Number	Ply Angle	Fabric	Description	
1	0°	D155		
2	0°	D155	Dropped ply	
3	+45°	DB120	DD5 Material	
4	-45°			
5	0°	D155		
6	0°	D155		
7	+45°	DB120		
8	-45°			
9	0°	D155		
Adhesive Layer Hysol EA 9309.2NA, 0.1 - 0.4 mm				
13	+45°	DB240		Web Material CH12 I - Beam shape, 3 mm thick $V_F = 0.35$
14	-45°			
15	0°	D155		
16	-45°	DB240		
17	+45°			

Flange laminate ESG

Beam 41

The flange of beam 41 was the ESG laminate, which had two exterior 0° ply drops, (plies 1 and 2, Table 13). It was fatigued at a rate of 3 Hz with a maximum load of 49 kN and a minimum load of 4.9 kN. The maximum load produced an initial maximum tension flange strain of 0.74% and a minimum compressive flange strain of -0.76%. The initial beam stiffness was measured as 5,213 kN/m. The tension flange ply drops were located at $x = 282$ and 327 mm and the compression flange ply drops were at $x = 287$ and

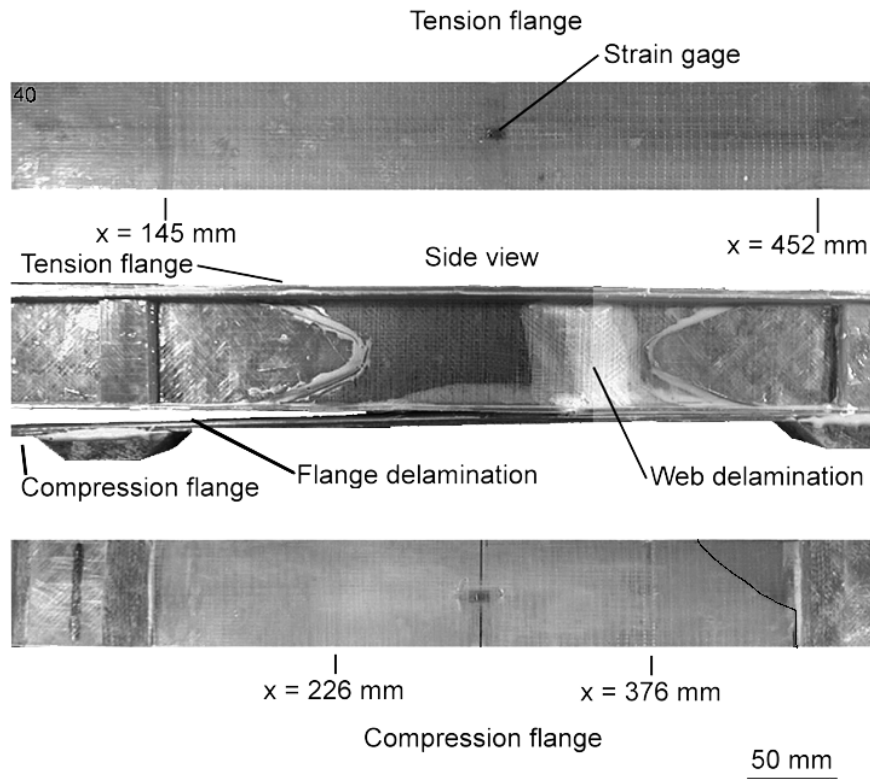


Figure 40. Beam 40

331 mm. On the tension side of the beam the delamination originally started between the 0° ply (ply 2, Table 13) and the $+45^\circ$ (ply 3, Table 13), but continued between the 0° (ply 5, Table 13) and the -45° ply (ply 4, Table 13). The average delamination length versus cycles is listed in Table 14. The calculated average delamination rate on the compression side was $1.75\text{E-}3$ mm/cycle, while the rate on the tension flange was calculated as $4.97\text{E-}3$ mm/cycle. The test was stopped after the delamination length extended into the shear stiffener area of the beam. No shear stiffener, torsional stiffener or other flange damage or delaminations were visible. Figure 41 shows the delaminated beam.

Table 13. Reference notation for Beams 41,42 with ESG laminate

Reference Notation for Beams 41,42 with ESG Laminate				
Ply Number	Ply Angle	Fabric	Description	
1	0°	D155	Dropped plies	
2	0°	D155		
3	+45°	DB120		
4	-45°			
5	0°	D155		
6	0°	D155		
7	+45°	DB120		
8	-45°			
9	0°	D155		
10	0°	D155		
11	+45°	DB120		
12	-45°			
13	0°	D155		
Adhesive Layer Hysol EA 9309.2NA, 0.1 - 0.4 mm				
14	+45°	DB240		I - Beam shape, 3 mm thick, $V_F = 0.35$
15	-45°			
16	0°	D155		
17	-45°	DB240		
18	+45°			

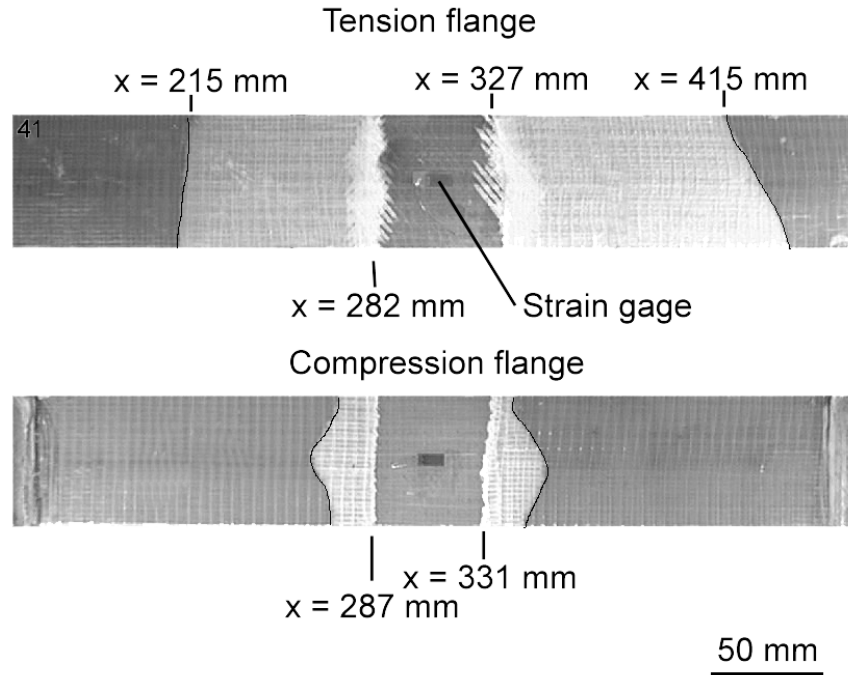


Figure 41. Beam 41

Table 14. Cycles vs. average tension and compression flange delamination length for Beam 41.

Cycles	Average Tension Flange Delamination length, mm	Average Compression Flange Delamination length, mm
20	11	--
200	13	--
600	21	--
1,000	25	--
1,500	29	--
2,100	33	3
3,700	34	3
13,997	70	21

Beam 42

The only difference with Beam 42 as compared to Beam 41 is the strain level which the beam were run. Beam 42 was fatigued at a rate of 4 Hz with a maximum load of 35.6 kN and a minimum load of 3.6 kN. The maximum load produced an initial maximum tension flange strain of 0.55% an a minimum compressive flange strain of -0.54%. The initial beam stiffness was measured as 5,524 kN/m. The tension flange ply drops were located at $x = 280$ and 325 mm and the compression flange ply drops were at $x = 280$ and 328 mm. On the tension side of the beam the delamination originally started between the 0° ply (ply 2, Table 13) and the $+45^\circ$ (ply 3, Table 13), but continued between the 0° (ply 5, Table 13) and the -45° ply (ply 4, Table 13). The average delamination length versus cycles is listed in Table 15. The average calculated delamination rate on the

Table 15. Cycles vs. average tension flange delamination for Beam 42.

Cycles	Average Tension Flange Delamination length, mm	Cycles (cont.)	Average Tension Flange Delamination length, mm
500	7	62,000	38
1,000	12	85,000	43
2,000	12	89,000	46
3,500	14	152,000	61
23,000	22	341,000	89
35,000	29	381,000	109
62,000	38	436,508	128

tension flange was $1.23\text{E-}4$ mm/cycle. The compression flange did not start to delaminate until almost 100,000 cycles and grew 9 mm with an average calculated delamination rate

was $3.84\text{E-}5$ mm/cycle for the remaining cycles. The delaminated beam is shown in Figure 42.

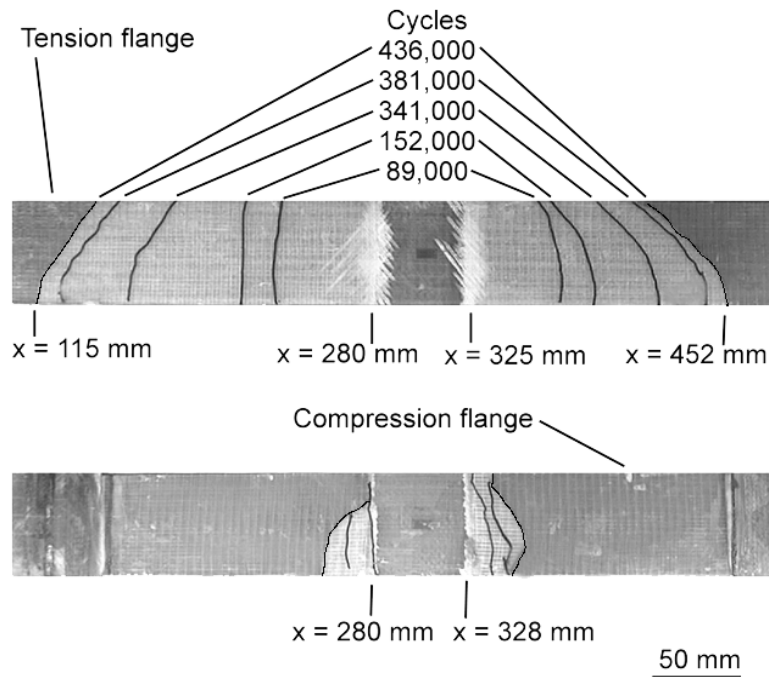


Figure 42. Beam 42, ESG laminate (two, exterior 0° ply drops) on flanges.

Flange laminate ESH

Beam 49

The flange material for beam 49 was the ESH laminate, which had two internal 0° ply drops (plies 2 and 3, Table 16). It was fatigued at a rate of 3 Hz with a maximum load of 57.8 kN and a minimum load of 5.8 kN. The maximum load produced an initial maximum tension flange strain of 0.76% and a minimum compressive flange strain of -0.73%. The initial beam stiffness was measured as 6,625 kN/m. The tension flange ply

drops were located at $x = 277$ and 326 mm and the compression flange ply drops were at $x = 290$ and 335 mm. The delamination on the tension side first propagated into the thin section of the flange, between the 0° and $+45^\circ$ plies (plies 1 - 4, Table 16), with a length of approximately 10 mm. After this initial delamination, the crack started to propagate into the thick section, starting two cracks between the 0° plies (ply 1 and 2, Table 16) and the 0° ply and the $+45^\circ$ ply (plies 3 and 4, Table 16). The delamination was uniform across the width of the flange and the average calculated tensile side delamination rate was $9.3E-5$ mm/cycle. Delamination on the compression flange did not start until approximately 6,800 cycles. Once the delamination did start on the compression flange, it grew at an average calculated rate of $4.2E-2$ mm/cycle until it reached the load pads at $x = 150$ and 455 mm. Even with the delamination on the compression side extending to the load pads, the stiffness of the beam remained approximately unchanged at 6,281 kN/m after 25,500 cycles. The average delamination length versus cycles is shown in Table 17. The delaminated beam is shown in Figure 43.

Table 16. Cycles for tension and compression flange delamination on beam 49.

Cycles	Average Tension Flange Delamination length, mm	Average Compression Flange Delamination length, mm
10	4	--
1,000	4	--
2,000	4	--
6,800	8	12
12,868	20	19
25,500	20	19

Table 17. Reference notation for Beams 49 and 50 with ESH laminate.

Reference Notation for Beams 49,50 with ESH Laminate				
Ply Number	Ply Angle	Fabric	Description	
1	0°	D155	Dropped plies	
2	0°	D155		
3	0°	D155		
4	+45°	DB120		
5	-45°			
5	0°	D155		
6	0°	D155		
7	+45°	DB120		
8	-45°			
9	0°	D155		
10	0°	D155		
11	+45°	DB120		
12	-45°			
13	0°	D155		
Adhesive Layer Hysol EA 9309.2NA, 0.1 - 0.4 mm				
14	+45°	DB240		I - Beam shape, 3 mm thick, $V_F = 0.35$
15	-45°			
16	0	D155		
17	-45°	DB240		
18	+45°			

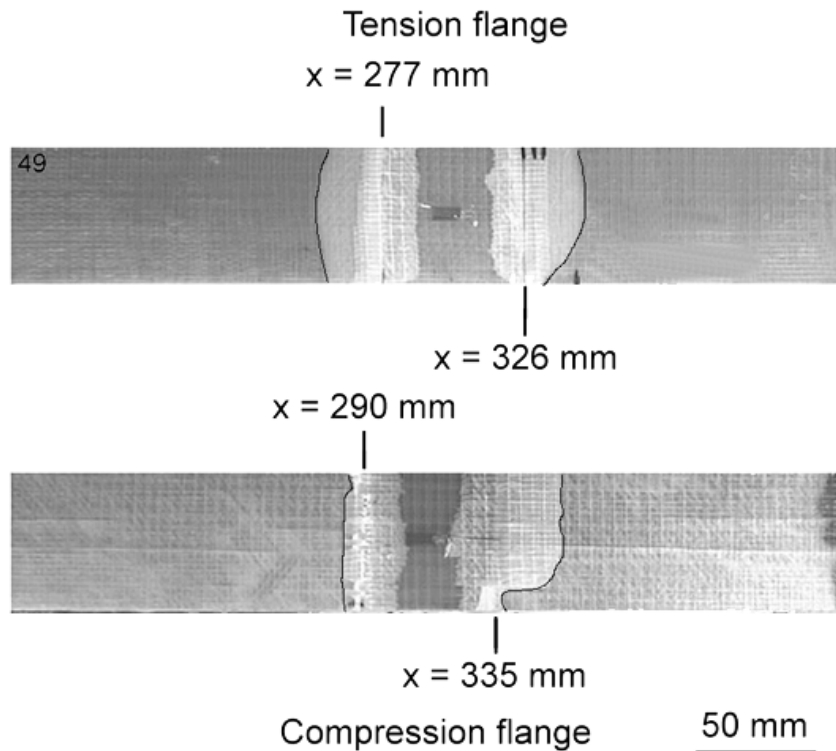


Figure 43. Beam 49 with ESH (two internal 0° ply drops) flange material.

Beam 50

Beam number 50 also contained ESH laminate flanges. It was fatigued at a rate of 3 Hz with a maximum load of 48.9 kN and a minimum load of 4.9 kN. The maximum load produced an initial maximum tension flange strain of 0.63% and a minimum compressive flange strain of -0.63%. The initial beam stiffness was measured as 6,054 kN/m. The tension flange ply drops were located at $x = 265$ and 325 mm and the compression flange ply drops were at $x = 270$ and 320 mm. Delamination on the tensile side started into the thin section and then arrested, just as the previous beams. The average delamination length versus cycles is shown in Table 18. The delamination on the

tensile flange started into the thick cross-section and propagated uniformly at an average calculated rate of $5.08\text{E-}4$ mm/cycle. The compression side of the beam showed delamination being initiated at one corner of the ply drop and slowly working its way along the flange edge and then across the flange. Once the crack had propagated across the flange width, the delamination grew unstably to the load pads. The beam was then

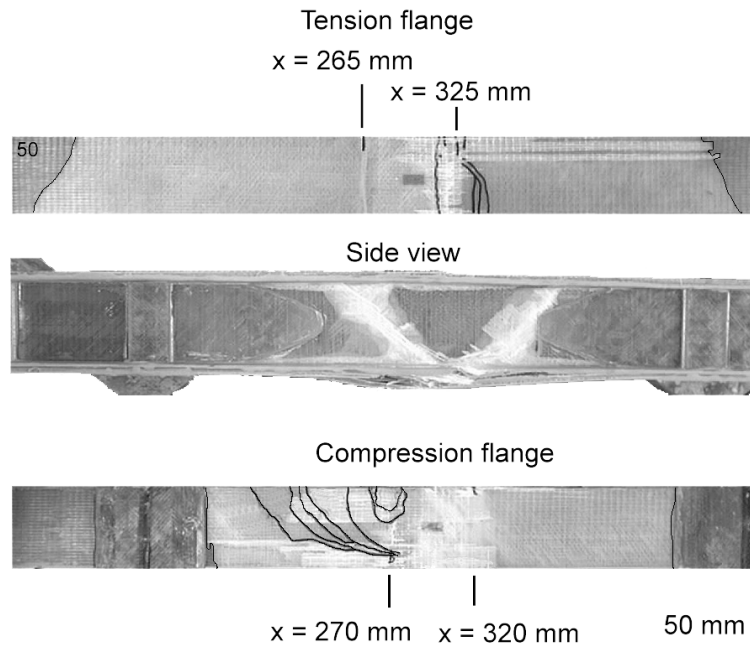


Figure 44. Beam 50 with ESH (two, interior 0° ply drops) laminate as flange material.

tested for residual strength after 204,100 cycles, with a residual load to failure of 88.2 kN determined. The failed beam is shown in Figure 44.

Comparison of Delamination Rate in Beams and Coupons

Two comparisons were made between beam and coupon delamination rates, the

first is the ESA laminate, a single exterior ply drop, and the second is the ESH laminate, containing two interior ply drops.

Table 18. Cycles vs. tension flange delamination length for beam 50.

Cycles	Average Tension Flange Delamination length, mm
500	4
2,500	19
7,000	24
12,000	30
31,800	30
82,000	30
105,000	43
131,000	52
176,000	102
204,100	102
Compression flange did not have a uniform delamination front. Once the delamination propagated across flange width, the delamination rapidly proceeded to the grips.	

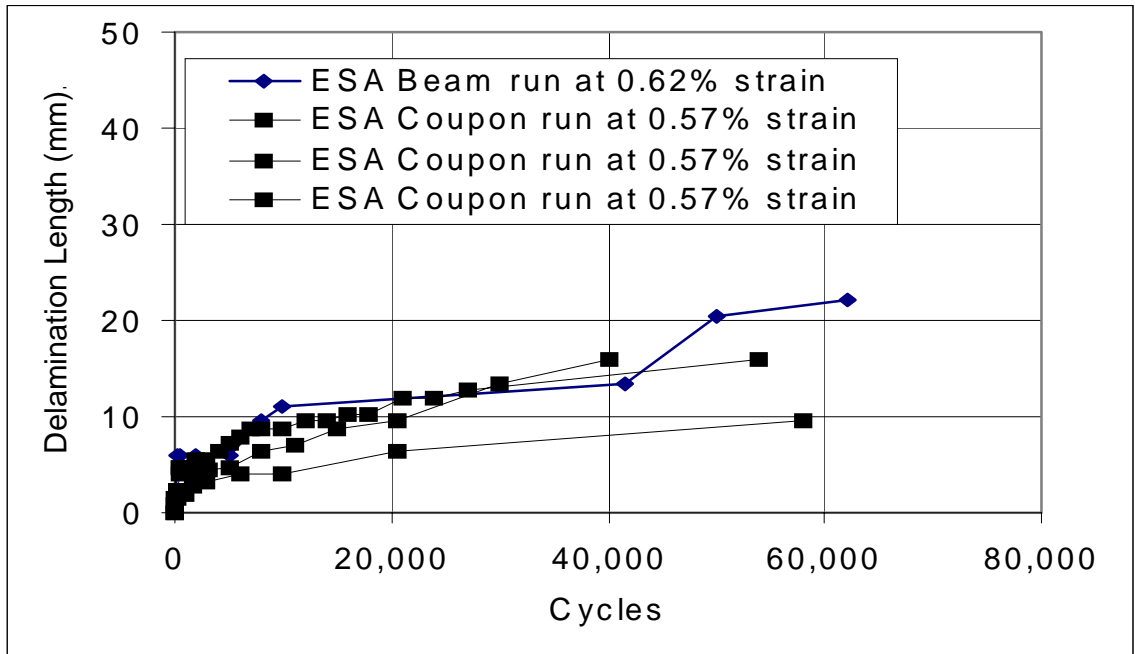


Figure 45. Beam (Tension Flange) vs. Coupon Data (R=0.1) for ESA (Single, exterior 0° ply drop), R=0.1.

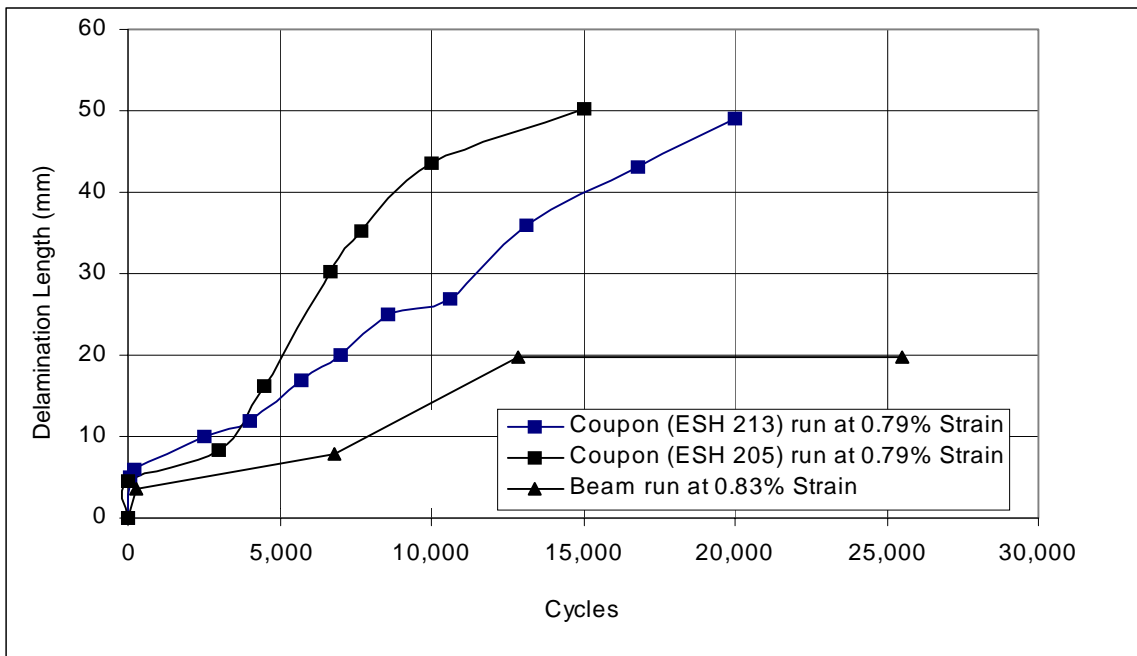


Figure 46. Beam (tension flange) vs. coupon data for ESH laminate (Two Interior ply drops), R=0.1.

These two comparisons are presented in Figures 45 and 46, respectively. Only one beam was run at each stress level. Therefore, no statistical tests were performed, two beams are necessary to form a population, to correlate the beam and coupon delamination rates. The beam and coupon delamination rates, in tension, for both interior and exterior ply drops were similar. If the strain levels had been exactly the same, the delamination rates might have been even closer together.

In compression, no stable delamination took place with the interior ply drops, delamination typically showed up only a few hundred cycles before total delamination of the ply drops. However, one beam (Beam 50) did not show this behavior until the delamination had been initiated across the whole width of the beam flange. This may be a typical scenario, since Beam 49 was left unattended during the cycles when the plies delaminated to the load pads. This was also common with compressive coupons, the delamination would propagate during the last few cycles across the width and then the ply drops would delaminate to the grips. Exterior ply drops behaved differently in compression than did interior ply drops. The delamination for exterior ply drops would initiate but would arrest, whereas on the tension side of the beam the delamination would continue to grow. No figures showing the delamination rate of coupons versus beams is shown in compression due to the sudden nature of the delamination propagation. In general, delamination was observed on the tensile flange well before it was observed on the compressive flange.

The compressive ESH coupons that were bonded together back to back as

described earlier do correlate well with the compressive side of the ESH beam. Back-to-back coupons delaminated to the grips after 32,025 cycles at 0.62% strain, while an ESH beam compressive flange delaminated to the load pads after 25,500 cycles at 0.73% strain. At first it was thought that bonding the flange material onto the beam would be the only way to get accurate results. This was expected because the beam could restrain the coupon material from buckling. However, by increasing the coupon thickness, and reducing non-symmetry by back-to-back bonding, the coupon results were consistent with the beam data. The overall set-up time and the ability to run higher testing frequencies is greatly improved with back-to-back coupons versus beams.

STRAIN ENERGY RELEASE RATE AND MODELING RESULTS

Determination of Critical Strain Energy Release Rate.

Most of the modeling of delamination is done in a separate finite element study by Maccagnano. Modeling of delamination at ply drops requires basic Mode I and II critical strain energy release rate (G_c) data. These G_c values were determined for Mode I cracks using a double cantilever beam (DCB) coupon and for Mode II cracks using an end-notched flexure (ENF) coupon. Three different coupons configurations were tested using the D155 fabric for 0° layers and DB120 fabric for the $\pm 45^\circ$ layers: the first laminate had the lay-up $[0]_{10}$ with a fiber content of 36 percent, the second laminate consisted of $[(0)_5/\pm 45/(0)_4]$ with a fiber content of 38 percent, and finally a plate constructed of $[\pm 45]_{10}$ with a fiber content of 26 percent. By using these three combinations it would be possible to determine G_c for cracks growing between a $0^\circ/0^\circ$, $0^\circ/\pm 45^\circ$ or a $\pm 45^\circ/\pm 45^\circ$ interface.

A 2.22 kN load cell was placed in series with the standard load cell of the 8501

Instron testing machine to obtain the required load sensitivity. The hinges that had been mounted on the Mode I coupons were clamped in the machine and the coupons were adjusted so that they would remain perpendicular to the load cell during the test. The

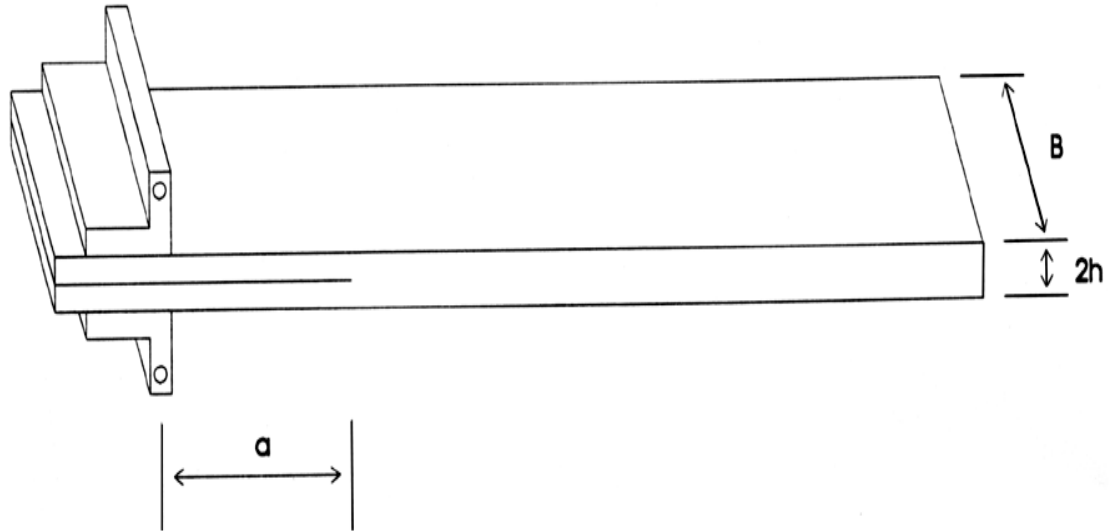


Figure 47. Mode I coupon geometry.

Instron machine was placed in displacement control, with a ramp rate of 0.04 mm/sec. To avoid the crack propagating through the resin rich region ahead of the Fluro-Peel insert in both the Mode I and II coupons, which could artificially influence the value of G , a flat faced screwdriver was used to extend the crack 2.5 mm past the resin rich region. The initial crack lengths for the coupons were measured from the hinges to the crack front. A diagram of a typical Mode I specimen showing the dimensions used to calculate the strain energy release rate is shown in Figure 47. All three of the load-displacement diagrams were very similar. The G_{Ic} values were calculated using the methods described in Chapter 2. During testing the crack stayed in the plane where it was initiated, except with coupons containing all $\pm 45^\circ$ layers. Therefore, values for these latter coupons are not reported.

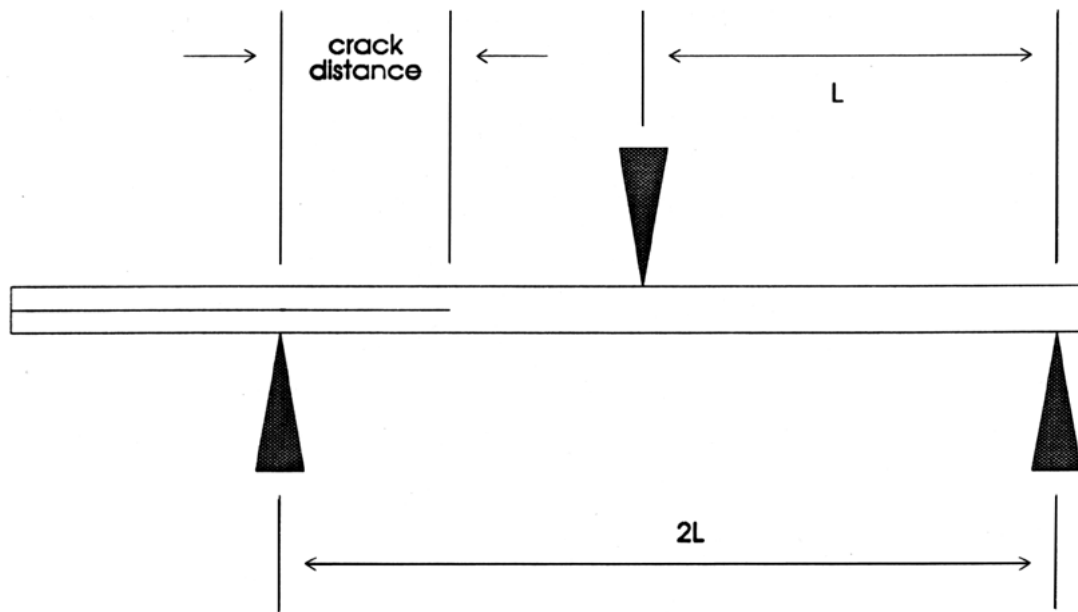


Figure 48. Mode II specimen geometry.

Mode II coupons did not require hinges for testing. An ENF coupon with the points of load application identified is shown in Figure 48. All the coupons were loaded until the crack propagated from the initial length to the point of load application, except the coupons containing all $\pm 45^\circ$ layers, which were too compliant and the crack did not grow. One solution to this problem might be to add 0° layers and keep two $\pm 45^\circ$ layers along the centerline, the stiffness of the coupon would be increased which would allow a value of G_{IIc} to be determined. The following table, Table 19, summarizes the results found from the Mode I and II tests.

Table 19. Critical strain energy release rate for Mode I and Mode II cracks

Average* Critical Strain Energy Release Rate for Mode I and Mode II Cracks		
Laminate	$G_{Ic} \frac{1.1 \dots 1.1}{\dots 2}$	$G_{IIc} \frac{1.1 \dots 1.1}{\dots 2}$
[0] ₁₀	0.49 ± 0.03	1.43 ± 0.35
[(0) ₅ /±45/(0) ₄]	0.78 ± 0.04	2.27 ± 0.53
*- Average of five specimens for each value.		

Static and Threshold Strain Energy Release Rates at Ply Drops

The ESA and ESB laminates were used to determine the static G values. In Table 20, the critical static stress causing delamination and the UTS of the ESA and ESB

Table 20. ESA and ESB critical static strength.

Laminate	Critical Static Stress, MPa	Static Strength, MPa
ESA	110	427
ESB	496	700

coupons are given. Values for G_c calculated from ply drop static tests were obtained using Eqn 5 [53] for exterior ply drops and Eqn 6 [26] for interior ply drops.

$$G = P^2 \frac{A_2 E_2 - A_1 E_1}{2w A_2 E_2 A_1 E_1} \quad (5)$$

$$G = \frac{\sigma^2 h t}{4E(h-t)} \quad (6)$$

In Eqn 5, P is the critical static strength to cause the delamination, A is the cross-sectional area, E is the modulus in the longitudinal direction and w is the width of the coupon. The subscript 2 refers to thick cross-section properties, while the subscript 1 refers to the thin cross-section. In Eqn 6, σ is the critical stress where delamination starts, h is the laminate thickness, t is the thickness of the dropped plies, and E is the modulus in the load direction, assumed to be the same for the thick and thin sides. The equations are based on simple mechanics of materials concepts. As the difference in modulus increases or the number of ply drops increase, the strain energy release rate will also increase. This shows the same trend as the experimental ESB and ESH coupons. Also, for a given ply drop case, increasing the thickness of the overall laminate reduces G . This is again consistent with the results for the ESB vs. ESH laminate. The static strain energy release rates for the ESA and ESB laminates are compared in Table 21 with values obtained from DCB and ENF coupons. The ESA laminate was compared to the critical strain energy release rate obtained from the DCB specimen with a $0^\circ/0^\circ$ crack interface. However, the crack in the ESB laminate propagated via Mode II as opposed to Mode I in the ESA laminate. Therefore, an ENF specimen with a $0^\circ/\pm 45^\circ$ interface was used as a comparison.

Table 21. Static strain energy release rates.

Laminate	Theoretical (N/mm)	Experimental (N/mm)	Percent Difference (%)
ESA	0.12	0.49	308
ESB	1.34	2.27	69

However, these equations do not correlate well the finite element predictions. Table 22 compares the results obtained using the equations to the finite element results. From the table the percent difference between the formulas found in literature and the finite element methods vary greatly . By experimentally determining the threshold stress level for some of the cases tested, finite element methods were capable of predicting the threshold stress of other laminates.

Table 22. Threshold strain energy release rates

Laminate	Theoretical Strain Energy Release Rate, N/mm	FEA Strain Energy Release Rate [55], N/mm	Percent Difference, %
ESA	0.08	0.12	51
ESB	0.34	0.73	114
ESH	0.15	0.74	380

For example, the ESB laminate had a threshold stress level of 276 MPa., which corresponded to a threshold strain energy release rate of 0.738 N/mm. The ESH geometry, with two interior ply drops, was then loaded at different stress levels until the threshold strain energy release rate of the ESH matched the ESB laminate. A threshold stress level for the ESH laminate of 200 MPa was obtained, which was only 3% lower than the experimental value of 207 MPa. The list of strains presented in Table 3 can be used in conjunction with finite element methods to predict threshold strain energy release rates for other laminates accurately.

CHAPTER 5

CONCLUSIONS AND RECOMMENDATIONS

Conclusions

Delamination at Ply Drops

The following detailed conclusions for delamination relate only to uniaxial tensile fatigue, $R = 0.1$, at ambient temperature with no environmental effects considered. A convenient comparison of results is given in Table 3 as the strain to produce a 25 mm delamination in 10^5 cycles, as well as arrest and threshold values.

- Internal ply drops are roughly twice as resistant to delamination as external ply drops.
- For the same number of ply drops, thicker laminates are better in resisting delamination.
- Dropping more than one ply at the same location increases the delamination growth rate.
- When the ply drops are separated, the delamination follows the same growth rate as a single interior ply drop until the delamination reaches the adjacent ply drop. The rate then increases.
- Dropping multiple $\pm 45^\circ$ layers is an effective way to taper the thickness without introducing delamination.
- The use of “Z-Spiking” and adhesives at ply drops in the manufacturing of parts substantially reduces the initial delamination rate.
- Incorporating adhesive into laminates containing interior ply drops prevents delamination, prior to tensile failure at the ply drop.

- Using “feathering” at the ply drops, on both interior and exterior ply drops, reduces the delamination rate.
- Random mat does not help and possibly has a detrimental effect on delamination resistance.
- Coupons can be successfully tested in compression, as long as care is taken to ensure the stiffness and symmetry of the coupon is sufficient to prevent buckling; back-to-back bonding of coupons worked well and correlated well with beam results.

I-Beam Study

- The delamination results between coupons and beam flanges containing ply drops were at similar strain levels.
- Ply drops, both interior and exterior, on the tension side of the beam showed similar delamination rates to coupons.
- Exterior ply drops on the compression flange arrested after growing a short distance. Interior ply drops gave little warning in compression before total delamination. In all cases, delamination occurred earlier on the tensile flange than on the compressive flange.

Effect of Ply Drops on Lifetime

- Introduction of ply drops reduces the fatigue life of the lower fiber content coupons more significantly than for the higher fiber content coupons.
- The fatigue resistance of lower fiber content coupons with ply drops was degraded to the level of the higher fiber content coupons without ply drops. The high fiber content coupons with ply drops did not show any significant loss in performance when compared to control coupons of the same fiber content.
- The A130 fabric for 0° reinforcement with ply drops has a very erratic, strand by strand delamination response at strains well below the values for the D155 fabric.
- The lifetime of laminates with A130 fabric converged with that of the D155 fabric in cyclic fatigue after 10^6 cycles.

G_c Tests

Determining the critical strain energy release rate was straight-forward, with Mode II values being 3 to 4 times higher than Mode I values. Testing of $[\pm 45]_{10}$ coupons did not provide any information due to the compliance of the coupons. Coupons that contained $\pm 45^\circ$ ply drops did not delaminate. Theoretical models for delamination growth are consistent with data trends, but disagree with some finite element results.

Recommendations

This set of data for ply drops establishes delamination rates and the performance of various lay-ups in cyclic fatigue loading at $R=0.1$ and $R=10$. The actual blade loading conditions need to be determined, so that coupon performance can be reevaluated under a worst loading case or spectrum loading conditions. Even though cracks form in composites which have no ply drops, the extensive delamination from ply drops causes even more severe cracks to form which makes the composite more susceptible to environmental attack. Therefore, an investigation of the environmental effects on the lifetime of laminates with ply drops should be investigated. Compression should also be explored in greater detail, along with understanding the influence of tapering coupons on buckling resistance.

Using the critical strain energy release rates from Mode I and II coupons, finite element modeling of laminates with ply drops should be used to predict static and threshold stress levels. Once the FEA results can be validated with the coupon data, ply drops can be incorporated into larger structures, such as wind turbine blades, with confidence.

REFERENCES CITED

1. Wilkins, D.J., Eisenmann, J.R. Camin, R.A., Margolis, W.S. and Benson, R.A., “ Characterizing Delamination Growth in Graphite-Epoxy,” *Damage in Composite Materials, ASTM STP 775*, 1982, pp. 168.
2. Broek, D. “Elementary Engineering Fracture Mechanics,” 4th edition, Kluwer Academic Publishers, 1986, pp 328-335.
3. Benbow, J.J. and Roesler, F.C., *Process Physical Society, London, B 70*, 1957, pp. 201.
4. Gilman, J.J. *Journal of Applied Physics*, Vol. 31, 1960, pp. 2205.
5. Russell, A.J. and Street, K.N., “ Factors Affecting the Interlaminar Fracture Energy of Graphite/Epoxy Laminates,” *Progress in Science and Engineering of Composites*, ed. Hayashi, T, Kawata, K., and Umekawa, S., ICCM IV, Tokyo, 1982, p. 279.
6. Lagace, P.A., Cannon, R.K., “ Effects of Ply Dropoffs on the Tensile Behaviour of Graphite/Epoxy Laminates, *4th Japan-U.S. Conference on Composite Materials*, Washington, DC, June 27-29, 1988.
7. Wisnom, M.R., “Prediction of Delamination in Tapered Unidirectional Glass Fibre Epoxy with Dropped Plies Under Static Tension and Compression,” *74th Meeting of the AGARD Structures and Material Panel*, Patras, Greece, May 24-29, 1992, pp. 25-1.
8. Mandell, J.F., Reed, R.M., Jr. and Samborsky, D.D., “ Fatigue of Fiberglass Wind Turbine Blade Materials, ”, *Contractor Report SAND92-7005*, Sandia National Laboratories, Albuquerque, NM, 1992.
9. Grimes, G.C., Dusablon, E.G., “ Study of Compressive Properties of Graphite/Epoxy Laminates with Discontinuities,” *Composite Materials: Testing and Design., ASTM STP 787*, 1982, pp. 513-538.
10. Ulman, D.A., Bruner, R.D., Owens, S.D., and Miller, H.R., “Damage Accumulation in Composites: Volume II- Experimental Data.” *Technical Report General Dynamics Technical Report AFWAL-TR-85-3070*. General Dynamics Fort Worth Division. Fort Worth, TX. September 1985.
11. Reifsnider, K.L., “Damage and Damage Mechanics,” *Fatigue of Composite Materials*, Elsevier Science Publishers, 1990, pp. 11.
12. Adams, D.F., Ramkumar, R.L., and Walrath, D.E., “Analysis of Porous Laminates in the presence of Ply Drop-Offs and Fastener Holes,” *Technical Report NOR 84-113*.

- Northrop Corporation, Hawthorne, CA. And University of Wyoming, Laramie, WY, May, 1984.
13. Fish, J.C., Lee, S.W., "Tensile Strength of Tapered Composite Structures," AIAA Paper No. 88-2252, *Proceedings of the AIAA/ASME/ASCE/AHS/ASC 29th Structures, Structural Dynamics, and Materials Conference. Part 1.* Monterey, CA., April, 1988.
 14. Fish, J.C., Lee, S.W., "Tensile Strength of Composite Structures with Internal Ply Drops," *PhD Thesis*, University of Maryland, 1988.
 15. Wu, C.M.L., Webber, J.P.H., "Analysis of Tapered (In Steps) Laminated Plates Under Uniform In-Plane Load," *Composite Structures*, Vol. 5, No. 1, pp. 87, 1988.
 16. Hoa, S.V., Daoust, J., Du, B.L., and VuKhanh, T., "Interlaminar Stresses in Tapered Laminates," *Polymer Composites*, Vol. 9, No. 5, pp. 337, October 1988.
 17. Dharani, L.R., Seaton, C.P., "Analysis of a Buffer Strip Laminate with Fiber and Matrix Damage and Interlaminar Debonding," *Composite Structures*, Vol. 7, pp. 139-158, 1987.
 18. Poe, C. C. and Kennedy, J. M., "Buffer Strips for Improving Damage Tolerance of Composite Laminates," *Journal of Composite Materials Supplement*, Vol. 14, p. 57, 1980.
 19. Hess, T. E., Huang, S. L., and Rubin, H., "Fracture Control in Composite Materials using Integral Crack Arresters," *Proceedings of the AIAA/ASME/SAE 17th Structures, Structural Dynamic and Materials Conference*, pp. 52-69, King of Prussia, PA, 1976.
 20. Fisher, K., "3D reinforcements: on the verge?," *High Performance Composites*, March/April 1996, p. 32.
 21. Tanzawa, Y., "Experimental Study of Interlaminar Delamination Toughness of 3-D Orthogonal Interlocked Fabric Composite," *Proceedings of the AIAA/ASME/ASCE/AHS/ASC 38th Structures, Structural Dynamics, and Materials Conference and Exhibit and AIAA/ASME/AHS Adaptive Structures Forum*, Vol. 4, pp. 2611, Kissimmee, FL, 1997.
 22. Chan, W.S., Rogers, C., and Aker, S., "Improvement of Edge Delamination Strength of Composite Laminates using Adhesive Layers," *Composite Materials: Testing and Design*, ASTM STP 893, 1986, p. 266.
 23. Masters, J. E., "Improved Impact and Delamination Resistance through Interleafing," *Interlaminar Fracture in Composites*, E. A. Armanios, editor, Trans Tech Publishing, Switzerland 23., 1989.

24. Kemp, B. L., Johnson, E. R., "Response and Failure Analysis of a Graphite/Epoxy Laminate Containing Terminating Internal Plies, AIAA Paper No. 85-0608, *Proceedings of the AIAA/ASME/ASCE/AHS 26th Structures, Structural Dynamic and Materials Conference, Part 1*, April 15-17, 1985, pp. 13-24.
25. Chan, W. S., and Ochoa, O. O., "Suppression of Edge Delamination in Composite Laminates by Termination of a Critical Ply Near the Edges," *Proceedings of the AIAA/ASME/ASCE/AHS 26th Structures, Structural Dynamic and Materials Conference, Part 1*, April 18-20, 1988, pp. 359-364.
26. Ochoa, O. O and Chan, W. S., "Tapered Laminates: A Study on Delamination Characterization," *Proceedings of the American Society for Composites, Third Technical Conference*, Sept. 25-29, 1988, pp. 633.
27. Hoa, S.V., Daoust, J., Du, B.L., and VuKhanh, T., "Interlaminar Stresses in Tapered Laminates," *Polymer Composites*, Vol. 9, No. 5, pp. 337, October 1988.
28. Curry, J.M., Johnson, E.R., and Starnes, J. H., "Effect of Ply Drop-offs on the Strength of Graphite/Epoxy Laminates," Technical Report CCMS 86-07, Center for Composite Materials and Structures, Virginia Polytechnic Institute and State University, Blacksburg, VA, December 1986.
29. O'Brien, T.K., "Towards a Damage Tolerance Philosophy for Composite Materials and Structures," *Composite Materials: Testing and Design (Ninth Volume)*. ASTM STP 1059, S.P. Garbo, Ed., American Society for Testing and Materials, Philadelphia, 1990, pp. 7-33.
30. Wilkins, D.J., Eisenmann, J. R., Camin, R. A., Margolis, W.S., Benson, R.A., "Characterizing Delamination Growth in Graphite-Epoxy," *Damage in Composite Materials*, ASTM STP 775, American Society for Testing and Materials, Philadelphia, June 1982, p. 168.
31. Mall, S., Yun, K. T., and Kochnar, N. K., "Characterization of matrix Toughness Effect on Cyclic Delamination Growth in Graphite Fiber Composites," presented at the 2nd ASTM Symposium on Composite Materials: Fatigue and Fracture, Cincinnati, OH, April 1987.
32. Russell, A.J. and Street, K.N., "Predicting Interlaminar Fatigue Crack Growth Rates in Compressively Loaded Laminates," presented at the 2nd ASTM Symposium on Composite Materials: Fatigue and Fracture, Cincinnati, OH, April 1987.
33. Gustafson, C. G., and Hojo, M., "Delamination Fatigue Crack Growth in Unidirectional Graphite/Epoxy Laminates," *Journal of Reinforced Plastics*, Vol. 6, No. 1,

January 1987, pp. 36-52.

34. O'Brien, T. K., "Generic Aspects of Delamination of Fatigue of Composite Materials," *Journal of the American Helicopter Society*, Vol. 32, No. 1, January 1987, pp. 36-52.
35. Martin, R. H. And Murri, G.B., "Characterization of Mode I and Mode II Delamination Growth and Thresholds in Graphite/PEEK Composites," NASA TM 100577, National Aeronautics and Space Administration, Washington, DC, April 1988.
36. O'Brien, T.K., "Characterization of Delamination Onset and Growth in a Composite Laminate," *Damage in Composite Materials, ASTM STP 755*, American Society for Testing and Materials, Philadelphia, 1982, pp. 140-167.
37. Russell, A.J. and Street, K. N., "Moisture and Temperature Effects on the Mixed-Mode Delamination Fracture of Unidirectional Graphite/Epoxy," *Delamination and Debonding of Materials, ASTM STP 876*, American Society for Testing and Materials, Philadelphia, October 1985, pp. 349-370.
38. Poursartip, A., "The Characterization of Edge Delamination Growth in Composite Laminates Under Fatigue Loading," *Toughened Composites, ASTM STP 937*, American Society for Testing and Materials, Philadelphia, 1987, pp. 222-241.
39. O'Brien, T. K., "Mixed-Mode Strain Energy Release Rate Effects on Edge Delamination of Composites," *Effects of Defects in Composite Material, ASTM STP 836*, American Society for Testing and Materials, Philadelphia, 1984, pp.125-142.
40. O'Brien, T.K., "Tension Fatigue Behavior of Quasi-Isotropic Graphite/epoxy Laminates," *Fatigue and Creep of Composite Materials, Proceedings, 3rd Riso International Symposium on Metallurgy and Materials Science, riso National Laboratory Roskilde, Denmark, 1982*, pp. 259-264.
41. O'Brien, T.K., "Fatigue Delamination Behaviour of PEEK Thermoplastic Composite Laminates," *Journal of Reinforced Plastics*, Vol. 7, No. 4, July 1988, pp. 341-359.
42. O'Brien, T.K., Murri, G.B., Salepekar, S. A., "Interlaminar Shear Fracture Toughness and Fatigue Thresholds for Composite Materials," *Composite Materials: Fatigue and Fracture- Second Volume, ASTM STP 1012*, American Society for Testing and Materials, Philadelphia, 1989, pp. 222-250.
43. Adams, D.F, Zimmerman, R. S., and Odem, E. M., "Frequency and Load Ratio Effects on Critical Strain Energy Release Rate G_c Thresholds of Graphite Epoxy Composites," *Toughened Composites, ASTM STP 937*, American Society for Testing and

Materials, Philadelphia, 1987, pp. 242.

44. O'Brien, T. K., Rigamonti, M., and Zanotti, C., "Tension Fatigue Analysis and Life Prediction for Composite Laminates," NASA TM 100549, National Aeronautics and Space Administration, Washington, DC, October 1988.

45. O'Brien, T. K., "Generic Aspects of Delamination in Fatigue of Composite Materials," *Journal of the American Helicopter Society*, Vol. 32, No. 1, January 1987, pp. 13-18.

46. Agarwal, B.D. and Broutman, L.J., "Analysis and Performance of Fiber composites," 2nd edition, John Wiley & Sons, 1990, pp. 430-435.

47. Freitas, G. and Fusco, T., "Z-Fiber Technology and Products for enhancing Composites Design," Aztec, Inc., Waltham, MA. pp. 1-7.

48. Hedley, C.W., "Mold Filling Parameters in Resin Transfer Molding of Composites," M.S. Thesis, April 1994, pp. 12.

49. Mandell, J.F., Samborsky, D.D., "DOE/MSU Composite Material Fatigue Database: Test Methods, Materials, and Analysis," *Sandia Contractors Report*, To be published.

50. Wung, E.C.J., Chatterjee, S.N., "On the Failure Mechanisms in Laminate Compression Specimens and the Measurement of Strength," *Journal of Composite Materials*, Vol. 26, No. 13, 1992, pp. 1885-1914.

51. Adams, D.F., Lewis, E.Q., "Influence of Specimen Gage Length and Loading Method on the Axial Compressive Strength of a Unidirectional Composite Material," *Experimental Mechanics*, March 1991, pp. 14-20.

52. Combs, D.W., "Design, Analysis and Testing of a Wind Turbine Blade Substructure," *MS Thesis*, March 1995, pp. 24-36.

53. Ramkumar, R.L. and Whitcomb, J.D., "Characterization of Mode I and Mixed-Mode Delamination Growth in T300/5208 Graphite/Epoxy," in *Delamination and Debonding of Materials*, ASTM STP 876, W.S. Johnson, ED., ASTM, Phi., 1985.

54. Mandell, J.F., Samborsky, D.D., Combs, D.W., Scott, M.E., and Cairns, D.S. "Fatigue of Composite Material Beam Elements Representative of Wind Turbine Substructure," *NREL Contractors Report*, To be published.

55. Maccagnano, Z., Personal Interview, 8 June 1997.

APPENDIX A

The coupon tests were given a letter which identified the material and individual coupons. This appendix contains results from cyclic fatigue tests using a constant stress amplitude sine waveform with R-values of 0.1 and 10, where the R-value is defined by:

$$R = \frac{\text{Minimum cyclic stress}}{\text{Maximum cyclic stress}}$$

and the compressive stresses are negative.

The individual test results are listed and summarized using eight columns with the following data structure:

Col. 1 & 2 Sample ID #	Col. 3 Max. Running Stress (MPa)	Col.4 E(GPa)	Col.5 %ε	Col. 6 Cycles	Col.7 Notes	Col. 8 R value
------------------------------	--	-----------------	-------------	------------------	----------------	-------------------

Col. 1: List the laminate being tested.

Col. 2: Lists the MSU test reference number.

Col. 3: This column indicates the maximum stress in megapascals (MPa) which was applied to the coupon. A positive number indicates tension while a negative number indicates compression. For a compression test the stress listed as maximum is actually the minimum stress.

Col. 4: Lists the initial measured elastic modulus (E) of the coupon in gigapascals (GPa).

Col. 5: Indicates the initial absolute maximum fatigue running strain (ε) in percent or the percent strain to failure for a static test.

Col. 6: Number of cycles the coupon was fatigued

Col. 7: Lists any other notation for comments.

The notations used in column 6 are summarized below:

- F- Failure of coupon
- RO - Run out, coupon has significant fatigue cycles but has not yet failed, test stopped.
- Z - Double coupon thickness, two coupons bonded together to increase the thickness.
- ~~~ Indicates that a value was unavailable
- DA - Delamination arrested
- EF - End failure of coupon

Other notations used in the test material summary tables include:

V_f - Fiber volume content of the material in percent

Laminate	Number	Max. Stress (MPa)	E (GPa)	% Strain	Cycles	Comments	R value
ESA	113	452	23.1	1.96	1	~	~
ESA	108	207	~	0.90	2,001	~	0.1
ESA	109	138	~	0.60	110,000	~	0.1
ESA	111	121	~	0.52	175,000	RO	0.1
ESA	112	103	~	0.45	400,000	DA	0.1
ESA	102	207	23.4	0.90	1,301	~	0.1
ESA	104	207	~	0.90	1,001	~	0.1
ESA	110	138	23.4	0.60	85,000	~	0.1
ESA	103	138	~	0.60	40,000	~	0.1
ESA	107	-276	~	-1.19	318	~	10
ESA	101	-207	~	-0.90	20,000	~	10
ESA	105	-138	~	-0.60	252,222	~	10
ESA	106	-172	~	-0.75	102,000	~	10
ESA	202s	410	~	1.77	1	~	~
ESA	203s	416	~	1.80	1	~	~
ESA	204s	436	~	1.89	1	~	~
ESA	205s	423	~	1.83	1	~	~
ESA	207s	477	~	2.07	1	~	~
(Vf=35%)							
ESB	112	524	22.1	2.27	1	~	~
ESB	106	207	24.1	0.90	90,001	~	0.1
ESB	109	345	~	1.49	7,326	EF	0.1
ESB	114	276	24.1	1.19	50,000	~	0.1
ESB	115	276	~	1.19	45,000	~	0.1
ESB	101	345	~	1.49	10,000	~	0.1
ESB	102	310	~	1.34	20,100	~	0.1
ESB	113	310	23.4	1.34	15,000	~	0.1
ESB	105	310	22.8	1.34	15,000	~	0.1
ESB	110	276	~	1.19	44,342	~	0.1
ESB	103	-276	~	-1.19	409	F	10
ESB	111	-241	~	-1.04	30,996	F	10
ESB	107	-241	~	-1.04	187,000	~	10

Laminate (Vf=35%)	Number	Max. Stress (MPa)	E (GPa)	% Strain	Cycles	Comments	R value
ESB	409	753	25.5	2.95	1	F	~
ESB	411	788	26.2	3.09	1	F	~
ESB	405	758	~	2.97	1	F	~
ESB	407	414	~	1.62	2,401	F	0.1
ESB	403	207	~	0.81	1,060,000	RO	0.1
ESB	404	414	25.5	1.62	3,567	F	0.1
ESB	414	207	~	0.81	1,277,000	F	0.1
ESB	401	276	25.5	1.08	58,501	F	0.1
ESB	402	276	~	1.08	164,000	F	0.1
(Vf=44%)							
ESC	101	555	22.8	2.37	1	~	~
ESC	110	345	24.1	1.47	8,700	~	0.1
ESC	109	345	23.4	1.47	4,000	~	0.1
ESC	108	276	~	1.18	41,000	~	0.1
ESC	104	276	~	1.18	20,000	~	0.1
ESC	107	345	~	1.47	10,000	~	0.1
ESC	105	276	~	1.18	25,001	~	0.1
(Vf=35%)							
ESD	110	396	14.5	2.13	1	~	~
ESD	109	138	18.6	0.74	300,000	RO	0.1
(Vf=37%)							
ESE	116	207	~	0.68	5,000	~	0.1
ESE	112	655	30.3	2.16	1	~	~
ESE	114	207	~	0.68	5,810	~	0.1
ESE	110	138	~	0.45	100,000	~	0.1
ESE	111	138	32.4	0.45	10,000	~	0.1
ESE	106	121	~	0.40	101,000	~	0.1
(Vf=40%)							

Laminate	Number	Max. Stress (MPa)	E (GPa)	% Strain	Cycles	Comments	R value
ESF	110	207	~	0.67	34,033	EF	0.1
ESF	105	276	31.0	0.89	74,428	EF	0.1
ESF	113	276	~	0.89	45,000	~	0.1
ESF	106	276	~	0.89	45,000	~	0.1
ESF	109	345	31.7	1.11	8,646	EF	0.1
ESF	108	276	~	0.89	9,785	EF	0.1
(Vf=40%)							
ESG	104	345	29.6	1.16	1	~	0.1
ESG	102	207	~	0.70	150	~	0.1
ESG	107	138	~	0.47	30,000	RO	0.1
ESG	105	138	29.6	0.47	50,000	~	0.1
ESG	106	103	~	0.35	225,000	~	0.1
ESG	101	121	~	0.41	42	~	0.1
(Vf=46%)							
ESH	101	276	~	0.93	24,000	~	0.1
ESH	102	454	29.6	1.53	1	~	~
ESH	105	207	~	0.70	50,000	~	0.1
ESH	106	276	29.6	0.93	25,000	~	0.1
(Vf=46%)							
ESH	202	634	33.09	1.88	1	F	0.1
ESH	204	630	33.78	1.87	1	F	0.1
ESH	208	345	~	1.02	1,300	F	0.1
ESH	209	345	~	1.02	1,350	F	0.1
ESH	213	276	~	0.82	20,000	RS	0.1
ESH	205	276	~	0.82	40,000	RS	0.1
ESH	211	379	~	1.12	57	F	0.1
ESH	212	379	~	1.12	63	F	0.1
ESH	207	276	~	0.82	15,000	F	0.1
ESH	210	207	~	0.61	92,479	F	0.1

Laminate (Vf=45%)	Number	Max. Stress (MPa)	E (GPa)	% Strain	Cycles	Comments	R value
ESH	301	733	32.40	2.42	1	F	~
ESH	312	770	31.02	2.54	1	F	~
ESH	313	798	~	2.63	1	F	~
ESH	304	414	~	1.36	1,935	F	0.1
ESH	305	414	~	1.36	2,021	F	0.1
ESH	303	414	~	1.36	2,693	F	0.1
ESH	307	207	~	0.68	953,762	F	0.1
ESH	311	345	30.33	1.14	3,929	F	0.1
ESH	310	207	~	0.68	526,064	F	0.1
ESH	306	276	31.71	0.91	39,000	F	0.1
ESH	314	276	~	0.91	82,921	F	0.1
ESH	309	276	~	0.91	56,938	F	0.1
(Vf=52%)							
ESH	413	747		2.64	1	F	~
ESH	407	207	27.58	0.73	731,521	F	0.1
ESH	412	728	28.27	2.58	1	F	~
ESH	411	414	~	1.46	813	F	0.1
ESH	406	414	~	1.46	748	F	0.1
ESH	410	276	~	0.98	28,019	F	0.1
ESH	405	276	27.58	0.98	30,689	F	0.1
ESH	404	207	28.27	0.73	1,093,000	RO	0.1
ESH	409	172	~	0.61	1,100,000	RO	0.1
ESH	408	207	27.58	0.73	968,675	F	0.1
ESH	403	207	~	0.73	685,000	F	0.1
(Vf=35%)							
ESI1	101	276	31.0	0.89	42,500	EF	0.1
	104	310	~	1.00	9,500		0.1
	105	276	~	0.89			0.1
	103	276	~	0.89	96,000	EF	0.1

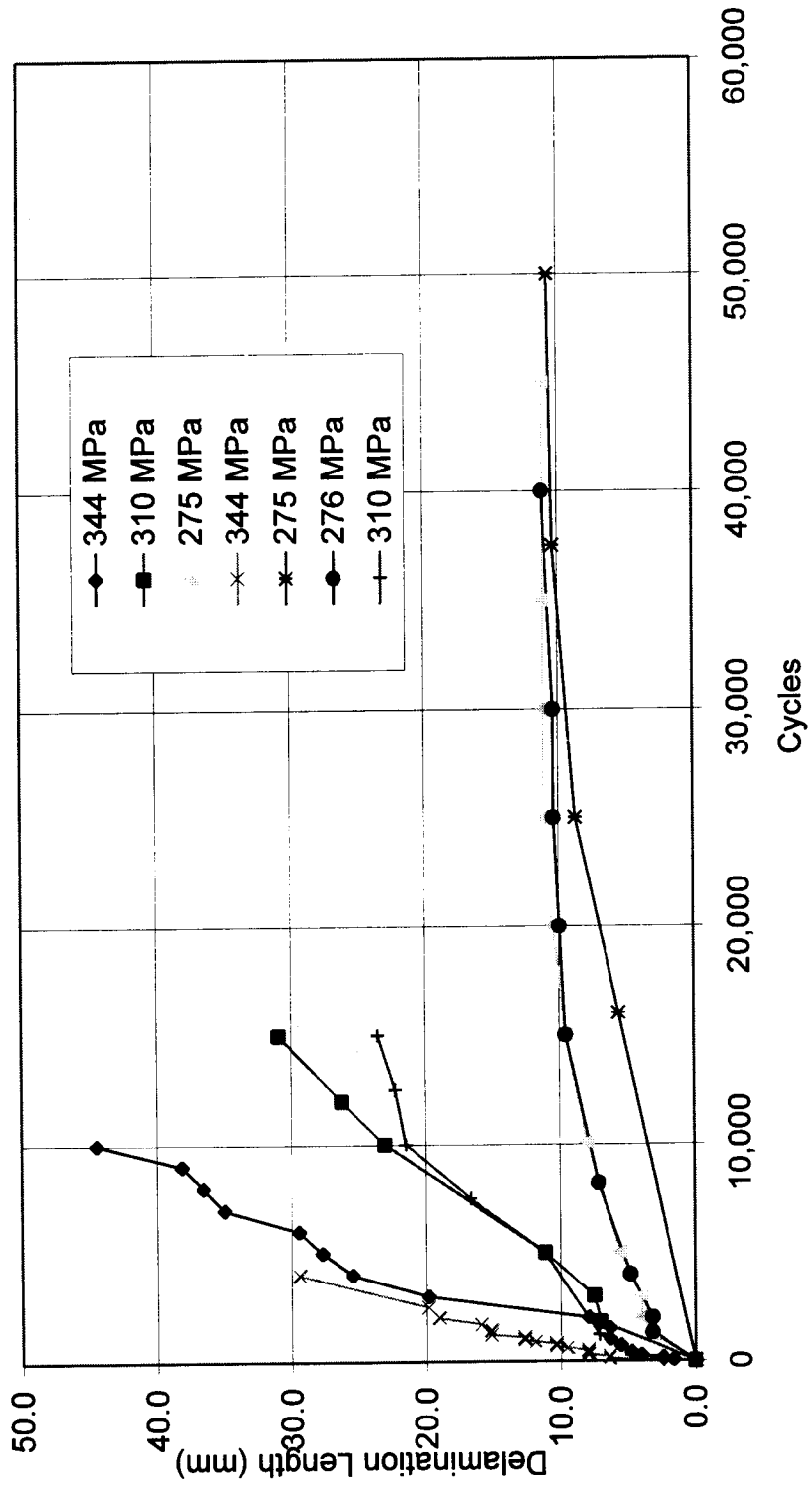
Laminate	Number	Max. Stress (MPa)	E (GPa)	% Strain	Cycles	Comments	R value
ES12	107	310	31.0	1.00	1,730	EF	0.1
	103	310	~	1.00	3,829	EF	0.1
	102	276	~	0.89	19,000	EF	0.1
	104	241	~	0.78	90,000	~	0.1
	106	276	~	0.89	19,100	EF	0.1
ES13	107	276	31.0	0.89	25,000	~	0.1
	104	276	~	0.89	52,000	~	0.1
	103	241	~	0.78	136,000	~	0.1
	108	207	~	0.67	1,121,809	~	0.1
	106	241	~	0.78	130,326	~	0.1
	102	276	~	0.89	87,090	~	0.1
ES14	108	276	31.0	0.89	9,500	EF	0.1
	106	276	~	0.89	51,000	~	0.1
	107	276	~	0.89	10,475	EF	0.1
	104	310	~	1.00	5,447	EF	0.1
	103	276	~	0.89	36,000	~	0.1
	101	241	~	0.78	162,000	~	0.1
(ES11 -ES14, Vf=36%)							
ESJ (Vf=37%)	101	207	~	0.79	90,000	~	0.1
	108	276	~	1.05	31,213	EF	0.1
	104	207	~	0.79	80,000	~	0.1
	106	207	26.2	0.79	110,000	~	0.1
ESK (Vf=37%)	104	207	~	0.71	30,000	~	0.1
	105	276	~	0.95	809	~	0.1
	107	207	~	0.71	10,000	~	0.1
	102	138	29.0	0.48	210,000	~	0.1

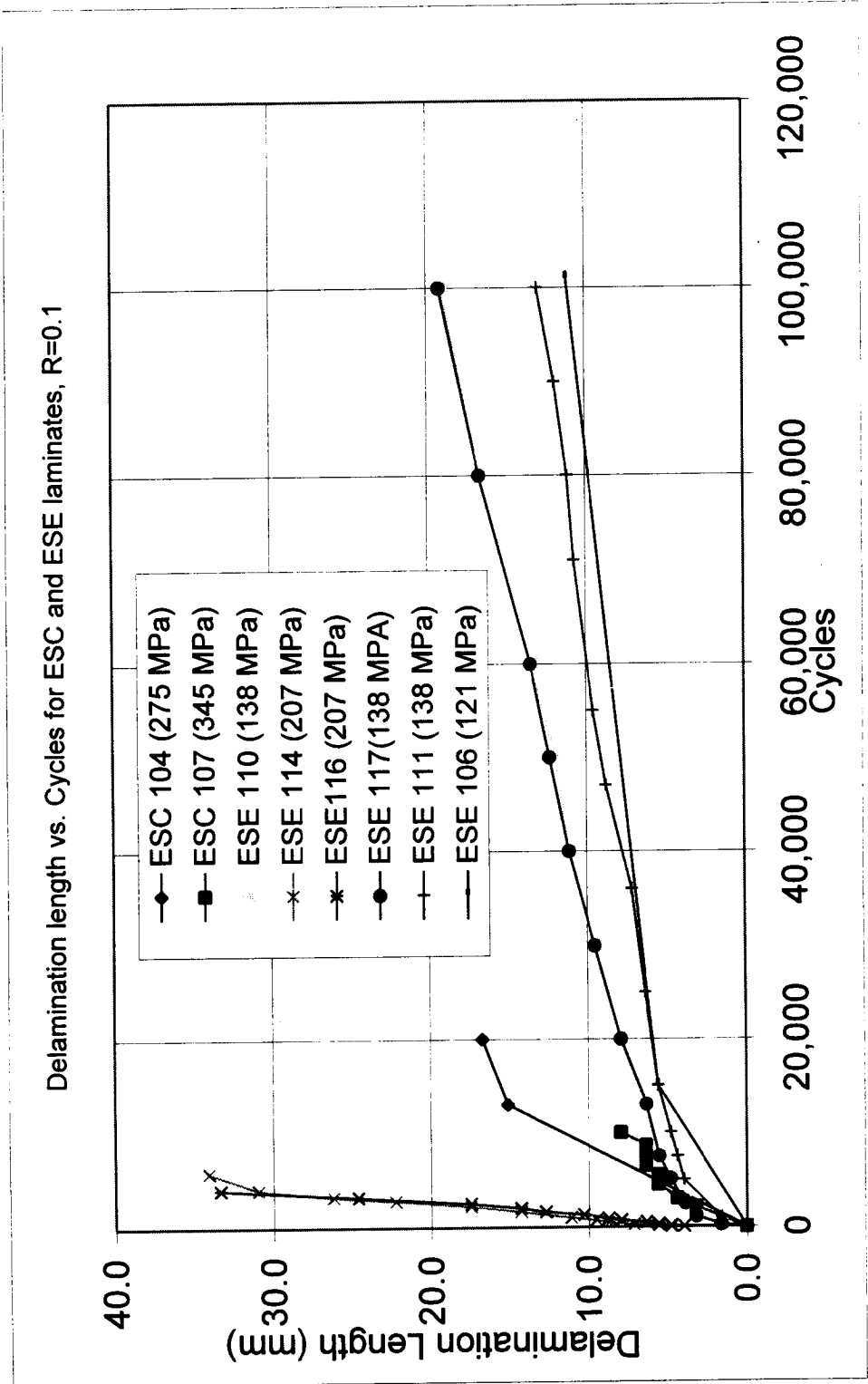
Laminate	Number	Max. Stress (MPa)	E (GPa)	% Strain	Cycles	Comments	R value
ESL	103	241	29.0	0.83	10	EF	0.1
ESL	107	241	~	0.83	365,000	~	0.1
ESL	102	276	~	0.95	83,400	~	0.1
ESL	101	276	~	0.95	80,000	~	0.1
(Vf=44%)							
ESM	107	276	~		142,000	~	0.1
(Vf=44%)							
ESN	101	276	24.1	1.14	1	~	0.1
ESN	102	172	24.8	0.71	1,500	~	0.1
ESN	103	138	~	0.57	17,000	~	0.1
ESN	104	103	~	0.43	102,000	~	0.1
ESN	105	103	~	0.43	187,000	~	0.1
(Vf=36%)							
ESO	101	276	24.8	1.14	120,000	EF	0.1
ESO	102	345	25.5	1.43	2,443	F	0.1
ESO	103	310	~	1.29	2,297	EF	0.1
ESO	104	310	~	1.29	8,379	EF	0.1
ESO	105	276	~	1.14	41,808	EF	0.1
ESO	106	276	~	1.14	19,500	EF	0.1
(Vf=36%)							
ESL	102	955	33.1		1	F	~
ESL	104	907	32.4		1	F	~
ESL	105	887	~	2.86	1	F	~
ESL	114	414	31.7	1.33	4,600	F	0.1
ESL	108	414	~	1.33	4,005	F	0.1
ESL	109	414	31.0	1.33	4,263	F	0.1
ESL	116	276	32.4	0.89	64,613	F	0.1
ESL	112	172	~	0.56	998,920	RO	0.1

Laminate	Number	Max. Stress (MPa)	E (GPa)	% Strain	Cycles	Comments	R value
ESL	115	207	~	0.67	922,651	F	0.1
ESL	110	276	31.7	0.89	116,740	F	0.1
ESL	113	276	~	0.89	108,767	F	0.1
ESL	111	552	~	1.78	311	F	0.1
ESL (Vf=44%)	106	552	~	1.78	381	F	0.1
ESQ	612	172	20.0	0.68	1,217,000	RO	0.1
ESQ	607	544	22.1	2.13	1	F	0.1
ESQ	603	552	~	2.17	1	F	0.1
ESQ	606	548	~	2.15	1	F	0.1
ESQ	608	276	21.4	1.08	12,405	F	0.1
ESQ	602	276	~	1.08	10,207	F	0.1
ESQ	601 610	310	23.4	1.22	2,704	F	0.1
ESQ	613	310	~	1.22	5,632	F	0.1
ESQ	614	276	~	1.08	19,000	F	0.1
ESQ	601	172	~	0.68	1,106,000	F	0.1
ESQ	611	241	22.1	0.95	210,000	F	0.1
ESQ (Vf=44%)	605	241	~	0.95	32,000	F	0.1

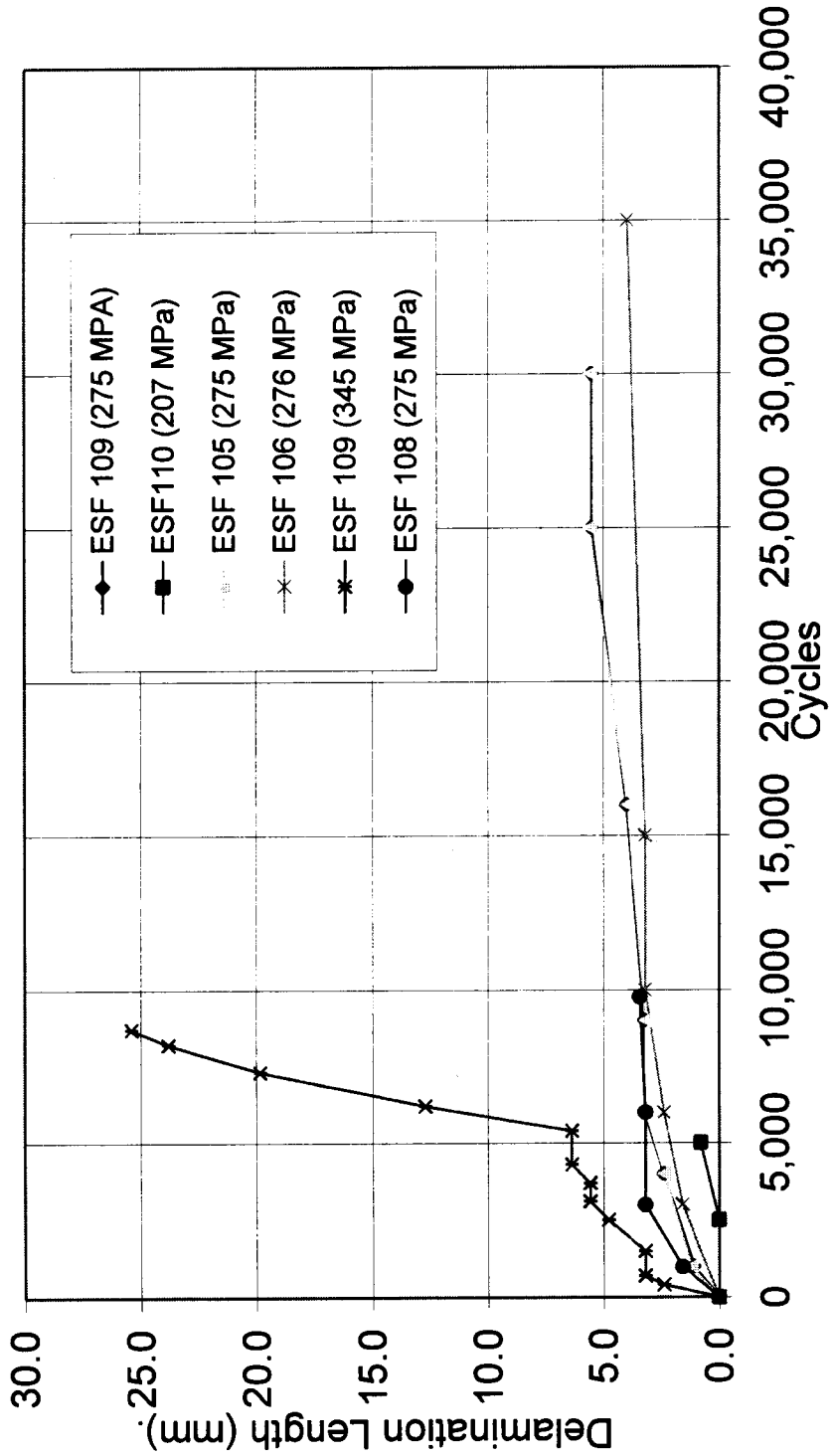
APPENDIX B
Delamination Length vs. Cycles for Coupons

Delamination Length vs. Cycles for ESB laminate, R=0.1

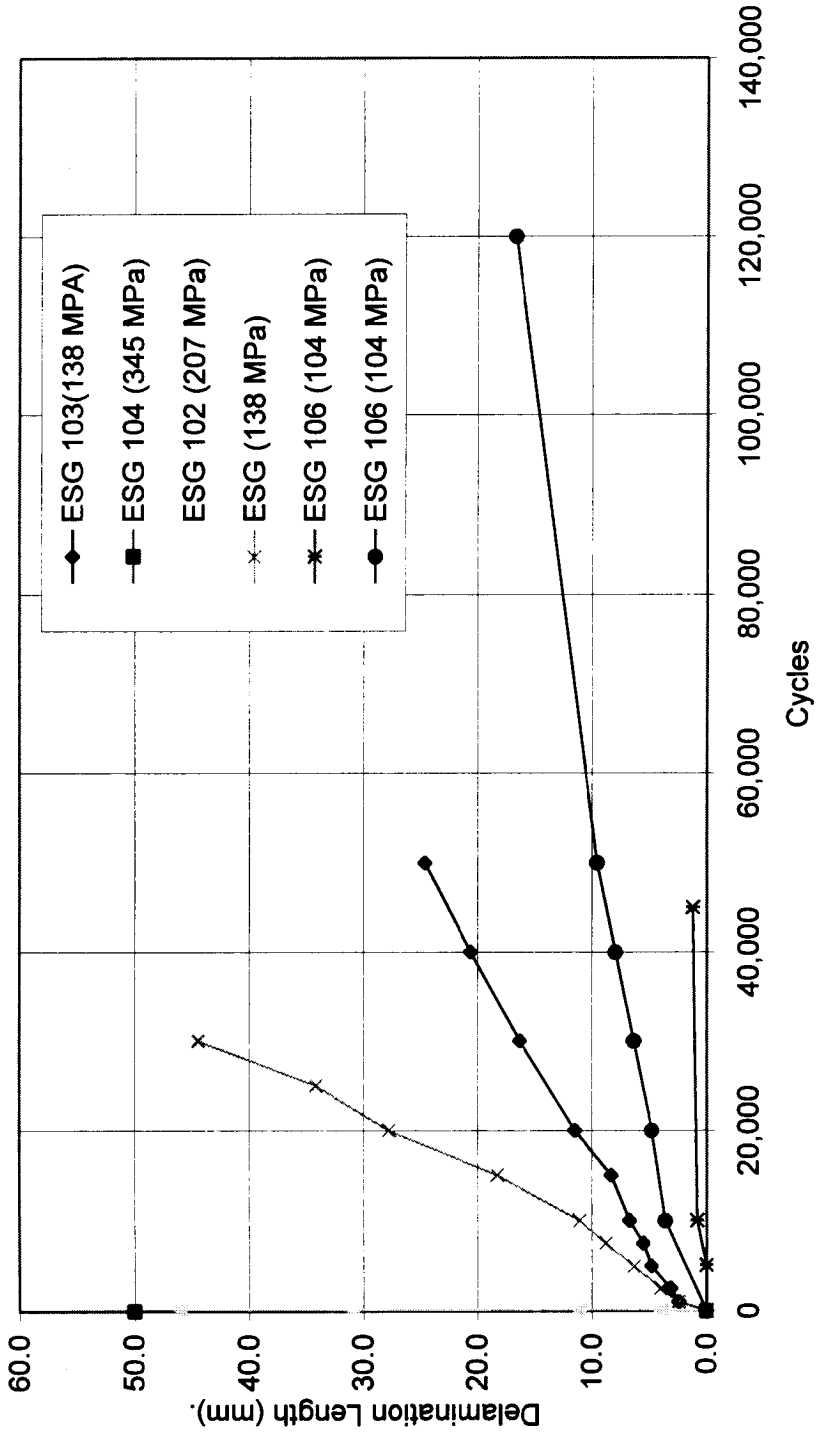




Delamination Length vs. Cycles for ESF laminate, R=0.1



Delamination Length vs. Cycles for ESG laminate, R=0.1



ESI 1			
ESI1 101 (276 MPa)			
CYCLES	UP CK.	LOW CK.	
0	0	0	
2,000	0	5	
3,700	0	7	
5,000	0	7	
8,000	0	8	
10,000	0	8	
16,000	0	8	
21,000	0	8	
25,000	0	8	
31,000	0	8	

ESI1 104 (310 MPa)			
CYCLES	UP CK.	LOW CR.	
0	0	0	
250	0	0	
500	4	4	
1,500	5	4	
2,600	5	5	
3,600	5	15	
5,000	10	15	
8,000	10	15	
9,000	20	15	

ESI1 105 (275 MPa)			
CYCLES	UP CK.	LOW CK.	
0	0	0	
3,400	5	8	
5,400	5	8	
8,000	8	8	

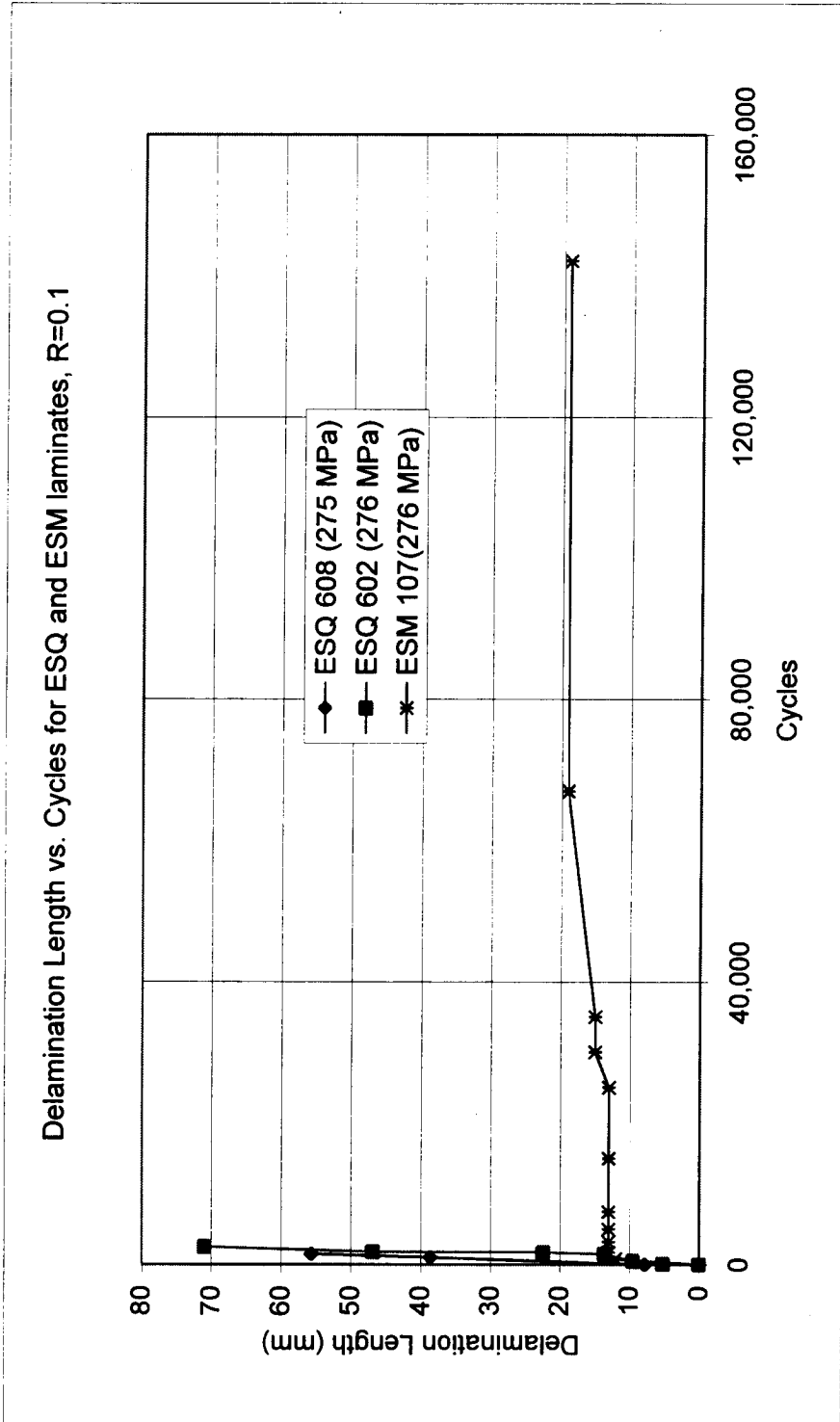
ESI2 107 (310MPa)			
CYCLES	UP CK	LOW CR.	
0	0	0	
500	5	5	
1,730	10	10	
1,750 EF			

ESI2 103 (310 MPa)			
CYCLES	UP CK	LOW CK.	
0	0	0	
500	2	10	
1,000	4	17	
1,600	8	17	
2,500	10	17	
3,829 EF			

ESI2 102 (275 MPa)			
CYCLES	UP CK.	LOW CK.	
0	0	0	
1,200	0	5	
3,000	0	9	
5,000	9	15	
10,000	9	15	
19,000 EF			

ES14 107 (275 MPa)		ES14 106 (275 MPa)		ES14 104 (310 MPa)	
CYCLES	UP CR.	CYCLES	UP CR.	CYCLES	UP CR.
0	0	0	0	0	0
3,600	0	4,000	0	50	0
5,600	5	6,500	0	200	0
7,600	5	8,500	0	400	0
		11,000	0	800	0
		20,000	0	1,300	0
		30,000	0	2,300	0
		51,000	0	3,000	0
		60,000	0	5,000	0
	LOW CR.		LOW CR.		LOW CR.
	0		0		0
	3		3		4
	5		5		6
	5		5		8
			5		10
			5		11
			5		12
			5		12
			5		15

ES14 103 (275 MPa)		ES14 101 (241 MPa)	
CYCLES	UP CR.	CYCLES	UP CR.
0	0	0	0
900	0	15,000	3
2,500	3	20,000	4
3,600	3	50,000	8
5,000	3	75,000	8
7,600	4	89,000	8
10,000	5	100,000	8
15,000	5	162,000	8
21,000	7		
26,000	8		
36,000	9		
	LOW CR.		LOW CR.
	0		0
	7		5
	10		9
	12		20
	12		20
	15		20
	17		20
	20		20
	20		20
	21		20
	23		20



Delamination Length vs. Cycles for ESA laminate with feathering, random mat, and repaired, R=0.1

